

POLITECNICO DI TORINO

Automotive Engineering

Master Thesis

Automatic design tool for timing belt tensioners



Supervisor:

Nicola Amati

Co-supervisor:

Andrea Tonoli

Tutor:

Federico Licata (Dayco)

Candidate

Bertoldo Emiliano

S231647

July 2018

Abstract

The timing belt has been introduced as an alternative for the timing chain. In the last decade, the timing belt in a lubricated environment has been introduced in the market (Belt In Oil system, developed by Dayco in 2007). The aim of this choice is to lower the friction of the system, allowing for a fuel consumption reduction, aspect becoming more and more important nowadays. But this brings also to face with some new issues. A critical issue is represented, for example, by the wider working temperature range, which can vary from -40°C up to 140°C. Another issue is represented by the higher sensitivity of the system, that brings to narrower belt drive components tolerance windows. For what concerns the timing belt tensioner, this is translated in narrower torque and damping tolerances, besides a higher average damping with respect to traditional applications.

The aim of this work is to take into account these more stringent requirements and, besides the packaging constraints, starting from the design input, to automatically obtain a raw but verified timing belt tensioner 3D model. This permits to save time in the early stages of the tool dimensioning.

In the first chapter of this thesis, a general overview of the timing belt tensioner tasks is added. Then, after the description of different typologies present in the market, the mathematical model describing its behaviour is introduced.

In the second chapter, instead, the components dimensioning flowchart is presented. It is a consequential process, that, given the working conditions as an input, looks for the best solution. The automation permits also to achieve a higher standardization level, with beneficial effects on the production process.

In the third chapter some practical applications have been considered. The same design inputs have been then inserted in the automatic design tool, analysing the differences between the program output and the real tensioner.

Finally, in the fourth chapter, the conclusions on this work can be found. In the same section some comments about possible improvements and integrations of this work have been included.

Content

<i>Introduction</i>	10
Vehicle longitudinal dynamics	12
Timing belt tensioner typologies	20
Tensioner mathematical model	24
<i>Tensioner design flowchart</i>	34
Design input	36
0) Tensioner execution selection	40
1) Ball bearing selection	48
2) Pivot diameter definition	49
3) Tensioner damping calculation	51
4) Pivot bushing size selection	53
5) Plastic friction element wear calculation	60
6) Stack-up calculation (axial)	66
7) Packaging constraints	67
8) Cone spring calculation	71
9) Main spring calculation	86
10) Tilting-Sliding verification	95
11) 3D CAD Parametric model	101
<i>Comparison with real tensioners</i>	103
Case study nr. 1	104
Case study nr.2	114
Case study nr. 3	124
<i>Conclusions</i>	132
<i>References</i>	134

List of Figures

Figure 1. Powertrain dynamic model	13
Figure 2. 4-cylinder engine model	14
Figure 3. Belt-drive dynamic model	15
Figure 4. Dual mass flywheel model	17
Figure 5. Longitudinal tire characteristic	18
Figure 6. Tire dynamic model	19
Figure 7. Tire frequency response	19
Figure 8. Autosetting tensioner model	20
Figure 9. Double eccentric tensioner model	21
Figure 10. Double eccentric with crank/rod loading system tensioner model	22
Figure 11. Linear guide loading system tensioner model	23
Figure 12. Tensioner model (no friction)	24
Figure 13. Tensioner model (loading condition)	25
Figure 14. Tensioner model (unloading condition)	26
Figure 15. Hysteresis cycle (load)	28
Figure 16. Hysteresis cycle (torque)	28
Figure 17. Tensioner sensitivity to differential angle	30
Figure 18. Tensioner sensitivity to pivot bushing friction coefficient	31
Figure 19. Tensioner sensitivity to plastic friction coefficient	32
Figure 20. Timing belt tensioner components	34
Figure 21. Tensioner design flowchart	35
Figure 22. Design input Excel table (1/2)	36
Figure 23. Design input Excel table (2/2)	36
Figure 24. Design input color legend	37
Figure 25. Design input Excel table (misalignment example)	38
Figure 26. Design input Excel table (suggested corrections example)	38
Figure 27. Rotary (left) and blade (right) tensioners	40
Figure 28. Standard (left) and reverse (right) layout	41
Figure 29. Flat (left) and toothed (right) pulley	42
Figure 30. Lock-up pin denied areas	43
Figure 31. Lock-up pin position reference system	45
Figure 32. Space constraints	46
Figure 33. Flowchart section 0) output	47
Figure 34. Flowchart section 1) output	48
Figure 35. Flowchart section 3) output	50
Figure 36. Flowchart section 4) output	52
Figure 37. Pivot bushing wear model	56
Figure 38. Flowchart section 5) output (1/3)	58
Figure 39. Flowchart section 5) output (2/3)	58
Figure 40. Flowchart section 5) output (3/3)	59
Figure 41. Plastic friction elements Simulink model	62
Figure 42. Flowchart section 6) output (1/5)	63
Figure 43. Flowchart section 6) output (2/5)	63
Figure 44. Flowchart section 6) output (3/5)	64
Figure 45. Flowchart section 6) output (4/5)	64
Figure 46. Flowchart section 6) output (5/5)	65

Figure 47. Maximum middle plane belt height definition (standard layout)	67
Figure 48. Minimum middle plane belt height definition (reversed layout)	68
Figure 49. Spring housing height definition for standard (left) and reverse (right) layout	68
Figure 50. Spring housing (highlighted in green) radial constraints	69
Figure 51. Section of a timing belt tensioner	70
Figure 52. Section of a cone spring	71
Figure 53. Cone spring characteristic as a function of h_0/t	73
Figure 54. Cone spring characteristics considered in the simulation	74
Figure 55. Damping trend over time as a function of the h_0/t parameter	74
Figure 56. Wear trend over time as a function of the h_0/t parameter	75
Figure 57. Damping variation during durability test simulation as a function of cone spring aspect ratio	75
Figure 58. Damping trend over time as a function of the h_0/t parameter (cone spring relaxation: 5% in 100hrs)	77
Figure 59. Damping trend over time as a function of the h_0/t parameter (cone spring relaxation: 10% in 100hrs)	77
Figure 60. Damping variation during durability test simulation as a function of cone spring aspect ratio	78
Figure 61. Wear trend over time as a function of the h_0/t parameter ($\frac{1}{2} * K_w$ plastic)	79
Figure 62. Wear trend over time as a function of the h_0/t parameter ($2 * K_w$ plastic)	79
Figure 63. Damping trend over time as a function of the h_0/t parameter (cone spring relaxation: 0%, $\frac{1}{2} * K_w$ plastic)	80
Figure 64. Damping trend over time as a function of the h_0/t parameter (cone spring relaxation: 0%, $2 * K_w$ plastic)	80
Figure 65. Damping variation during durability test simulation as a function of cone spring aspect ratio ($\frac{1}{2} * K_w$ plastic)	81
Figure 66. Damping variation during durability test simulation as a function of cone spring aspect ratio ($2 * K_w$ plastic)	81
Figure 67. Cone spring-guide pin coupling scheme	84
Figure 68. Flowchart section 8) output (1/2)	85
Figure 69. Flowchart section 8) output (2/2)	85
Figure 70. Spring stress level comparison as a function of presetting	86
Figure 71. Flowchart section 9) output (1/2)	93
Figure 72. Flowchart section 9) output (2/2)	94
Figure 73. Flowchart section 10) output (1/2)	99
Figure 74. Flowchart section 10) output (2/2)	100
Figure 75. Exploded view of a simplified 3D model	101
Figure 76. Section view of a simplified 3D model	102
Figure 77. 1 st case study 3D model	104
Figure 78. 1 st case study 3D model (section view)	104
Figure 79. 1 st case study bushing wear vs. time	107
Figure 80. 1 st case study pulley parallelism vs. time	108
Figure 81. 1 st case study damping decay vs. time	108
Figure 82. 1 st case study cone spring characteristic	109
Figure 83. 1 st case study plastic friction elements wear vs. time	109
Figure 84. 1 st case study cone spring axial force vs. time	110
Figure 85. 1 st case study cone spring force tolerance	110
Figure 86. 1 st case study Smith-Goodman diagram	111
Figure 87. 1 st case study pivot base contact pressure vs. contact angle	111
Figure 88. 2 nd case study 3D model	114
Figure 89. 2 nd case study 3D model (section view)	114
Figure 90. 2 nd case study bushing wear vs. time	117

Figure 91. 2 nd case study pulley parallelism vs. time	118
Figure 92. 2 nd case study damping decay vs. time	118
Figure 93. 2 nd case study cone spring characteristic	119
Figure 94. 2 nd case study plastic friction elements wear vs. time	119
Figure 95. 2 nd case study cone spring axial force vs. time	120
Figure 96. 2 nd case study cone spring tolerance	120
Figure 97. 2 nd case study Smith-Goodman diagram	121
Figure 98. 2 nd case study pivot base contact pressure vs. contact angle	121
Figure 99. 3 rd case study 3D model	124
Figure 100. 3 rd case study 3D model (section view)	124
Figure 101. 3 rd case study bushing wear vs. time	127
Figure 102. 3 rd case study pulley parallelism	128
Figure 103. 3 rd case study Smith-Goodman diagram	128
Figure 104. 3 rd case study pivot base contact surface vs. contact angle	129

List of tables

Table 1. Input data for ball bearing size selection _____	48
Table 2. Input data for the pivot diameter definition _____	49
Table 3. Damper pad dimensions as a function of the axial damping _____	52
Table 4. Endcap spacer dimensions as a function of the axial damping _____	52
Table 5. Pivot bushing threshold values _____	54
Table 6. Tolerance value of cone spring gap height influencing elements _____	66
Table 7. Cone spring fundamental parameters optimal range _____	72
Table 8. Cone spring-pivot clearance _____	83
Table 9. 1 st case study design input _____	106
Table 10. 1 st case study simulation output summary _____	107
Table 11. 2 nd case design input _____	116
Table 12. 2 nd case study simulation output summary _____	117
Table 13. 3 rd case study design input _____	126
Table 14. 3 rd case study simulation output summary _____	127

Introduction

A timing belt or a timing chain is a component of an internal combustion engine that connects the crankshaft and the camshaft(s). It is needed in order to synchronize the lift of the intake and exhaust valves, but usually it drives also the water pump, the oil pump and, in case of diesel engines, the fuel pump.

An alternative to the timing belt or timing chain is the direct gear drive, which is a more reliable and durable solution, but it introduces more geometrical constraints between the crankshaft and the camshaft, as a very short distance between the two; this is the reason why this solution is adopted almost uniquely on trucks. On cars, instead, in most cases this solution is discarded because of the need of more freedom for the camshaft location, either respect to the crankshaft, either respect to the other camshaft (if it is present). Another important aspect to be underlined is that the rubber composite belts produce less noise, they are less expensive and, since they are lighter, they waste a lower amount of energy, bringing the system to a higher efficiency. While the noise is a key factor from a selling point of view, since it is a customer higher quality perception, the higher efficiency is a crucial factor for the fuel consumption and the pollution, aspects that are becoming predominant either from the selling point of view, but especially because of more and more stringent environmental regulations. This is the main reason for the introduction of the Belt In Oil system, which permits to waste a lower amount of energy due to friction. Besides this, the timing belt presents an economical advantage with respect to the chain configuration, since, in this last case, the sprockets are expensive due to the refined thermal treatments needed. In most of modern engines, part of the stroke of one of more valves is overlapped with respect to the piston one. This is done in order to achieve higher compression ratios. These engines are referred to as interference engines. This aspect underlines that this timing device requires a very careful design process, since its failure would bring to a contact between a valve and a piston. This would cause the valve failure and heavy damages to the engine itself.

The most common failure modes are the unpacking of the fibre cores, or the tearing of teeth. In this last failure mode, the belt tensioner plays a key role. It has to maintain a sufficient belt tension to avoid its slippage, that would bring to the teeth failure and at the same time it has to maintain the tension under the maximum tensile strength of the timing belt itself.

Besides this, the timing belt system life can be significantly reduced by the working environment. In fact, if it is lubricated by the engine oil, its working temperature can reach, even if only for small periods of time, 140°C. This brings to a critical issue, since the rubber degrades with high temperatures. Then, in case of dry solutions, the contact with water or antifreeze is detrimental. This aspect has to be carefully evaluated in vehicles in which this situation currently occurs, such as off-road vehicles.

An additional worsening of the working condition of the system is the presence of impurities in the engine oil, such as combustion residuals; in fact, these particles can be pressed on the

belt, which acts as an abrasive tool on the tensioner pulley. In order to improve the mechanical properties of the timing belt, high-tensile fibres are usually implemented.

Besides these mechanical considerations, also vibrational issues have to be accounted for, since the comfort in modern vehicles is becoming a key selling factor.

Indeed, the engine is one of the principal sources of internal excitation (together with the wheels and the driveline). Aside from the vibrations arising from the thermodynamic cycle and those due to the unbalancing of the rotating parts, a principal role in this sense is covered by the torsional born ones. Historically these were considered as marginal contributions, almost negligible. The only concern for the dimensioning of the system was the avoiding of the collapse of the mechanical components of the engine, with particular attention for the crankshaft. Nowadays, instead, these contributes are more important also due to the growth of the number of the driver assisting components; some examples are constituted by the power steering pumps (either hydraulic, since the oil pump has to continuously be driven by the engine through the auxiliary belt, either electrical, which imposes the need for a more powerful alternator, so bigger and with a bigger inertia) and by other electrical energy consuming devices (they introduce as well the need for a bigger alternator). So, the torsional vibration of the engine is transferred to the accessories, which are in turn transferred also to the vehicle body. This aspect is particularly enhanced in diesel engines, due to the stronger variation of pressure in the combustion chamber. In order to smooth this phenomenon, through the reduction of vibration of the crankshaft and the insulation of the accessories, torsional vibration dampers have been introduced.

Vehicle longitudinal dynamics

The timing belt has an important role for what concerns comfort, principally due to the contact between the teeth and the pulley. Besides this, there is the contribution of the pumping effect of the air that remains between the belt and the pulley. It is worth to be noticed that at high temperatures, due to the higher viscosity of the belt (becomes stickier), a noise can arise. This is due to the stick-slip phenomena of the belt against the pulley. In addition, the noise can be produced from the transversal vibration of the belt between a pulley and the following one. The triggering phenomenon of the just mentioned vibrations can be either the engine orders, either some geometrical defects of the structure of the pulley.

Another kind of discomfort source is introduced by the powertrain. In fact, these operations introduce a torsional vibration of the transmission, that in turn is converted in longitudinal vibrations of the whole vehicle.

Torsional dynamics of the drivetrain can introduce longitudinal accelerations, which have an impact on comfort. A typical manoeuvre to evaluate a vehicle from this point of view is to actuate the throttle with a step function (tip-in tip-out). This brings the flywheel to linearly increase its rotational speed (clutch springs are packed) and then to linearly decrease its rotational speed as well. This is not true for the seats, in fact they experience oscillating longitudinal accelerations. Since these oscillations are source of discomfort for passengers, they have to be avoided. From this point of view, the performance of a vehicle is evaluated considering the smoothness of the engine during its rpm increase: the drivability. In order to handle this problem, the powertrain layout plays a key role, due to the different transmission shaft configuration.

In order to study the driveline impact on the longitudinal vehicle dynamics a 6-dofs model can be used:

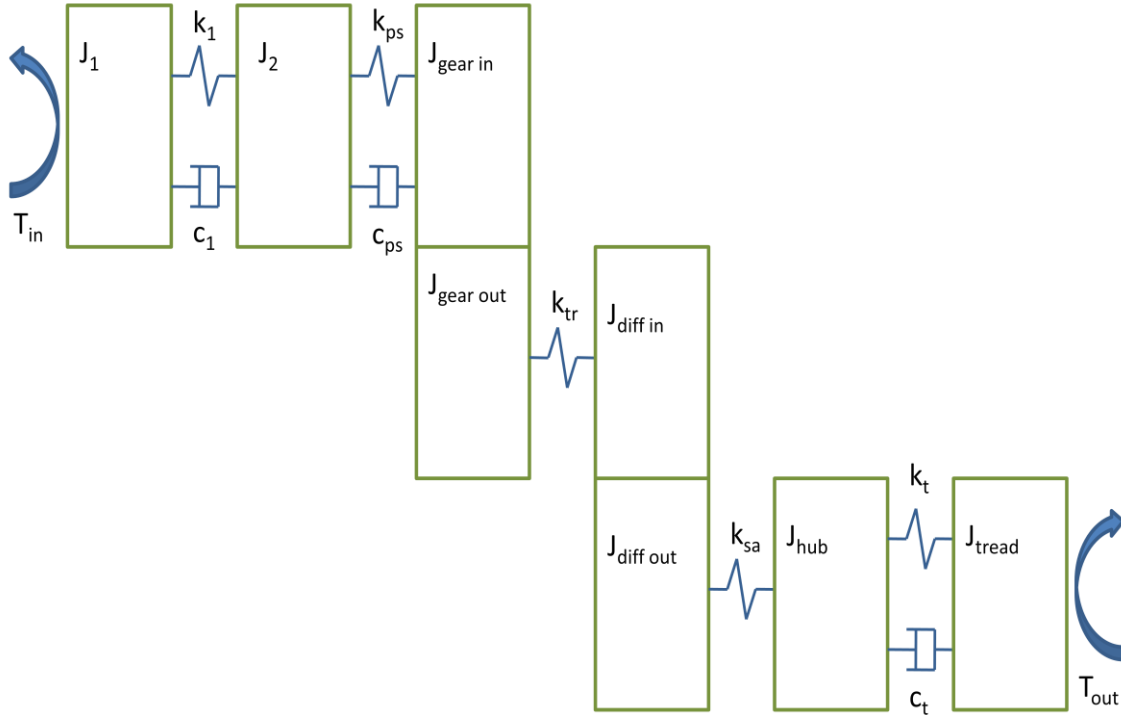


Figure 1. Powertrain dynamic model

where:

- J_1 is the inertia contribution of the engine, of the belt-drive system and of the primary mass of the dual mass flywheel
- k_1 and c_1 are representing the dual mass flywheel
- J_2 is the inertia contribution of the secondary mass of the dual mass flywheel and of the clutch cover
- k_{ps} and c_{ps} are representing the clutch
- J_{gear} is the inertia contribution of the gearbox
- k_{tr} represents the transmission shaft torsional stiffness
- J_{diff} is the inertia contribution of the differential
- k_{sa} represents the semi-axis torsional stiffness
- J_h is the inertia contribution of the wheel hub
- k_t and c_t represents the tyre model
- J_{tread} is the inertia contribution of the wheel tread band

The moment of inertia of the crankshaft is a function of the position of the crankshaft itself, since it is not axis-symmetric. Each piston can be modelled as an equivalent flywheel, in such a way to obtain a linear dynamic equation with constant coefficients:

$$J_{pi}\ddot{\theta} + c_{\theta}\dot{\theta} + k_{\theta}\theta = M_i(\theta) \quad (1)$$

where:

ϑ is the angular position of the crankshaft [deg]

J_{pi} is the equivalent moment of inertia of the i^{th} piston [kg*m²]

c_{ϑ} is the crankshaft damping [Nm*s]

k_{ϑ} is the crankshaft equivalent stiffness [Nm/deg]

M_i is the torque deriving from the i^{th} piston [Nm]

Since the crankshaft is a deformable body, the distance between two adjacent equivalent flywheels has to be chosen in such a way to obtain a rotational stiffness equal to the crankshaft real one:

$$k_{\theta} = \frac{G \cdot I_p}{l_{eq}} \quad (2)$$

where:

G is the crankshaft shear modulus [MPa]

I_p is the polar moment of inertia of the crankshaft [m⁴]

l_{eq} is the equivalent length of the bar between two adjacent pistons [m]

The polar moment of inertia is evaluated by considering the main diameter of the crankshaft. J_i is a function of the crankshaft angular position, but, by performing a MacLaurin expansion at the first term (which is constant), J_{pi} can be approximated with a constant value, obtaining an equivalent flywheel with constant moment of inertia for each piston.

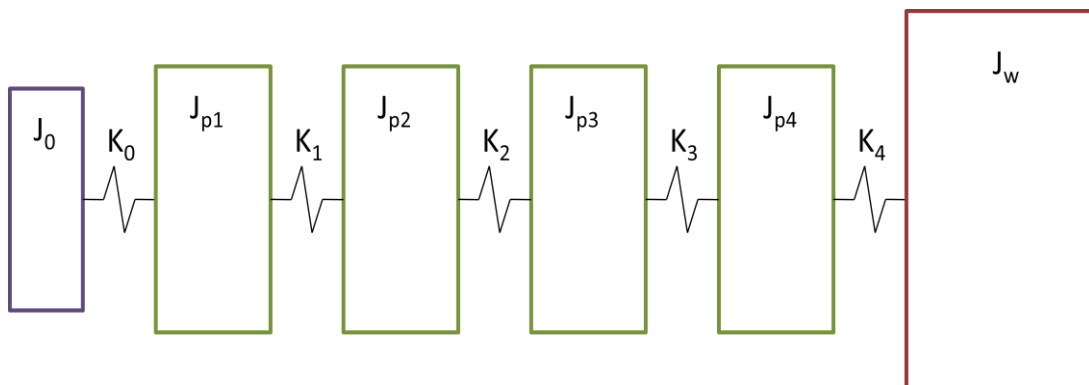


Figure 2. 4-cylinder engine model

In the figure 2, a 4-cylinder engine model is represented. Besides the above described piston equivalent flywheels (J_{p1} , J_{p2} , J_{p3} , J_{p4}), two additional flywheels can be seen. The first one represents the crank-nose pulley, that drives the timing belt and the multi-rib belt and has an inertia value equal to J_0 . The second one represents the flywheel actually present on the engine. It is characterized by an inertia value equal to J_w , which is quite high since it is

needed to smooth the crankshaft rotation irregularities. It is worth to be noticed that, while K_1 , K_2 and K_3 have a similar value, K_0 has a different value, which is different also from K_4 . If the vehicle longitudinal dynamics is investigated, a simpler engine model is sufficient. In fact, the frequency of motion concerning the crank-nose and the equivalent flywheels is higher than 200Hz, while the drivetrain one is less than 50Hz. Due to this aspect, usually the engine is modelled as a 1-dof model with just one flywheel.

Moving the attention to the crank-nose pulley, since it drives both the timing belt and the multi-rib belt, it is interested by a fluctuating resisting torque. In the first case the fluctuating resisting torque is due to the contact between the cams and the valve springs. The fluctuations are enhanced by the cam shape. During its rotation, the spring axial force, that can be considered linear, has to be won. Despite its linearity the arm through which the force is applied is changing, so a great force variation is experienced. In Diesel engines also the fuel pump has to be synchronized with the crankshaft, so it must be driven by the toothed belt as well. For what concerns the auxiliary belt, instead, a multi rib belt is usually implemented. This last belt-drive system is composed by many components, but, in order to study its dynamics, only the most important are considered: the crankshaft pulley, the alternator pulley and the automatic tensioner.

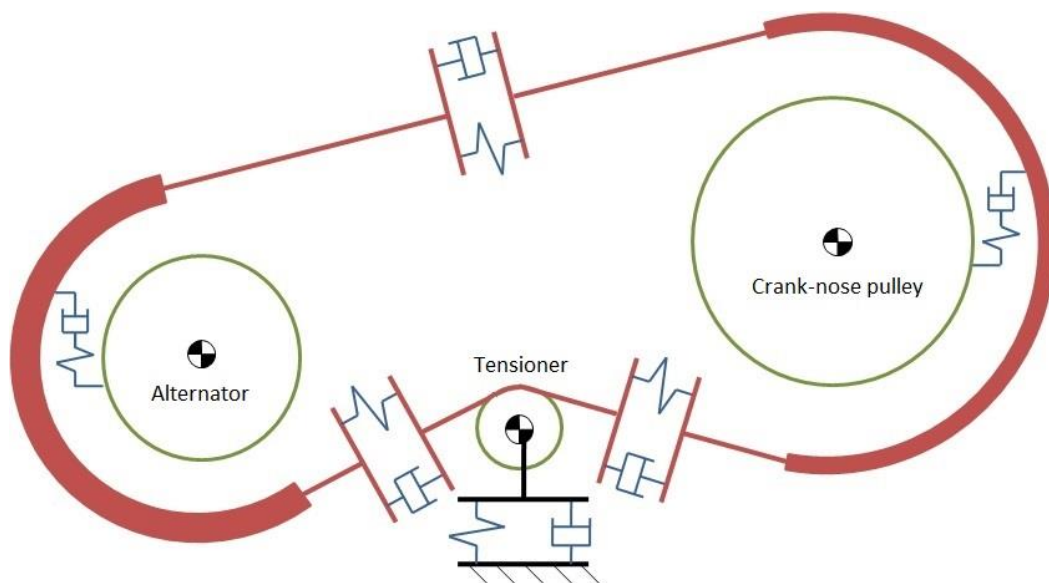


Figure 3. Belt-drive dynamic model

The model represented in figure 3 is characterized by 5 degrees of freedom:

- shear deformation of belt at the crank-nose pulley
- shear deformation of belt at the alternator pulley
- rotation of alternator pulley
- rotation of automatic tensioner pulley
- vertical movement of automatic tensioner pulley

As it can be seen from the figure, the shear deformation of the belt due to the relative movement with respect to the pulleys has been schematized through a series-connection of a spring with a viscous damper. This mathematical description of the shear deformation is not needed in correspondence of the automatic tensioner pulley, since it is an idle one. The belt deformability, instead, is reproduced through a parallel connection of a spring with a damper. The input of the system is the rotation of the crank-nose pulley.

The model represented in figure 3 is about the accessories system, but very similar considerations can be done for the timing belt system. In fact, despite the presence of the teeth, the great amount of torque is transmitted by shear as well. Only a small portion of torque is transmitted through the teeth, which are in charge to guarantee the synchronization between the crankshaft and the elements driven by the belt itself. If the timing belt tension is not sufficient, the torque transmitted by shear deformation falls under a given threshold. This event forces the teeth to transmit higher loads with respect to the ones for which have been designed for, bringing to teeth failure. This is a critical situation since synchronization is lost and the engine can be damaged.

In most cases by moving to the opposite side of the engine, the flywheel can be found. It is needed in order to smooth the engine rotational speed oscillations, which are intrinsically present due to the thermodynamic cycle. The torque is irregular throughout the cycle (720° of crankshaft revolution considering a 4-strokes engine) and an irregularity parameter permits to evaluate it:

$$\delta = \frac{\omega_{max} - \omega_{min}}{\omega_{mean}} = \frac{\Delta L}{(J_{shaft} + J_{flywheel}) * \omega_{mean}^2} \quad (3)$$

where:

δ is the kinematic irregularity index [-]

ω_{max} is the maximum crankshaft rotational speed achieved in one cycle [rad/s]

ω_{min} is the minimum crankshaft rotational speed achieved in one cycle [rad/s]

ω_{mean} is the mean crankshaft rotational speed achieved in one cycle [rad/s]

ΔL is the energy variation in one cycle [J]

J_{shaft} is the crankshaft inertia [Kg*m²]

$J_{flywheel}$ is the flywheel inertia [Kg*m²]

As it can be seen from equation nr. 3, by increasing $J_{flywheel}$, the irregularity δ can be reduced. But, by increasing $J_{flywheel}$, the flywheel contribution to the vehicle equivalent mass is increased as well, so the acceleration performance is worsened. Due to this aspect, a trade-off between the irregularity and the acceleration performance has to be found. In order to simplify this task, the dual mass flywheel has been introduced:

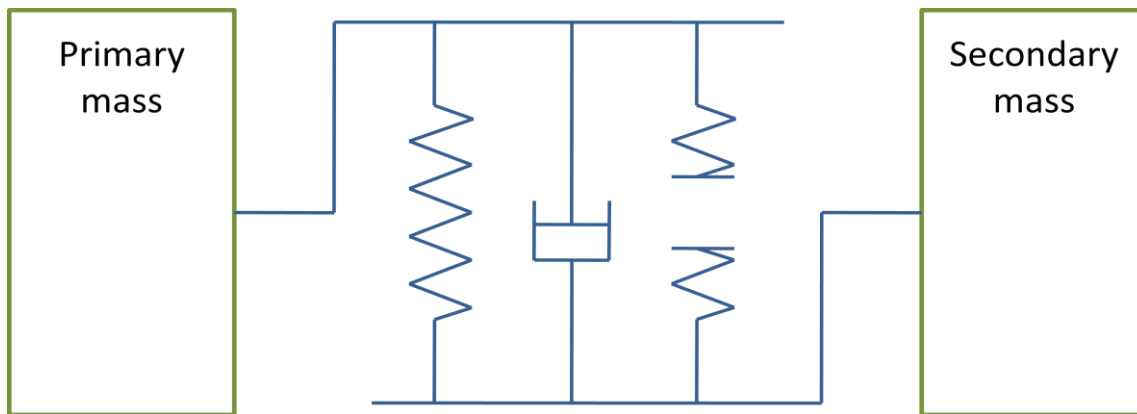


Figure 4. Dual mass flywheel model

As it can be seen from figure 4, dual mass flywheel is composed by two parts:

- the primary mass
- the secondary mass

The primary mass is constrained to the crankshaft, in fact it hosts also the teeth needed during the cranking operation. The secondary part, instead, is linked to the clutch (and so to the powertrain).

As depicted in the scheme above, between the two masses there are two sets of springs and a damper. The first set of springs and the damper are always working, while the second set of springs starts to work only over a certain angular displacement. In this condition the two sets of springs are working in parallel, so assuring a higher stiffness. This system is aimed to filter most of vibrations coming from the crankshaft. Thanks to this system the same irregularity level can be achieved with a lower J_{flywheel} (with respect to the single mass flywheel), so better acceleration performances are obtained.

The clutch is transferring the torque between the crankshaft and the primary shaft of the gearbox. This is performed through friction, which is guaranteed by a spring that presses the two plates of the clutch. In order to disengage it, the spring is pressed thanks to a thrust bearing. Some additional helical springs are present in this device. They are positioned between the high-friction outer part and its inner part. They are needed to smooth the vibrations brought by the engagement and disengagement of the clutch itself.

The following component of the driveline is the gearbox. This element is composed by two shafts, the primary one and the secondary one. Gears of the two shafts are always engaged, but they are free to rotate on them, in such a way to not transmit torque. In fact, only a pair of gears at a time is angularly constrained to the shafts in order to transmit torque. This is done through selectors, engaged by synchronizers.

Then, the differential can be found. It is composed by a cage and bevel gears. Its main task is to permit to the vehicle wheels of the same axle to rotate at different speeds. This degree of freedom is exploited every time the vehicle trajectory deviates from the straight one.

The torque coming from the differential is transferred through semi-axis to the wheel rim. In order to obtain the vehicle motion, the torque has still to be transferred through an element:

the wheel tread. The torque transfer between these two last elements must comply with the tread deformation.

Knowing the characteristic of the tyre, depicted in the figure 5:

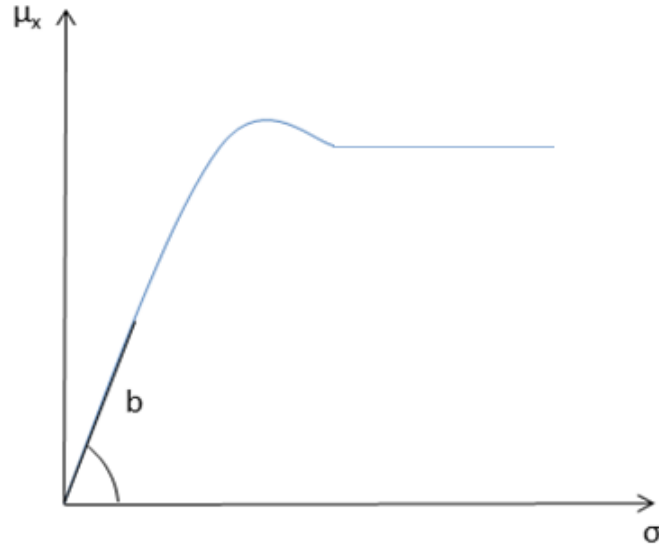


Figure 5. Longitudinal tire characteristic

Since

$$\mu_x = \frac{F_x}{F_z} \quad (4)$$

in the linear range it can be written:

$$F_x = F_z * \mu_x = b * F_z * \sigma \quad (5)$$

where

$$\sigma = \frac{\Omega - \Omega_0}{\Omega_0} \quad (6)$$

where:

μ_x is the longitudinal force coefficient [-]

F_x is the longitudinal tyre force [N]

F_z is the vertical tyre force [N]

b is the longitudinal tyre characteristic slope in the linear range [-]

σ is the tyre longitudinal slip [-]

Ω_0 is the rim rotational speed [rad/s]

Ω is the tread rotational speed [rad/s]

Since the tyre longitudinal slip is the difference in rotational speed between the wheel rim and the wheel tread, in case of steady-state conditions it can be schematized with a damper, like it is depicted in the picture 6.

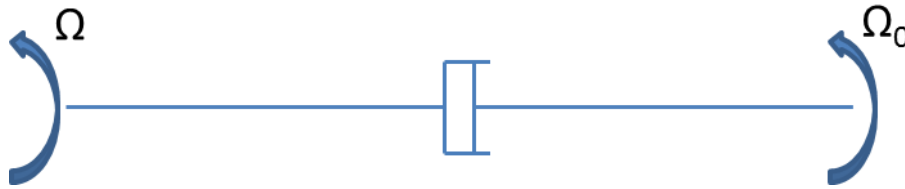


Figure 6. Tire dynamic model

In transient conditions, instead, the tire frequency response has to be considered. It presents a pole at a given frequency, which is changing as a function of the tire type and which cannot be changed, but it must be accepted as it is.

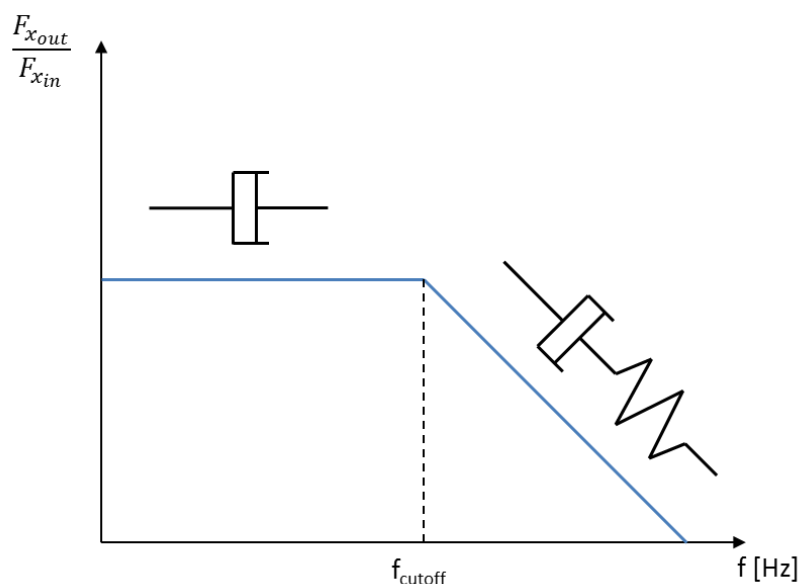


Figure 7. Tire frequency response

In figure 7 the tire frequency response has been depicted. As it can be seen, it acts as a low pass filter. In fact, below the pole frequency (f_{cutoff}) it behaves as a damper and the output corresponds to the input force, while above that frequency the tire behaves as a damper and a spring in series, so the tire response is delayed.

The 6 degrees of freedom longitudinal dynamics model is a tool that helps to understand how a varying engine torque can bring to longitudinal varying acceleration, decreasing in this way the passenger comfort. This aspect highlights the importance of a correct functioning of the belt-drive system, achieved with a correct belt tension. This is in turn achieved with a correct dimensioning of the timing belt tensioner.

Timing belt tensioner typologies

There are 4 main types of timing belt drive tensioners:

- I. Single eccentric “autosetting”
 - II. Double eccentric
 - III. Double eccentric with “crank/rod” loading system
 - IV. Sliding single eccentric
-
- I. Single eccentric “autosetting”

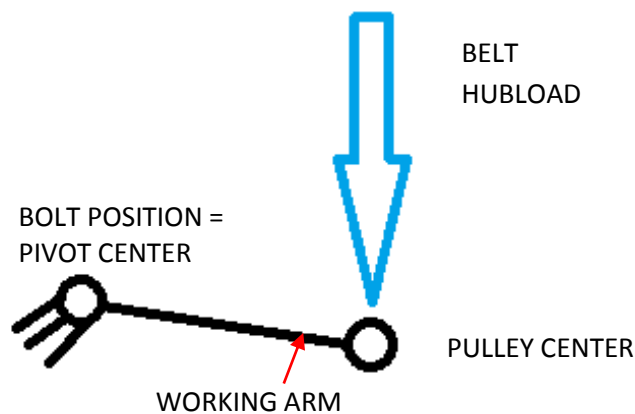


Figure 8. Autosetting tensioner model

In this configuration the fixation bolt and the pivot are coaxial. The working arm is obtained by exploiting the eccentricity of the bearing seat axis of rotation with respect to the arm bushing hole. Thanks to these characteristics this is the simplest and the cheapest tensioner typology. This is due also to the simpler components, as the absence of the anti-rotation milling on top of the pivot. It is called autosetting, since in the assembly plant it does not require any loading operation. From this description can be deduced that this type of tensioner is checked as a first attempt, since it is the most convenient to be used from an economical point of view. However, it must be noticed that does not allow neither the control of the installation torque (so the control of the belt load), neither the control of the differential angle. In addition, it presents a high sensitivity as a function of the layout tolerance. For this reason, particular attention must be paid to its angular position with respect to the engine front end. Usually this is done through a hole on the support plate that, during the assembly phase is constrained to be concentric to a reference point present on the engine front end. Once the bolt (concentric with the pivot axis) has been fastened at the prescribed torque, if the friction between the pivot and support plate bases and the engine surface is sufficient, the angular position constrain tool is removed. The coupling between the pivot and the support plate can be performed in 3 different ways:

- calking

- press-fit
- axially constrained, but free to rotate

it is worth to be noticed that in this last case the reaction to the spring torque passes completely through the support plate orientation feature. Due to the characteristics of this type of tensioner, a circular profile is sufficient to join the pivot superior extremity and the steel end cap. In fact, only the press-out force is linked to the tensioner functionality and not the torque-out.

II. Double eccentric

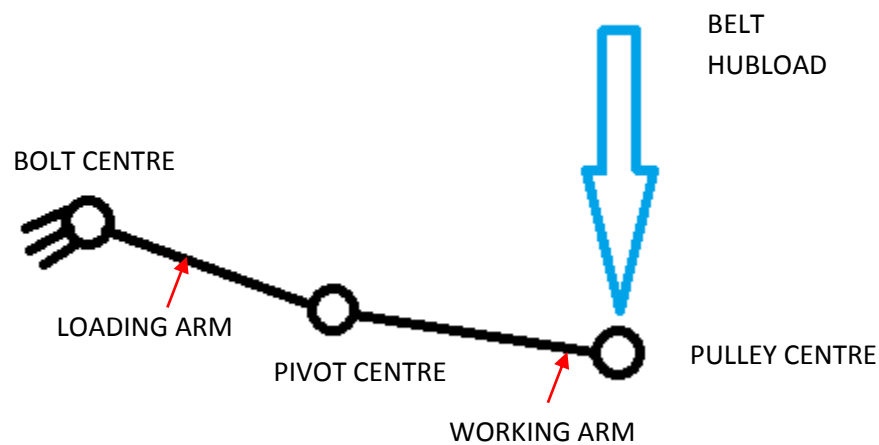


Figure 9. Double eccentric tensioner model

In a double eccentric tensioner, instead, the bolt centre is no more coincident with the pivot one. The eccentricity of the pivot tube introduced the so-called loading arm, while the working arm is obtained exactly in the same way of the previous tensioner typology: by exploiting the eccentricity between the bearing seat axis and the bushing hole one. Such a configuration permits to keep under control belt installation tension, being able to manage layout and recover the belt length variability due to the tolerances. These features bring to a substantial difference of the assembly operation seen above. In fact, the support plate does not need any more to be angularly referenced respect to the engine front end, while the pivot is rigidly connected to the support plate itself (this means that only caulking or press-fit joints can be used). In this case the steel end cap is angularly constrained with respect to the pivot or with the eccentric loading pivot, which has to be fitted with radial clearance into a centric pivot tube. Here the need of a visual indicator arises. It can be obtained with a hole or a recessed notch on the endcap that has to be aligned with another hole or notch on the plastic endcap spacer or on the arm. Another solution is to combine two marks on the other tensioner side, so one on the arm and one on the support plate.

III. Double eccentric with “crank/rod” loading system

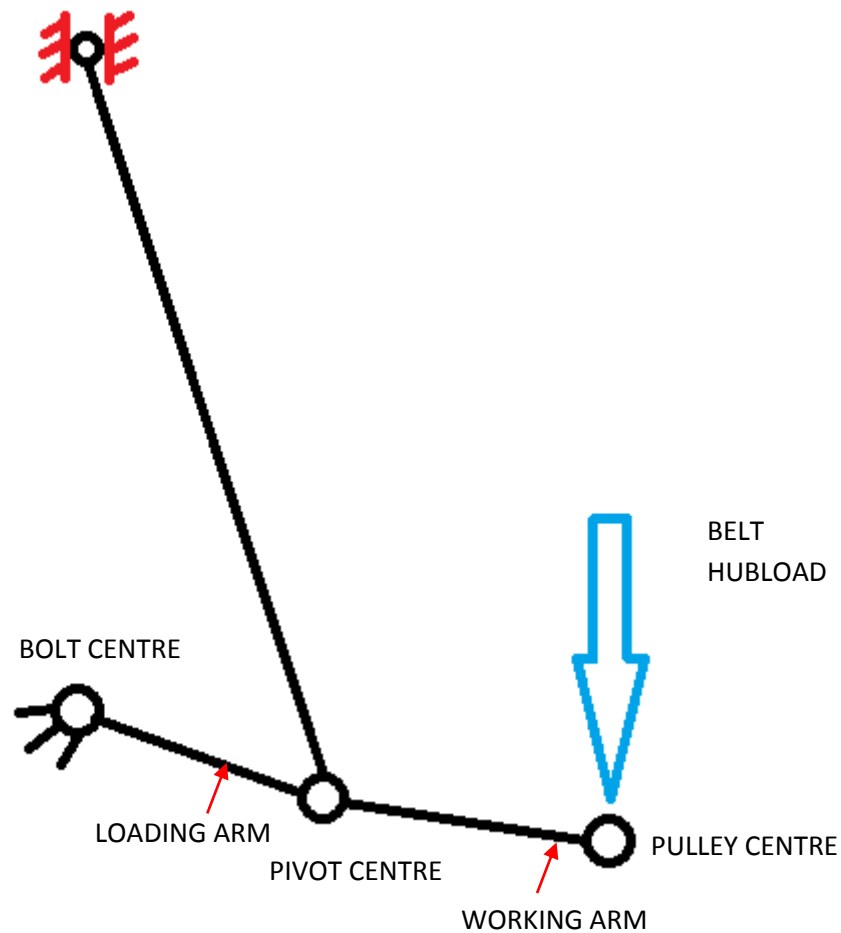


Figure 10. Double eccentric with crank/rod loading system tensioner model

This layout is comprehensive of two arms as above (the loading one and the working one), but it is also comprehensive of a rod. Usually this rod is not physically present in the system, since its function is performed by the support plate, which needs to have a special shape. This is geometrically connected through a rotational joint to the pivot tube center and through a hook sliding in a slot to the engine front end. In order to introduce the loading arm, there are again two possibilities, the eccentric pivot tube, or the loading pivot tube. Also the working arm is obtained in the same way of the cases seen above. The main advantage of this layout is the good control either of the installation tension, either of the differential angle. This is possible since, while the belt is not in contact with pulley, tensioner working arm approaches the belt with quasi-translational movement. This configuration needs a support plate with a hook, which, by engaging in a slot in the engine front end, can slide in that slot and limit the steel plate rotation. This is the reason of the better control of the installation torque and of the differential angle during the installation and loading operations. Loading features are needed also in this case. They are obtained as explained in the previous case.

IV. Linear guide

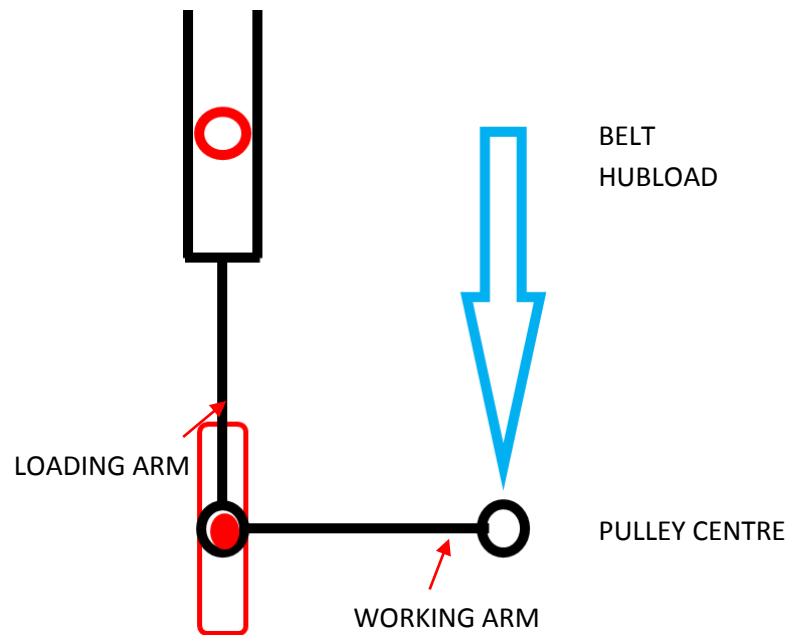


Figure 11. Linear guide loading system tensioner model

In this case the tensioner is fixed through a pin that can slide into a slot, but it cannot rotate (permitting in this way the tightening). A visual indicator is needed in order to be able to detect the nominal position. Besides this, a hook geometry in the support plate is needed too, in order to permit the sliding motion.

Tensioner mathematical model

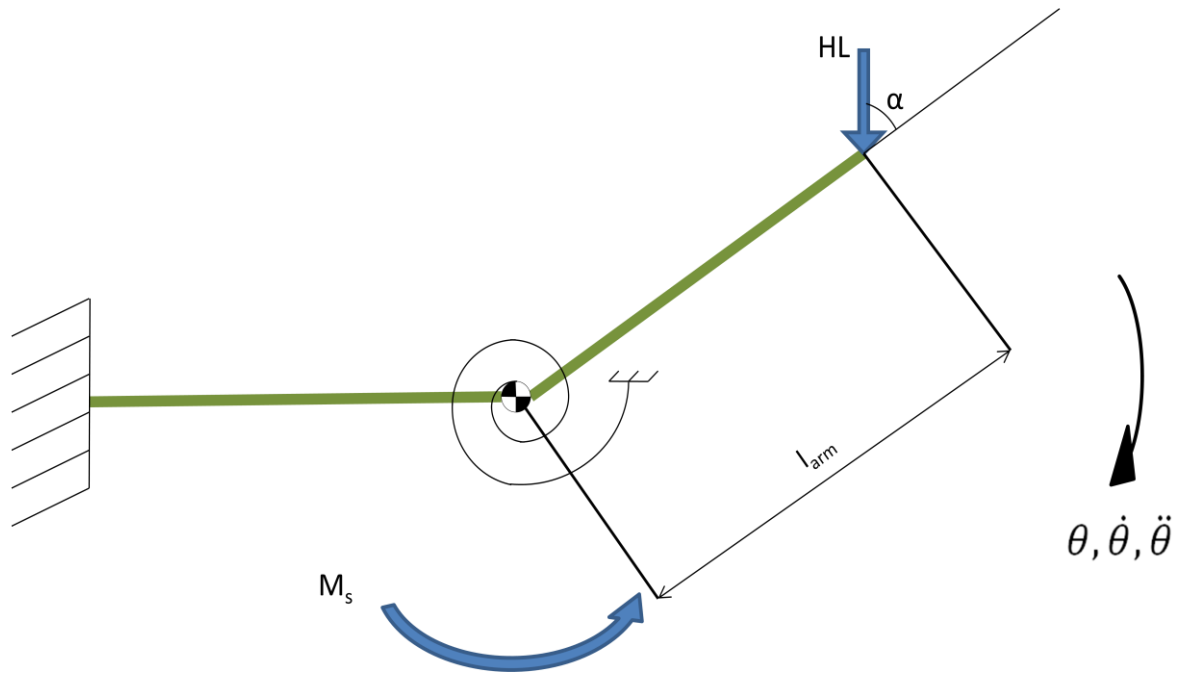


Figure 12. Tensioner model (no friction)

In order to study the system a mathematical model has been developed. It consists on a lever constrained in an extremity with a hinge, so permitting its rotation, while, in the other extremity, a force is applied. This force represents the load applied by the belt while the tensioner is operating, or the load applied by the testing machine while the tensioner is being measured. Actually, the force is applied on the pulley, but under the assumption of ideal components, it is transferred to the centre of the pivot. This load is counteracted by a torsional spring installed in the constrained side. The angle between the force and the tensioner arm (angle α in the figure 12) is defined as differential angle. Even if a single arm is represented in the model, it describes successfully also a double-eccentric tensioner. In fact, once the degree of freedom introduced by the presence of the loading arm has been exploited, the pivot bolt is tightened, and the pivot is locked. From this time on, the tensioner behaves as a single-eccentric type.

The equation of equilibrium of this simple system is:

$$HL = \frac{M_s}{\cos(\alpha) * l_{arm}} \quad (7)$$

where:

HL is the load applied by the belt/testing machine on the pivot [N]

M_s is the spring torque with tensioner at differential angle [Nm]

α is the differential angle [deg]

l_{arm} is the eccentricity of the tensioner [m]

It is worth to notice that the spring torque can be computed as:

$$M_s = T_{nom} + k_t * (\theta(t) - \theta_{nom}) \quad (8)$$

where

T_{nom} is the spring torque in nominal position [Nm]

k_t is the torsional stiffness of the spring [Nm/deg]

$\vartheta(t)$ is the angular position of the tensioner [deg]

ϑ_{nom} is the angular nominal position [deg]

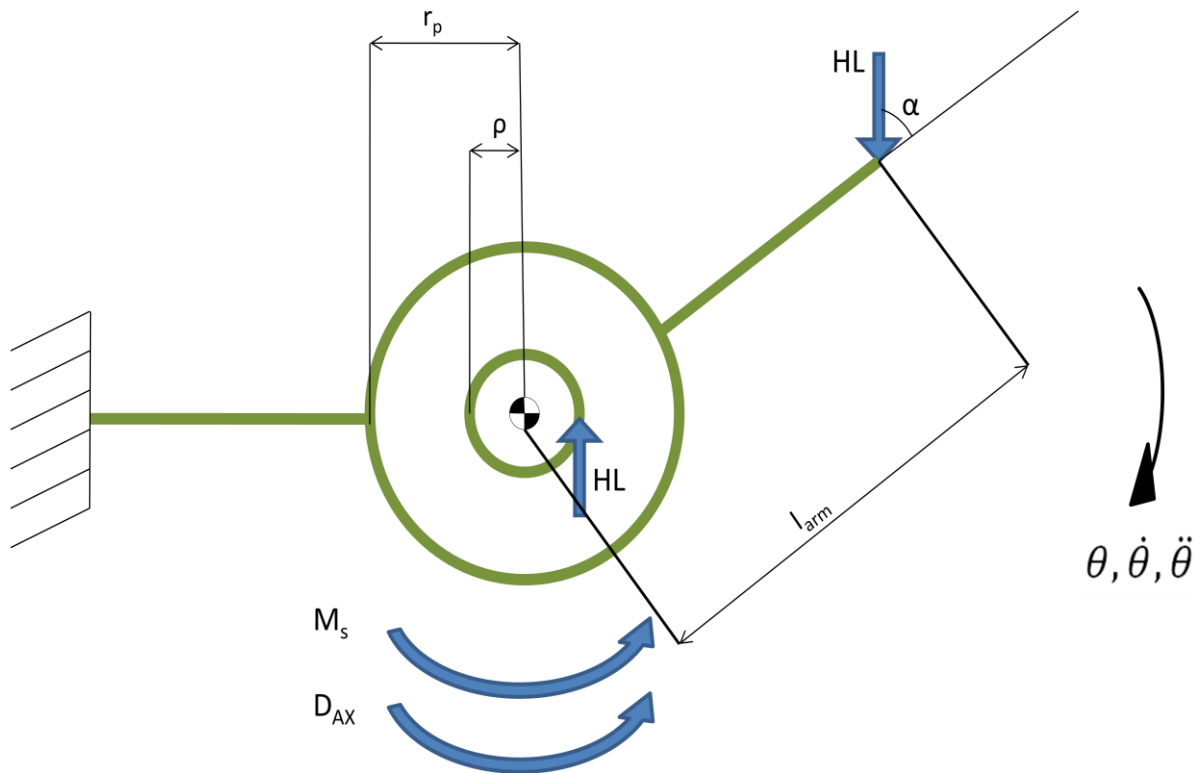


Figure 13. Tensioner model (loading condition)

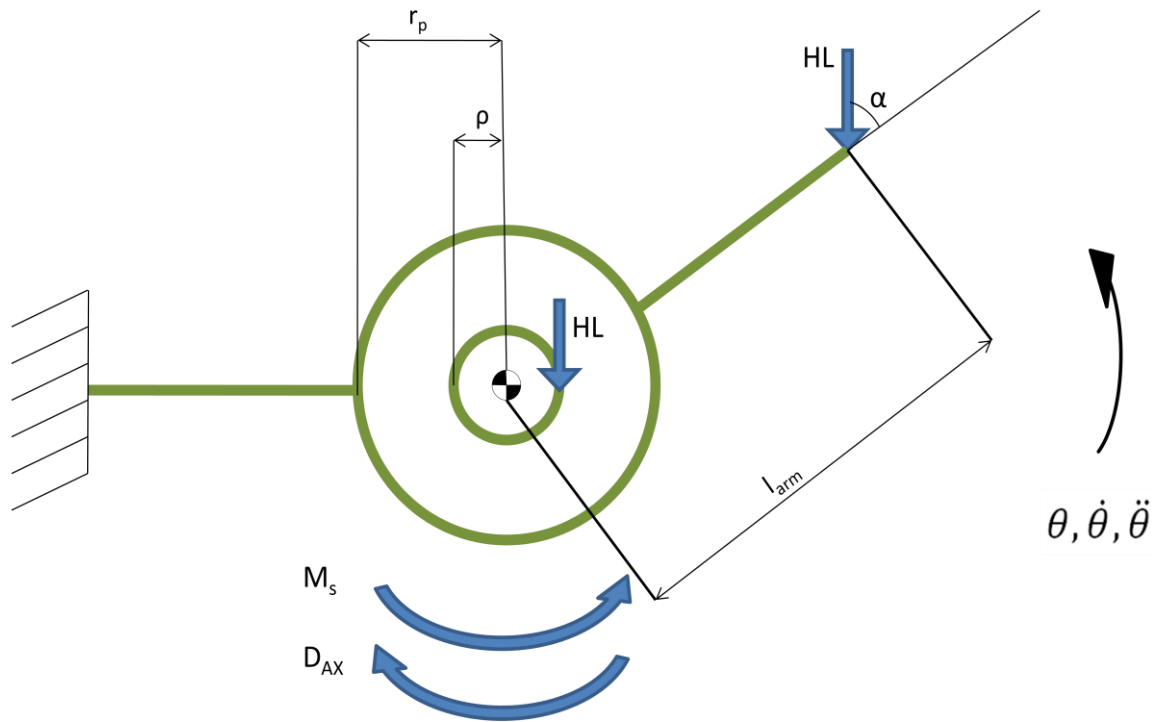


Figure 14. Tensioner model (unloading condition)

Besides this, the damping phenomenon has to be considered. In fact, it is obtained by friction, so by wasting energy in such a way to reduce the vibrations of the system. The damping is obtained by the combination of two main contributions:

- the axial damping
- the radial damping

It is worth to notice that the damping phenomena change sign from loading conditions to unloading one (as it can be seen from pictures 13 and 14), since they are always opposing the motion.

The axial damping is introduced by a cone spring. It exerts an axial load, in such a way to compress the tensioner axial stack-up. This is done in order to assure a pressure between the arm (oscillating part of the tensioner) and two plastic elements, the damper pad and the endcap spacer. By so doing, a friction torque is introduced (assumed constant along the tensioner travel) that can be computed as follows:

$$D_{AX} = F_{AX} * \phi_{plastic} * (R_{mdp} + R_{mes}) \quad (9)$$

where:

D_{AX} is the damping axial component

F_{AX} is the axial force exerted by the cone spring

R_{mdp} is the medium radius of the contact surface between the arm and the damper pad

R_{mes} is the medium radius of the contact surface between the arm and the endcap spacer

$\phi_{plastic}$ is the plastic friction coefficient

The radial damping, instead, is introduced by the friction of the pivot. In fact, it generates a torque opposing the tensioner movement. This torque cannot be considered constant along the whole tensioner travel, since it is a function of the hubload, as it can be seen from the equation 10:

$$D_{RAD} = HL * r_p * \sin \varphi_{pb} \quad (10)$$

where

D_{RAD} is the radial damping [Nm]

HL is the hubload [N]

r_p is the pivot radius [m]

φ_{pb} is the pivot bushing friction coefficient [-]

At this point, through equation nr. 11, is possible to compute the total damping of the tensioner, that, as explained above, is the sum of the two just mentioned contributions:

$$D_{tot} = D_{AX} + D_{RAD} \quad (11)$$

Since the friction phenomena are related with the direction of motion of the tensioner, while the spring and the friction torque are related to its position, it is possible to write two equations of equilibrium (equations 12 and 13). In fact, one is describing the hubload in loading condition, while the other is describing the hubload in unloading condition and they are:

$$HL_{max} = \frac{M_s + D_{AX}}{l_{arm} * \sin \alpha(t) - \sin(\tan^{-1} \varphi_{pb})} \quad (12)$$

$$HL_{min} = \frac{M_s - D_{AX}}{l_{arm} * \sin \alpha(t) + \sin(\tan^{-1} \varphi_{pb})} \quad (13)$$

This aspect permits to explain why, during the characterization of a tensioner, a hysteresis cycle is obtained. In fact, a spring would not present a hysteretic behaviour, which is introduced by the presence of friction forces: the damping.

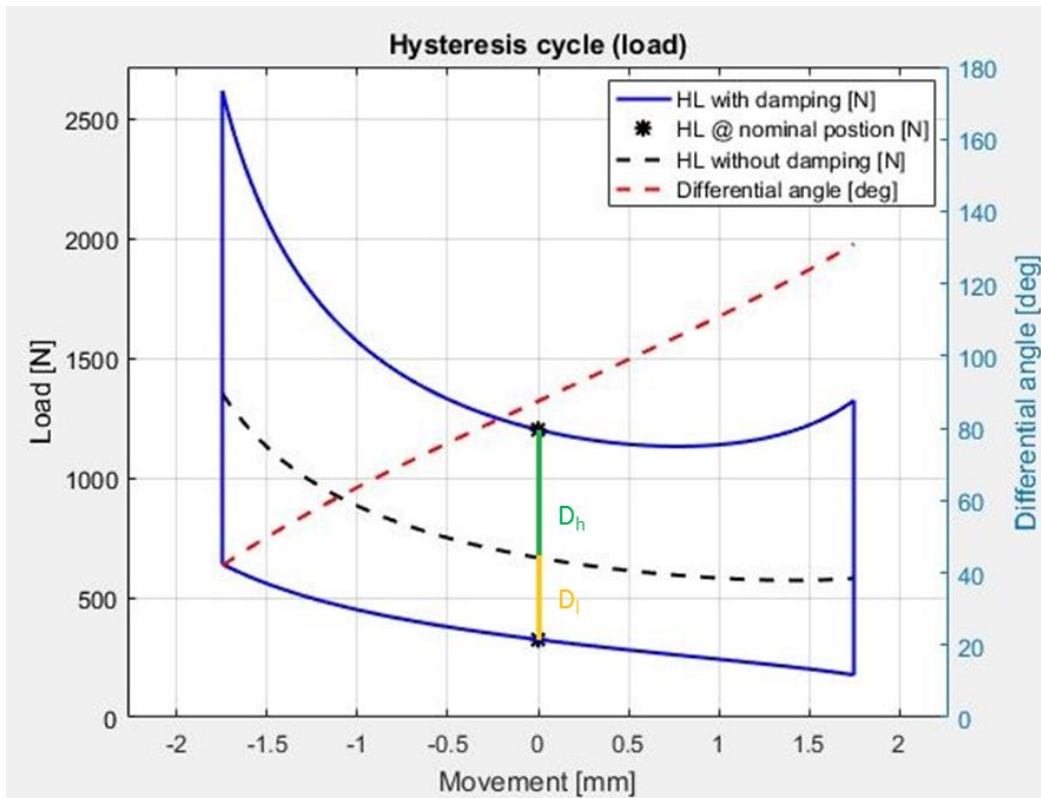


Figure 15. Hysteresis cycle (load)

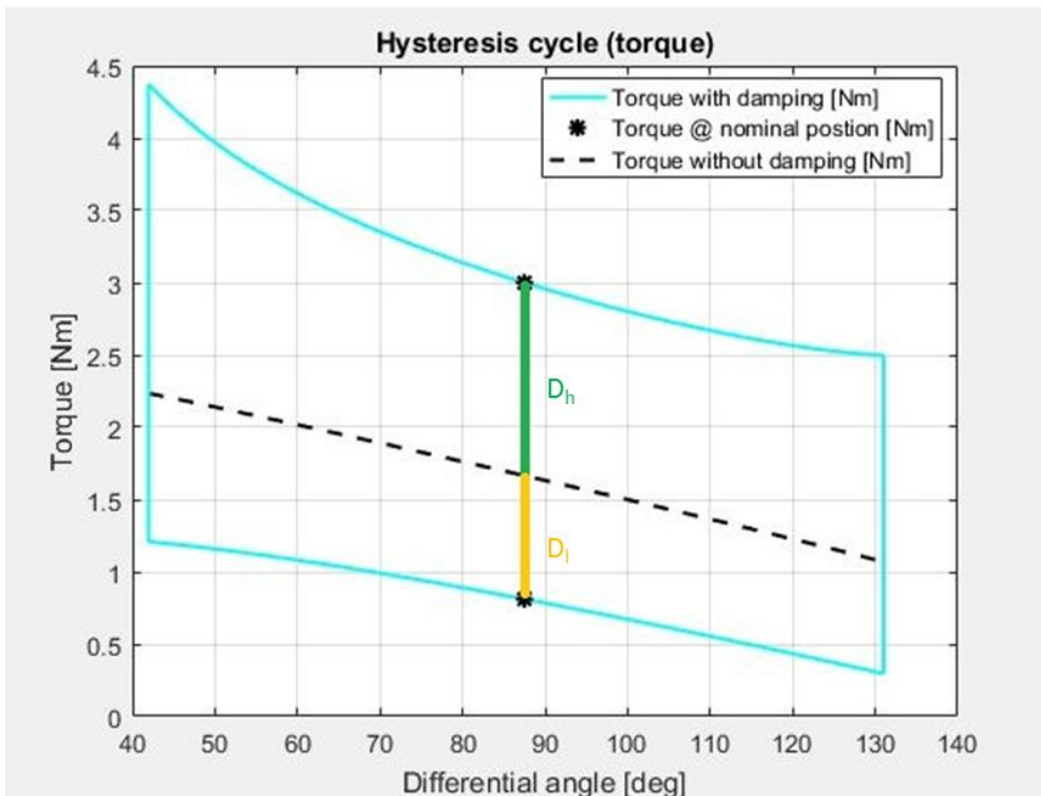


Figure 16. Hysteresis cycle (torque)

The graphs here represented are the reproduction of a tensioner static characterization. This procedure is aimed to study the tensioner response on its whole working range, which is delimited by two extremes positions, the free arm position and the installation position. The first corresponds to the tensioner without any force applied to it. In this condition the arm of the tensioner is in contact with the free arm endstop (the so-called cold stop). In the characterization graphs this condition corresponds to the right extreme. The opposite working range limit is the installation condition. The spring torque is at maximum and the tensioner arm comes in contact with the installation endstop (the so-called hot stop). In the graphs above, this condition is the left extreme. The main outputs of the characterization are:

- calculated torque: it is the calculated spring torque. In fact, under the assumption of symmetrical damping, the spring torque can be calculated as the average between the maximum and the minimum torque for each differential angle
- damping: it is calculated as the difference between the maximum torque and the calculated torque, or the difference between the calculated torque and the minimum torque, so the assumption of the symmetrical damping is still considered

During the simulation, thanks to the mathematical model, the spring torque can be computed. In this way the model of the symmetrical damping can be abandoned, so an additional output can be achieved: the damping asymmetry ratio (equation 14).

$$ASY_{ratio} = \frac{D_h}{D_l} \quad (14)$$

where

$$D_h = D_{AX} + HL_{max} * r_p * \sin \varphi_{pb} \quad (15)$$

$$D_l = D_{AX} + HL_{min} * r_p * \sin \varphi_{pb} \quad (16)$$

where:

D_h is the friction torque in loading condition

D_l is the friction torque in unloading condition

HL_{max} is the hubload in loading condition

HL_{min} is the hubload in unloading condition

Under the assumption of the symmetrical damping, this ratio would be equal to 1. As soon as the radial damping starts to grow, this ratio assumes values bigger than 1. This sentence highlights the interest on evaluating the influence of fundamental tensioner parameters such as the differential angle, the pivot bushing friction coefficient and the damper pad on the tensioner performances. The sensitivity analysis has been performed with this aim:

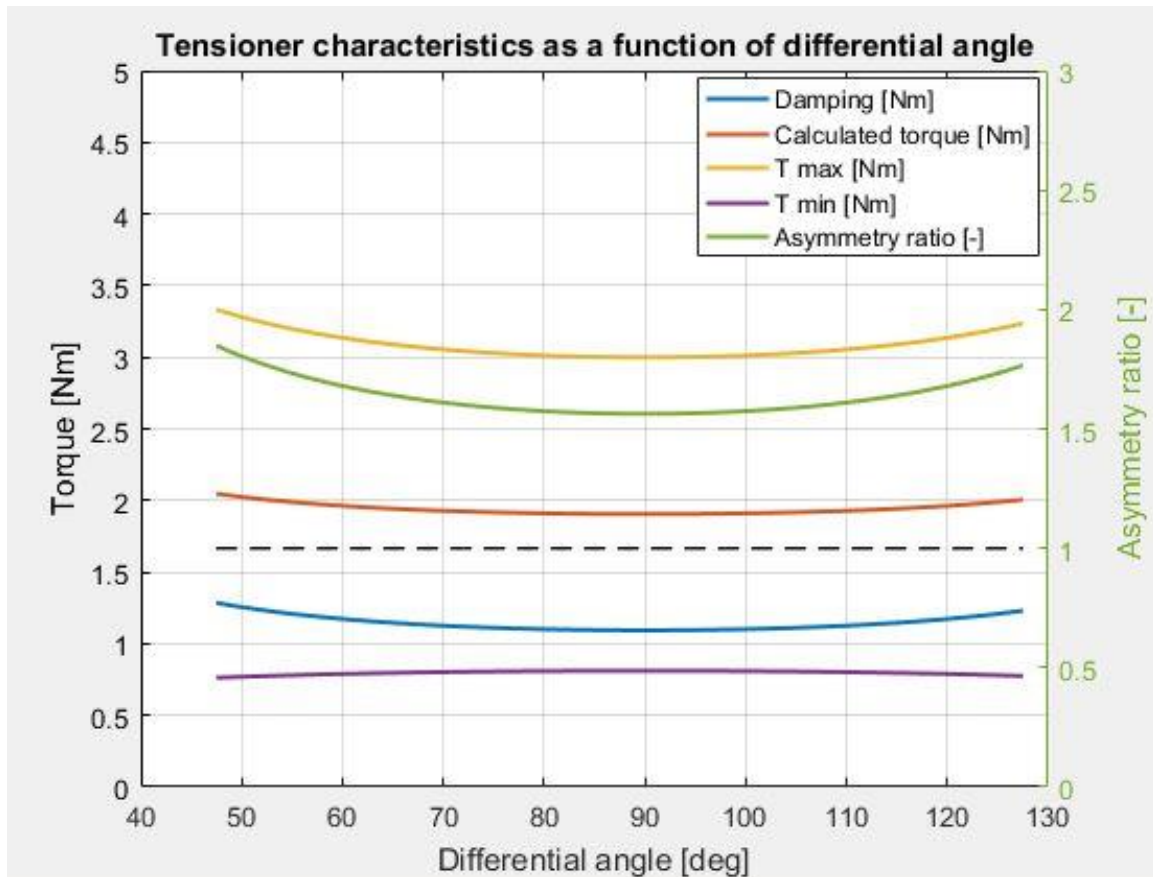


Figure 17. Tensioner sensitivity to differential angle

As it can be seen from the graph above, the differential angle has a limited impact on the tensioner characteristics. In fact, a difference can be noticed only with differential angles strongly different from nominal ones. It is worth to underline that a tensioner working on an engine is oscillating at an amplitude of about +/- 8 degrees. In this interval almost null variation can be noticed.

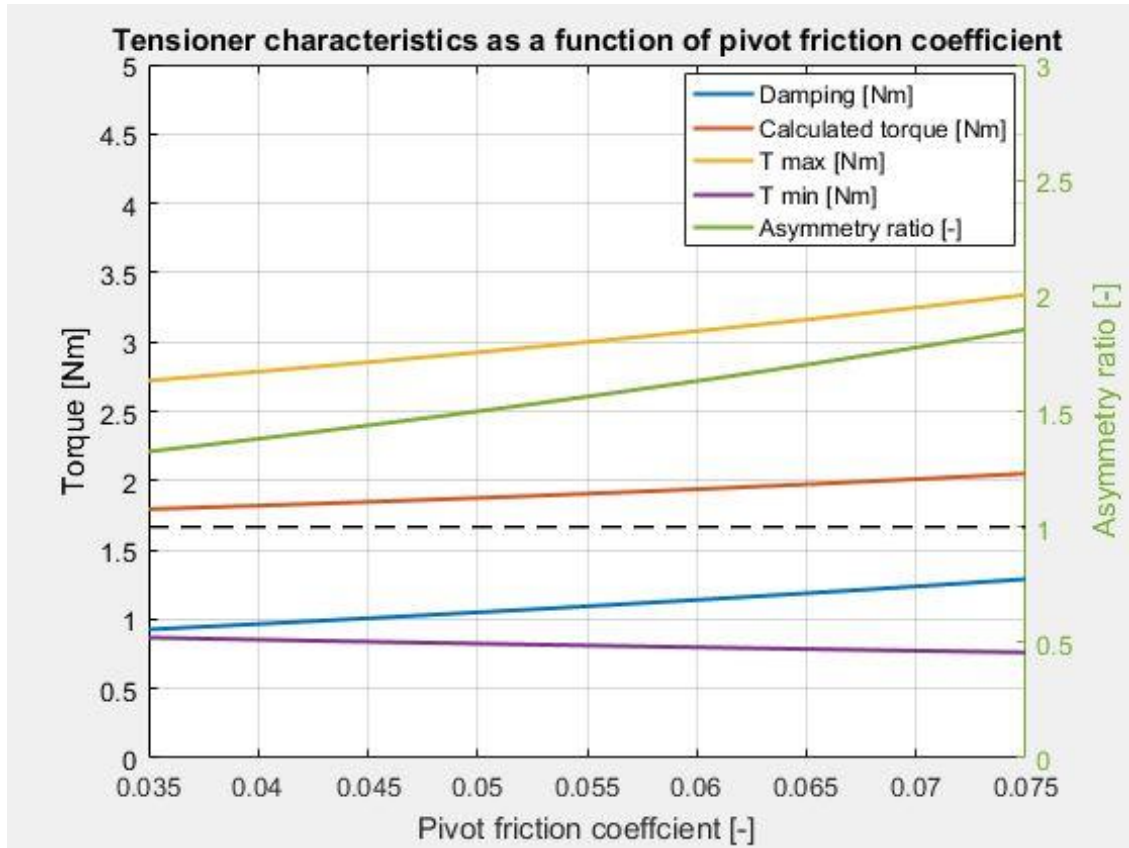


Figure 18. Tensioner sensitivity to pivot bushing friction coefficient

By analysing picture 18, the pivot bushing friction coefficient influence can be evaluated. The radial damping can be computed through equation 10, reported here below:

$$D_{RAD} = HL_{nom} * r_p * \sin \varphi_{pb} \quad (10)$$

the damping grows linearly with the pivot bushing friction coefficient and the calculated torque as a consequence. A linear trend can be seen in the asymmetry ratio as well. In fact, as the pivot bushing friction coefficient grows, the difference between HL_{max} and HL_{min} is increasing, as it can be seen analysing equations 12 and 13, reported here below:

$$HL_{max} = \frac{M_s + D_{AX}}{l_{arm} * \sin \alpha(t) - \sin(\tan^{-1} \varphi_{pb})} \quad (12)$$

$$HL_{min} = \frac{M_s - D_{AX}}{l_{arm} * \sin \alpha(t) + \sin(\tan^{-1} \varphi_{pb})} \quad (13)$$

This difference is enhanced with the pivot friction coefficient increase in the D_h and D_l calculation, since a constant term is adding two growing terms, as It can be seen in equations 15 and 16:

$$D_h = D_{AX} + HL_{max} * r_p * \sin \varphi_{pb} \quad (15)$$

$$D_l = D_{AX} + HL_{min} * r_p * \sin \varphi_{pb} \quad (16)$$

So the almost linear increase of the asymmetry ratio as a function of the pivot bushing friction coefficient is confirmed.

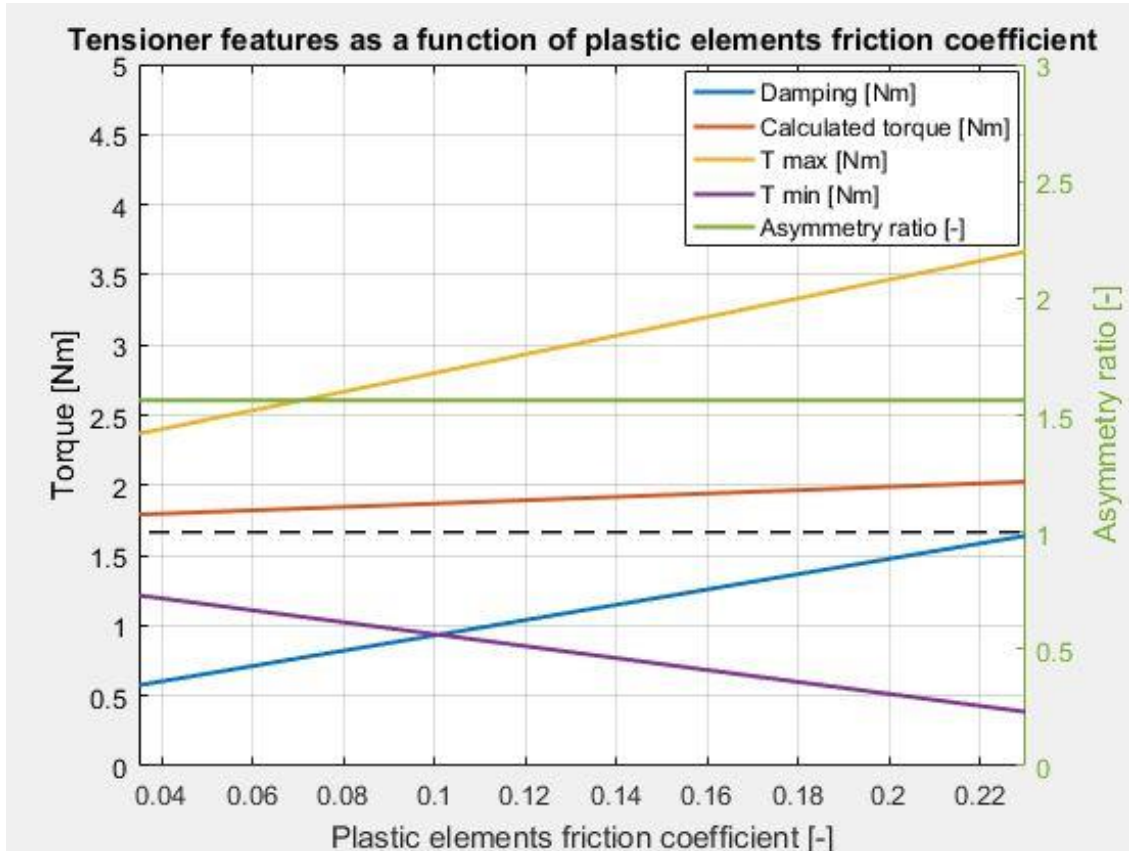


Figure 19. Tensioner sensitivity to plastic friction coefficient

By observing figure 19, the plastic elements friction coefficient impact on tensioner features can be analysed. First of all, it is possible to notice that the damping is the most influenced characteristic. It is in line with what was expected, since, by recalling equation 11, the damping can be calculated as

$$D_{tot} = D_{AX} + D_{RAD} \quad (11)$$

and the axial damping is computed according to equation nr. 9:

$$D_{AX} = F_{AX} * \varphi_{plastic} * (R_{mdp} + R_{mes}) \quad (9)$$

By moving the attention to the calculated torque, a slightly growing trend can be observed. In fact, since the damping is becoming higher as the plastic coefficient is increasing, also the loads will grow as well. Since the friction torque in loading and unloading operations are computed through equations 15 and 16:

$$D_h = D_{AX} + HL_{max} * r_p * \sin \varphi_{pb} \quad (15)$$

$$D_l = D_{AX} + HL_{min} * r_p * \sin \varphi_{pb} \quad (16)$$

the damper pad and endcap spacer friction coefficient does not introduce any asymmetry in the tensioner characteristics.

Tensioner design flowchart

A timing belt tensioner is an assembly of several components (see figure 20 here below).

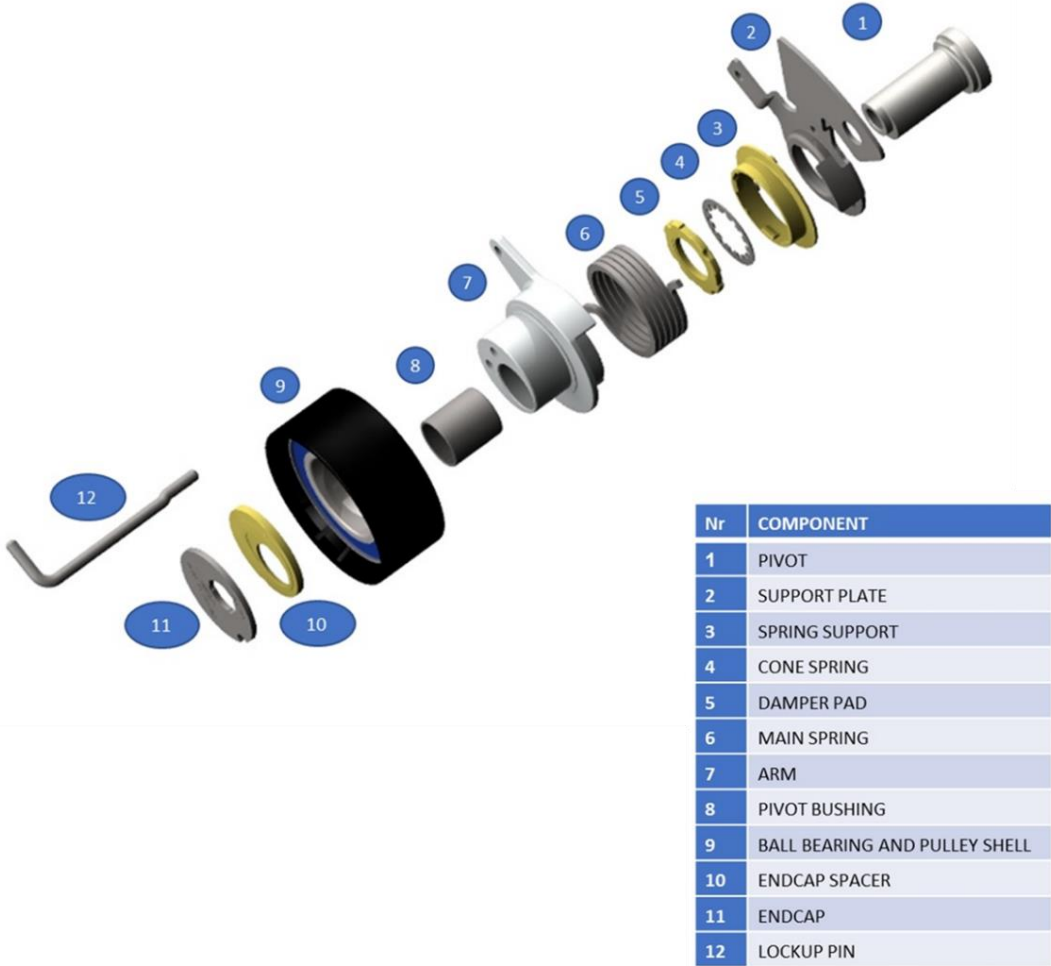


Figure 20. Timing belt tensioner components

The support plate is customized as a function of the application. It is needed in order to impose an angular reference of the tensioner with respect to the engine crankcase, so it has to cope with the tensioner support morphology. All other components dimensions and features, instead, are depending only on tensioner specifications and its packaging constraints. The aim of this work is to automate the components dimensioning process, permitting in this way to start from the tensioner design input and to obtain from this a raw but verified 3D CAD model. The design input has been structured in an Excel table, while the dimensioning is performed in Matlab environment. The outputs of this work, besides the above-mentioned 3D CAD model, are numerical results summarized in a second Excel table, together with Matlab graphs.

The design of a timing belt tensioner can be divided in different phases or steps:

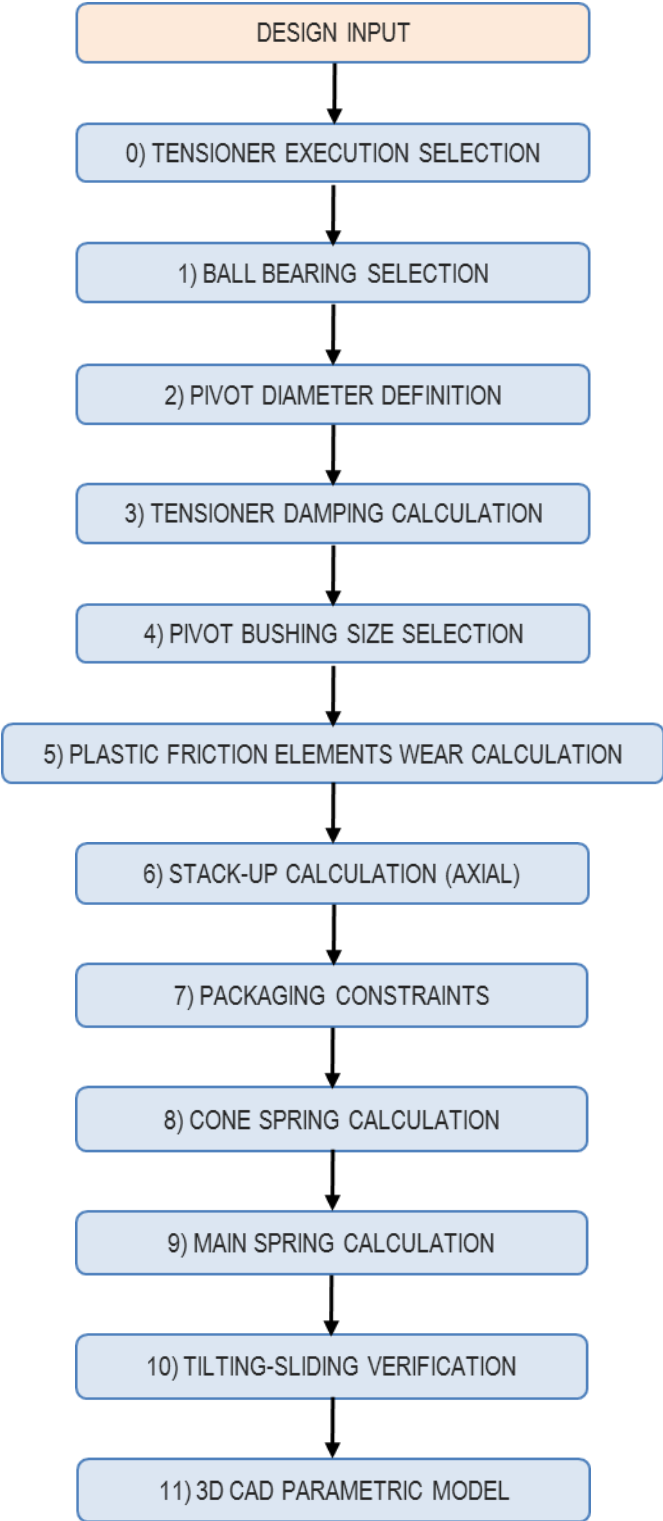


Figure 21. Tensioner design flowchart

Design input

A	B	C	D	E	F	G
TENSIONER INPUTS (Data coherent with Matlab last iteration)						
See colour legend below			Standard values	Customized values	Data read by Matlab during last iteration	Suggested corrections / Comments
Engine application						
Application type	[-]	Standard only	Belt In Oil		Belt In Oil	
Engine Fuel	[-]	Standard only	Diesel		Diesel	
Tensioner architecture typology	[-]	Standard only	Rotary		Rotary	
Pulley						
Pulley shell type	[-]	Standard only	Toothed		Toothed	
Pulley diameter	[m]	Standard	0,06		0,06	
Pulley max parallelism EOLife	[µm]	Standard	300		300	
Tensioner geometrical data						
Belt loading type	[-]	Standard only	Double eccentric		Double eccentric	
Working arm length	[m]	Standard only	0,0025		0,0025	
Loading arm length	[m]	Standard	0,0035		0,0035	
Differential angle	[deg]	Custom only		87,5	87,50	
Wrap angle	[deg]	Custom only		90,00	90,00	
Nominal arm angle with respect to HER	[deg]	Custom only		71,5	71,50	
Belt						
Belt width	[m]	Standard	0,02		0,020	
Middle plane belt height	[m]	Custom only		0,016	0,0160	
Middle plane belt height increment (worst case)	[m]	Standard	0,002		0,002	
Lock-up pin						
Lock-up pin position radius (respect to pulley center)	[m]	Custom only				Not checked due to optional data missing
Lock-up pin angular position (respect to H.E.R.)	[deg]	Custom only				Not checked due to optional data missing
Lock-up pin diameter	[m]	Standard				Not checked due to optional data missing
Space constraints						
Max pivot height	[m]	Custom only		0,042	0,042	
Max axial displacement	[m]	Custom only				
minimum belt-crankcase clearance	[m]	Custom only		0,002	0,002	
Pivot						
Pivot class diameter	[m]	Standard	0,020		0,020	
Pivot bushing radial thickness	[m]	Standard only	0,001		0,001	
Durability test						
Duty cycle	[-]	Defined				
Engine size	disp[L_layout [-]					
Theta peak-to-peak	[deg]	Custom only		16	16	
Frequency	[Hz]	Custom only		50	50	
Time durability test	[hrs]	Custom only		1350	1350	
Tensioner specifications						
Calculated torque target	[Nm]	Custom only		2	2	

Figure 22. Design input Excel table (1/2)

A	B	C	D	E	F	G
Tensioner specifications						
Calculated torque target	[Nm]	Custom only		2	2	
Damping target	[Nm]	Defined		0,75	0,75	
Damping tolerance	[Nm]	Custom only		0,2	0,2	
Damping EOLife limit	[Nm]	Custom only		0,8	0,8	
Main spring						
Spring stiffness	[Nm/deg]	Custom only		0,0131	0,0131	
Spring dimensioning methodology	[-]	Automatic			Automatic	
Spring material	[-]					
Working condition	[-]					
Wire section type	[-]					
Wire section sizes	[mm x mm]					
Wire section sizes	[mm]					
Mean winding diameter	[mm]					
Spring torque tolerance	[%]	Custom only				
Bolt						
Bolt dimensioning methodology	[-]	Automatic			Automatic	
Tilting safety factor (min)	[-]	Standard	3		3,0	
Sliding safety factor (min)	[-]	Standard	3		3,0	
Tightening torque	[Nm]					
Bolt class	[-]					
Bolt pitch	[mm]					
Bolt material class	[mm]					
Fixation dimensional features						
Engine support internal diameter	[m]	Standard	0,0082		0,0082	
Engine support external diameter	[m]	Standard	0,028		0,028	
Contact angle	[deg]	Standard	360		360	
Bolt head contact external diameter	[m]	Standard	0,011		0,011	
Number of active threads	[-]	Custom only		1,5	1,5	
σ_a support (compression)	[MPa]	Custom only		400	400	
σ_a support (traction)	[MPa]	Custom only		400	400	

Figure 23. Design input Excel table (2/2)

In the figures 22 and 23, the design input Excel table is shown. It is organized in sections or themes (by rows). The user, either during the data filling-in, either during the result reading, is helped by the colors of the cells, through the color legend shown in the figure 24 here below.

Information data
Mandatory data
Optional data
No input - Output from automatic calculation
Data not verified due to optional data missing
Warning

Figure 24. Design input color legend

Data have to be inserted in a matrix, composed by three columns (C, D and E). In the first columns of this matrix, a selector has been introduced, in order to pass from standard values (column D) to customized values (column E) and vice versa (if possible). As it can be seen this is not present in all rows, since for some data only standard or only customized values are available, in fact, in these rows, the selector is an information data type, reporting “Standard only” or “Custom only” descriptions. Some exceptions are present:

- **Defined/Assumed:** this selector has been implemented for the durability test parameters and for the damping tensioner typology. In the first case, if it is assumed, the user is asked to insert an engine typology from a list. As a function of this choice, some durability test parameters are selected. If the duty cycle is defined, instead, the user is asked to insert the exact parameters. Moving to the tensioner damping typology, if the selector is set as “Defined”, the user has to insert a numerical value (the average between upper and lower values), while if it is assumed, the possible inputs are “Only radial” or “Radial and Axial”.
- **Automatic/Manual:** this selector has been implemented for the main spring and for the fixation bolt. These are very similar sections, in which if the selector is in “Manual”, the user has to insert all the parameters requested and the flowchart section will be run as a verification, while if the selector is set as “Automatic”, all design standards that have been embedded in Matlab libraries are checked until a positive outcome is obtained.

Another important aspect to be noticed is the difference between mandatory and optional data. Optional data can be omitted and dimensioning flowchart can still be run. This possibility has been introduced since information missing is quite frequent in the early stages of a project. An incomplete data filling could bring to an incomplete tensioner verification, highlighted by alerts (in an orange cell) as shown in picture 25, in the lock-up pin section.

In column F, the data read by Matlab are printed. This is done in order to guarantee the alignment between the design input parameters and the outputs. If a change is performed, a red alert turns on in correspondence of the misaligning input and in the table title, as shown in the figure 25 here below.

TENSIONER INPUTS (Warning: data not coherent with Matlab last iteration)						
See colour legend below			Standard values	Customized values	Data read by Matlab during last iteration	Suggested corrections / Comments
Engine application						
Application type	[-]	Standard only	Belt In Oil		Belt In Oil	
Engine Fuel	[-]	Standard only	Diesel		Diesel	
Tensioner architecture typology	[-]	Standard only	Rotary		Rotary	
Pulley						
Pulley shell type	[-]	Standard only	Flat		Toothed	
Pulley diameter	[m]	Standard	0,06		0,06	
Pulley max parallelism EOLife	[µm]	Standard	300		300	
Tensioner geometrical data						
Belt loading type	[-]	Standard only	Double eccentric		Double eccentric	
Working arm length	[m]	Standard only	0,0025		0,0025	
Loading arm length	[m]	Standard	0,0035		0,0035	
Differential angle	[deg]	Custom only		87,5	87,50	
Wrap angle	[deg]	Custom only		90,00	90,00	
Nominal arm angle with respect to HER	[deg]	Custom only		71,5	71,50	
Belt						
Belt width	[m]	Standard	0,02		0,020	
Middle plane belt height	[m]	Custom only		0,016	0,0160	
Middle plane belt height increment (worst case)	[m]	Standard	0,002		0,002	
Lock-up pin						
Lock-up pin position radius (respect to pulley center)	[m]	Custom only				Not checked due to optional data missing
Lock-up pin angular position (respect to H.E.R.)	[deg]	Custom only				Not checked due to optional data missing
Lock-up pin diameter	[m]	Standard				Not checked due to optional data missing
Space constraints						
Max pivot height	[m]	Custom only		0,042	0,042	

Figure 25. Design input Excel table (misalignment example)

Finally, in column G, some comments or suggested corrections are shown (if needed). If an issue is detected, a value able to solve it is suggested to the user, in order to avoid time-wasting trial and error procedures. As an example, the figure 26 is shown here below.

Bolt						
Bolt dimensioning methodology	[-]	Automatic			Automatic	
Tilting safety factor (min)	[-]	Custom		8,000	8,0	
Sliding safety factor (min)	[-]	Standard	3		3,0	
Tightening torque	[Nm]					
Bolt class	[-]					
Bolt pitch	[mm]					
Bolt material class	[mm]					
Fixation dimensional features						
Engine support internal diameter	[m]	Standard	0,0082		0,0082	Not compatible with bolt dimensions
Engine support external diameter	[m]	Standard	0,022		0,022	
Contact angle	[deg]	Standard	360		360	
Bolt head contact external diameter	[m]	Custom		0,0148	0,0148	
Number of active threads	[-]	Custom only		1,5	1,5	
σ_{cs} support (compression)	[MPa]	Custom only		400	400	Suggested bolt head ext diameter: >0.0148
σ_{cs} support (traction)	[MPa]	Custom only		400	400	Suggested number of active threads: >2.5

Figure 26. Design input Excel table (suggested corrections example)

As it can be seen, three warnings have been highlighted. The first one is referring to the pivot inner diameter: the fixation bolt needed to fulfil the requirements imposed in the design input is a M10x1,50, so a $\varnothing 10,2$ mm pivot diameter internal hole is needed (at least)

to host the bolt. The second and third warnings are concerning the engine crankcase stress. Regarding the compression stress, the limit has been overcome, so a under bolt head external diameter contact bigger than 14.9 mm is needed to increase the contact surface and so to avoid overcoming the yield strength. Moving the attention to the last warning, an analogous consideration can be done: at least 2.5 active threads are needed to avoid plastic deformation due to traction forces.

0) Tensioner execution selection

In order to choose the correct type of tensioner for a given application a careful study of the working conditions has to be performed. The first aspect to focus on is the type of environment in which the tensioner has to work in. In fact, it can be;

- dry (in absence of oil)
- lubricated (Belt In Oil or BIO)

The main difference between these two options is the friction coefficient. Another important aspect to take into consideration is the fuel of the engine. In fact, the Diesel engine is characterized by lower rpm, but presents a higher percentage of soot. This is the product of an incomplete combustion and it is detrimental for the tensioner and the belt. In fact, a portion of the soot produced by the engine during its running, is blended to the engine oil. In the case of BIO application, soot particles contact the belt and they are pressed on it. Due to this reason, the belt behaves like an abrasive tool and it shortens the life of the tensioner. After these considerations, the attention can be moved to the tensioner itself. There are two tensioner families (figure 27):

- rotary type
- blade type

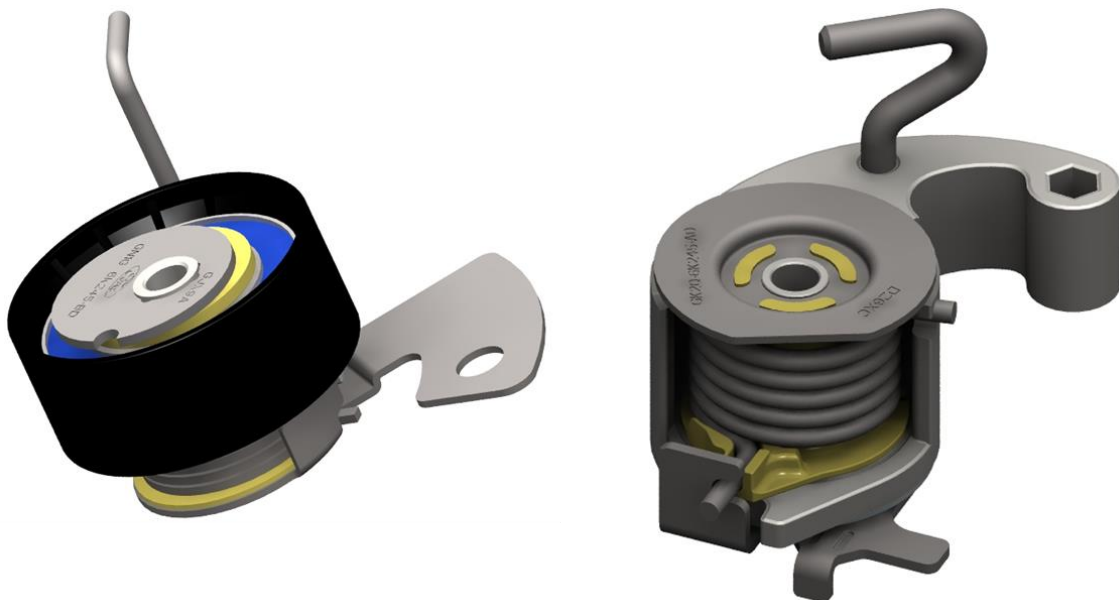


Figure 27. Rotary (left) and blade (right) tensioners

The rotary type is the most common typology present in the market. The belt is put in tension through a pulley, free to rotate on a ball bearing, which has the centre of rotation not coincident with the centre of the pivot. This is the working arm. As anticipated above,

the second family is the blade tensioner type. As the name suggests, there is a blade that puts in tension the belt. Since the blade is not rotating, there is a rubbing between the belt and the blade itself. This brings to a higher friction, so to a higher wear of the system. For this reason, the blade tensioner has to be preferred to the rotary typology only in case of strict constraints of packaging. Another important condition to be fulfilled prior to choose the blade configuration is the application type: it is not compatible with the dry configuration (due to the too much high friction, that would bring to premature system failure).

If the rotary tensioner type has been chosen, there are two layout possibilities (figure 28):

- standard
- reverse

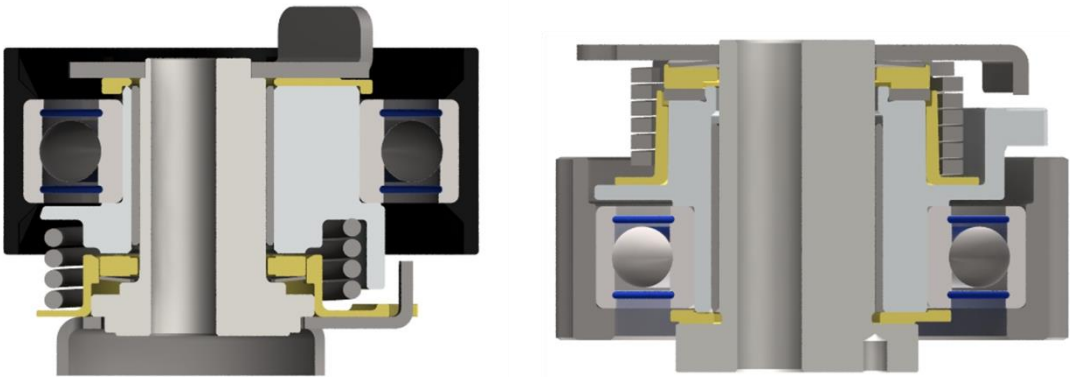


Figure 28. Standard (left) and reverse (right) layout

Standard tensioner is simpler to be assembled, so it is economically convenient respect to the reverse configuration. Due to this aspect, it has to be preferred when space constraints permit it. In fact, the choice between the two is to be kept on the basis of the belt offset. In particular the standard configuration is selected if the inequation 17 is verified:

$$h_{middle\ plane\ belt} \geq \frac{h_{max}}{2} \tag{17}$$

where:

- $h_{middle\ plane\ belt}$ is the belt offet [m]
- h_{max} is the maximum height available [m]

If, instead:

$$h_{middle\ plane\ belt} < \frac{h_{max}}{2} \tag{18}$$

the reverse configuration is chosen.

As it can be seen, if the middle plane belt height coincides with the semi-maximum height, the standard layout is selected.

There are two possibilities for the pulley type (figure 29):

- cylindrical
- toothed

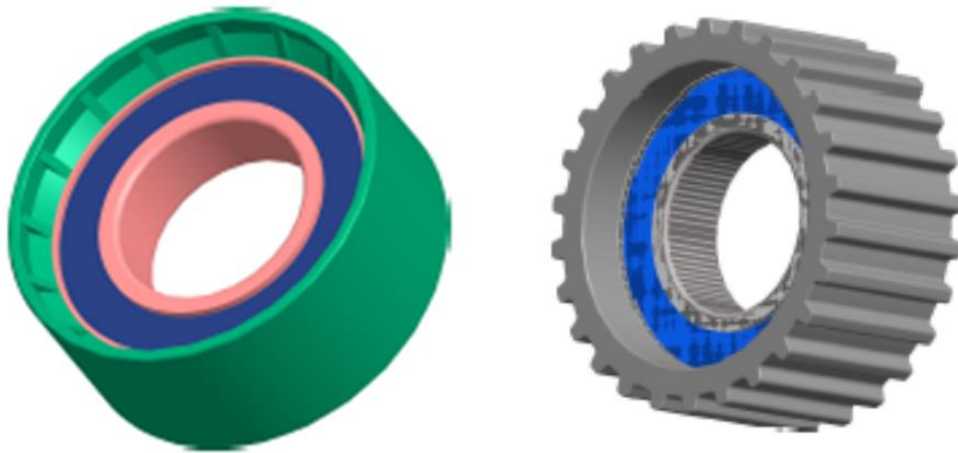


Figure 29. Flat (left) and toothed (right) pulley

The first type is implemented if the belt is put in tension by pushing it in the backside, while the second one is implemented if the belt is pushed on the toothed side.

In this flowchart section also some checks have been performed. In fact, the lock-up pin position is investigated. The lock-up pin is needed in order to keep the tensioner in installation position, so the arm goes against the end-stop towards the loading direction (in fact it is also called hot stop). This is done in such a way to permit to the operator to assemble the timing belt tensioner (by tightening the screw passing through the pivot hole on the crankcase) and to position the belt without any effort. Once these operations have been performed, the lock-up pin can be removed, so the tensioner goes to nominal position and the belt is put into tension.

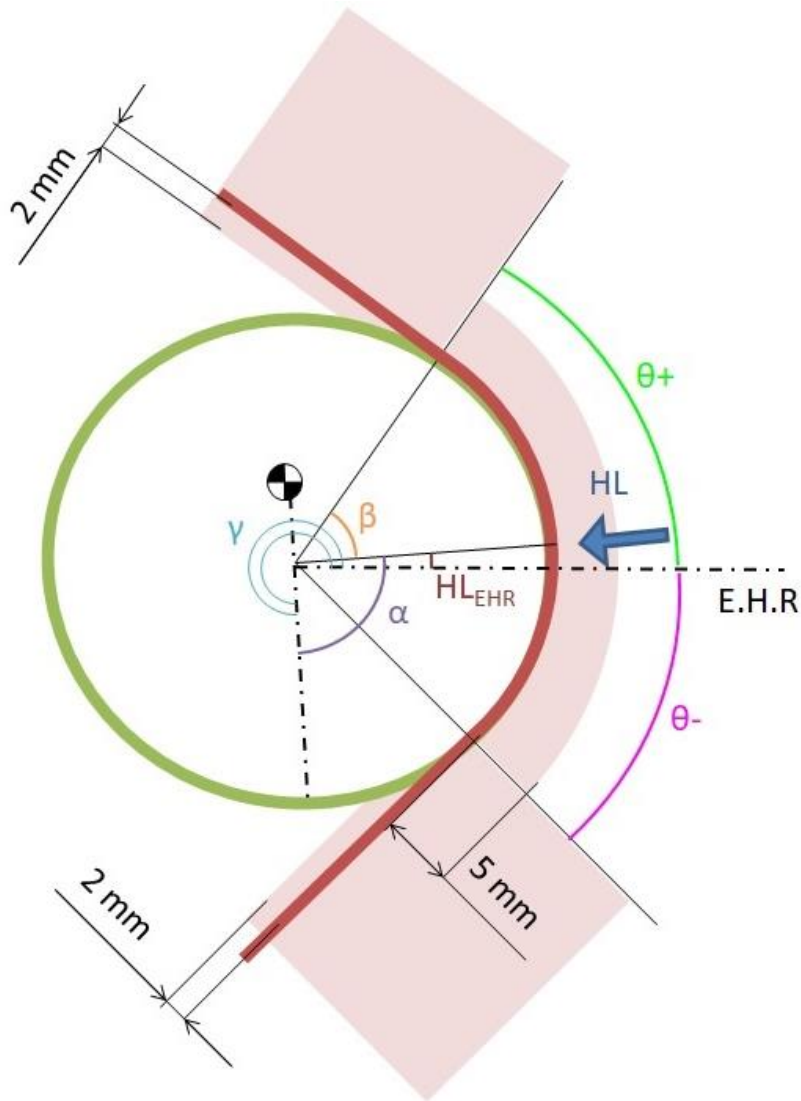


Figure 30. Lock-up pin denied areas

The lock-up pin has to be positioned in such a way to not contact the belt during assembling. In order to assure this, the pin cannot be positioned in some areas (depicted in the picture 30 in light pink colour). As it can be seen, some tolerances have been considered. The hubload position with reference to the E.H.R. (Engine Horizontal Reference) can be computed through equation 19:

$$HL_{EHR} = 360^\circ - (\alpha + \gamma) \quad (19)$$

where:

HL_{EHR} is the angle between the hubload and the E.H.R. [deg]

α is the differential angle [deg]

γ is the nominal arm position angle [deg]

Once HL_{EHR} is known, the wrap angle upper and lower extremes can be defined through equations nr. 20 and 21:

$$\theta_+ = HL_{EHR} + \beta \quad (20)$$

$$\theta_- = HL_{EHR} - \beta \quad (21)$$

where:

ϑ_+ is the E.H.R. to upper belt-pulley contact limit [deg]

ϑ_- is the E.H.R. to lower belt-pulley contact limit [deg]

β is the semi-wrap angle [deg]

The first check that needs to be performed is that the pin does not touch the pulley, so inequation 22 must be verified:

$$R_{pin\ position} - \frac{\Phi_{pin}}{2} \leq \frac{\Phi_{pulley}}{2} \quad (22)$$

where:

$R_{pin\ position}$ is the radial position of the pin [mm]

Φ_{pin} is the pin diameter [mm]

Φ_{pulley} is the pulley diameter [mm]

$\Phi_{pulleytol}$ is the pulley diameter tolerance [mm]

The second check, instead, depends on the lock-up pin angular position. If it is comprised between θ_+ and θ_- , a clearance equal to 5mm has to be assured, fulfilling requirements imposed by inequation 23:

$$R_{pin\ position} - \frac{\Phi_{pin}}{2} \geq \frac{\Phi_{pulley}}{2} + 0.005 [m] \quad (23)$$

Then, if the lock-up pin is positioned at an angle bigger than θ_+ , a clearance of 2mm with respect with the belt must be assured. To do this, a reference system has to be defined:

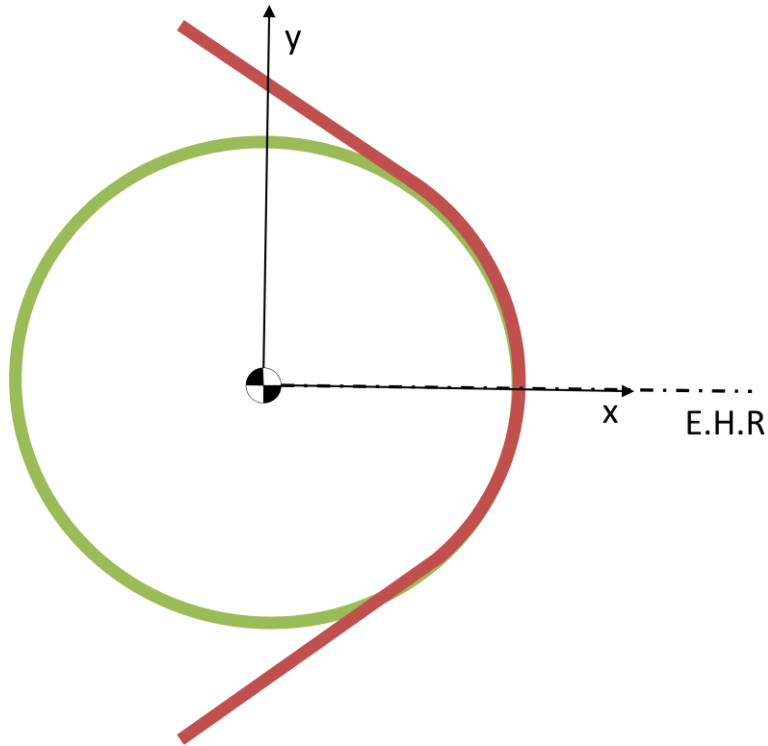


Figure 31. Lock-up pin position reference system

So, by considering the belt tangency in correspondence of the upper belt-pulley contact limit, the inequation 24 must be verified:

$$y_{pin\ position} + \frac{\varnothing_{pin}}{2} + 0.002 [m] < y_{pin\ limit} \quad (24)$$

where:

$y_{pin\ position}$ is the vertical lock-up pin position (function of horizontal lock-up pin position)

$y_{pin\ limit}$ is the belt vertical position (function of horizontal lock-up pin position)

If the lock-up pin angular position is lower than θ , through analogous considerations with respect to the case analysed above, the condition to be fulfilled stated in inequation 25:

$$y_{pin\ position} - \frac{\varnothing_{pin}}{2} - 0.002 [m] > y_{pin\ limit} \quad (25)$$

As a last step of this section of the design flowchart, the axial displacement is verified. To do this, first of all the type of tensioner has to be considered.

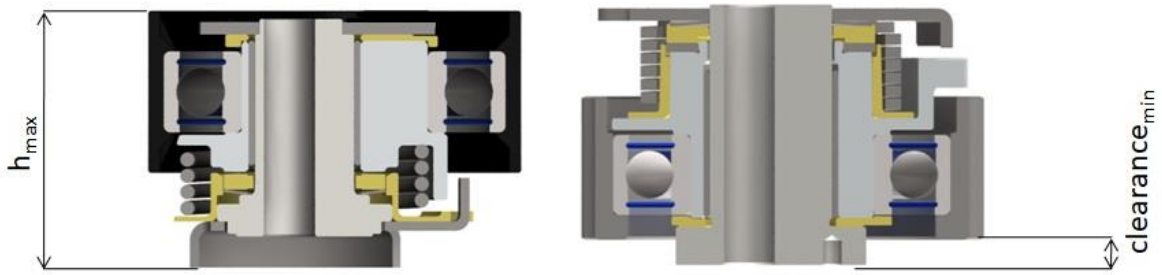


Figure 32. Space constraints

If it is a standard configuration (to the left in the picture 32), the critical issue is found on the top of the pivot. In fact, the top side of the pulley has to be lower than the maximum height available, according to inequation 26:

$$h_{middle\ plane\ belt} + \frac{w_{pulley}}{2} \leq h_{max} \quad (26)$$

where:

w_{pulley} is the pulley width [mm]

h_{max} is the maximum height available [mm]

If it is a reverse configuration (to the right in the picture 32), instead, the attention must be moved to the bottom of the element. In fact, a minimum clearance has to be considered between the pulley lower side and the crankcase. This is done in order to avoid pulley-crankcase contact in whatever working condition, through equation nr. 27:

$$h_{middle\ plane\ belt} - \frac{w_{pulley}}{2} \geq clearance_{min} \quad (27)$$

where:

$clearance_{min}$ is the minimum clearance between belt and crankcase [mm]

The outputs of this stage are the suggested corrections (if any) of the above-mentioned performed checks. Besides this, the tensioner architecture typology and the pulley width are printed in the outputs Excel table, as shown in the figure 33.

TENSIONER OUTPUTS		
Tensioner architecture		
Tensioner architecture typology	[-]	Rotary, Standard
Pulley		
Pulley width	[m]	0,026

Figure 33. Flowchart section 0) output

1) Ball bearing selection

In this section of the workflow the ball bearing size is investigated. As it can be seen in the table 1, it is a function of the nominal hubload and of the type of engine fuel.

HLnom		Gasoline	Diesel
Ball bearing	6006	<1000N	<1200N
	6007	>1000N	>1200N

Table 1. Input data for ball bearing size selection

Gasoline engine is a more stringent condition due to the higher medium engine rpm. In fact, since there is a given transmission ratio (changing for an application to another one) between engine crankshaft and timing belt tensioner pulley, this aspect is translated in higher medium rpm also for the pulley itself and, as a consequence, for the ball bearing too. The output of this stage is the bearing typology, which is printed in the outputs Excel table, as depicted in the picture 34 here below.

Ball bearing		
Ball bearing typology	[-]	6006

Figure 34. Flowchart section 1) output

2) Pivot diameter definition

The pivot diameter is a crucial factor for the timing belt tensioner. It has to be maximized in order to achieve a higher radial damping, which is less sensitive to the time with respect to the axial one. It is directly proportional to the pivot diameter, since it can be computed through equation 10, which has been reported here below:

$$D_{RAD} = HL_{nom} * r_p * \sin \varphi_{pb} \quad (10)$$

Another beneficial aspect achieved through the maximization of the pivot diameter is that a lower pressure on the pivot bushing is obtained. This is very important because a pivot bushing presents a threshold for the maximum pressure achievable. Then, since the pressure is directly linked to the wear, a higher pressure can bring also to durability problems.

Pivot diameter depends on following tensioner features:

- tensioner working arm (from system calculation)
- ball bearing size (from ball bearing calculation)
- pivot bushing thickness

The tensioner working arm is set during the system simulation. The ball bearing size is set in point 1). Bushing thickness is assumed at this stage, since it depends on the pivot bushing supplier. The choice is among two suppliers; one presents a radial thickness equal to 1mm, while the other has a radial thickness of 0.5mm. Due to this reason, pivot diameter is firstly chosen according to the following table, then, if the pivot bushing is 0.5mm thick, pivot diameter is increased of 1mm (in order to recover the 0.5mm radial thickness difference).

Ball bearing		6006				6007
Input	Working arm [mm]	2.5	3	4	5	4.5
	Max loading arm [mm]	4.5	4.5	4	3.5	5.5
Output	Pivot class diameter [mm]	21	21	19	17	22

Table 2. Input data for the pivot diameter definition

Pivot is characterized by a hole needed for the fixation bolt. It can be concentric with respect to the pivot (in case of single eccentric tensioner), or at a distance from the pivot axis, which is equal to the loading arm length. In addition, its diameter can be equal to 8,2mm or 10,2mm, as a function of the implemented fixation bolt size (M8 and M10 respectively).

Then, ball bearing inner diameter has to be considered:

- 6006 size: 30mm
- 6007 size: 35mm

This is an important feature since a minimum thickness of 1mm of the arm has to be assured in the most critical side, so the one in the direction of the eccentricity.

Given a tensioner working arm length, the standard value for the loading arm length (if present) and for the pivot class diameter correspond to the value that can be found in the same column. For both these parameters, it is possible to manually impose customized values, but only smaller values with respect to standard ones can be chosen. The Excel design input table is set in such a way to show only acceptable values, but a check is performed in Matlab to avoid incompatibilities prior to freeze this degree of freedom. As a matter of fact, the only output of this stage of the flowchart is the pivot diameter, which is printed in the outputs Excel table, as depicted in the picture 35 here below.

Pivot		
Pivot diameter	[m]	0,016

Figure 35. Flowchart section 3) output

3) Tensioner damping calculation

In this workflow section the tensioner damping is investigated. In fact, through the equation 10 here below reported, the radial damping can be computed as:

$$D_{RAD} = HL_{nom} * r_p * \sin \varphi_{pb} \quad (10)$$

At this stage of the workflow, the radial damping can be considered fixed because is a function of parameters that have already been set before. In fact, the pivot bushing friction coefficient depends only on working conditions, the pivot radius value has been set in the previous workflow section and the average hubload is obtained through the calculated torque target, differential angle and the working arm. Since the tensioner total damping can be computed through equation 11 reported here below:

$$D_{tot} = D_{AX} + D_{RAD} \quad (11)$$

if the tensioner damping required is higher than the radial one, the axial damping group has to be introduced. It is worth to remember that the axial damping can be computed through equation 9:

$$D_{AX} = F_{AX} * \varphi_{plastic} * (R_{mdp} + R_{mes}) \quad (9)$$

The plastic friction coefficient is a function of the working conditions and it is fixed, so the parameters on which is possible to act are:

- the axial force
- the medium radii

In order to evaluate the axial force of the cone spring, the value of the medium radii of the contact surfaces can be retrieved from the tables here below reported.

Damper pad		OUTPUT			
		Contact surface [mm ²]	Mean radius [mm]	∅ _{outer} [mm]	Axial height [mm]
INPUT	D _{AX} <0,7 [Nm]	290	12	31.5	2,5
	0,7<D _{AX} <1.10 [Nm]	460	12.5	31.5	3,5
	1.10<D _{AX} <2,00 [Nm]	490	13.5	34.5	2,5

Table 3. Damper pad dimensions as a function of the axial damping

Endcap spacer		OUTPUT		
		Contact surface [mm ²]	Mean radius [mm]	Axial height [mm]
INPUT	$D_{AX} < 0,7$ [Nm]	350	12,5	1,5
	$0,7 < D_{AX} < 1.10$ [Nm]	490	13,5	1,5
	$1.10 < D_{AX} < 2,00$ [Nm]	670	14,5	1,5

Table 4. Endcap spacer dimensions as a function of the axial damping

The output of this stage are the tensioner spring torque computed in nominal position, the axial damping presence and, if this is the case, how the tensioner damping is subdivided between axial and radial, as shown in the picture 36 reported here below.

Tensioner characterization		
Axial damping	[Y/N]	Yes
Axial damping	[Nm]	0,599
Radial damping	[Nm]	0,151
Spring torque @ nominal position	[Nm]	1,633

Figure 36. Flowchart section 4) output

4) Pivot bushing size selection

Once the pivot diameter has been set (at point 2 of the flowchart), the remaining free parameter that influences the pressure (and the wear as well) is the pivot bushing length. In fact, the pressure applied on the pivot bushing can be computed through equation 28:

$$p_{bush} = \frac{HL_{nom}}{\Phi_{bush} * L_{bush}} \quad (28)$$

where:

p_{bush} is the pressure on the pivot bushing surface [N/mm²]

HL_{nom} is the nominal hubload [N]

Φ_{bush} is the pivot bushing external diameter [mm]

L_{bush} is the pivot bushing length [mm]

It is worth to be noticed that the hubload is independent from the bushing wear, since is due to external forces. For this reason, as a first approximation, it is assumed to be constant during the durability test. Then, it is possible to compute the average pivot bushing sliding speed, through equation 29:

$$v_{av\ bush} = \frac{2 * \theta_{pp} * \pi * \frac{\Phi_{bush}}{2} * f}{180} \quad (29)$$

where:

$v_{av\ bush}$ is the pivot bushing mean sliding speed [m/s]

θ_{pp} is the oscillation amplitude [deg]

Φ_{bush} is the pivot bushing diameter [m]

f is the oscillation frequency [Hz]

So, it is possible to compute also the $p * v$ term, as defined in equation 30:

$$p * v_{bush} = p_{bush} * v_{av\ bush} \quad (30)$$

and the $p * v * t$ term, as defined in equation 31:

$$p * v * t_{bush} = p_{bush} * v_{av\ bush} * t_{durability} \quad (31)$$

where:

$t_{durability}$ is the durability test duration [hrs]

At this point is possible to compare these three factors with existing application ones (see table 5), in order to check if they are below the attention threshold, or if they need to be more deeply investigated.

Max reference values		Dry	BIO
p_{bush} [MPa]	Supplier A	2,5	5
	Supplier B	3	NA
$p*v_{bush}$ [Mpa* m/s]	Supplier A	0,8	0,95
	Supplier B	0,6	NA
$p*v*t_{bush}$ [Mpa* m/s * hrs]	Supplier A	800	850
	Supplier B	600	NA

Table 5. Pivot bushing threshold values

Finally, the pivot bushing wear can be computed thanks to equation 32:

$$w_{bush} = \int k_w bush * p_{bush} * v_{av bush} \quad (32)$$

where:

w_{bush} is the average wear of the pivot bushing [mm]

k_{wbush} is the constant of wear of pivot bushing [mm*m*s/N]

p_{bush} is the pressure on the pivot bushing surface [N/m²]

v_{avbush} is the mean sliding speed of the pivot bushing [m/s]

Once the pivot bushing average wear has been obtained, the maximum allowed average wear has to be considered. Its value depends on the bushing typology and it corresponds to the depth of the sliding material, so before to reach the support steel sheet, that would mean to lose the low friction properties of the bushing itself.

If pivot bushing does not reach the verification, pivot bushing length must be increased. The pivot bushing length must not overcome the maximum available space on the pivot, whose dimension is a function of the maximum pivot height and of the presence or not of the axial damping. In fact, if the axial damping group is not needed, it is evaluated according to equation 33:

$$L_{bush max} = h_{maxpivot} - \Delta bush_crank_{no_ax_damp} - \Delta bush_head_{no_ax_damp} \quad (33)$$

where:

$L_{bush max}$ is the maximum bushing length which is possible to implement [m]

$\Delta bush_crank_{no\ ax\ damp}$ is minimum gap between the lower pivot bushing extreme and the pivot base in case of only radial damping [m]

$\Delta bush_head_{no\ ax\ damp}$ is minimum gap between the upper pivot bushing extreme and the pivot head in case of only radial damping [m]

instead, if the axial damping presence is forecast, the maximum space available for the pivot bushing is evaluated according to equation 34:

$$L_{bush\ max} = h_{maxpivot} - \Delta bush_crank_{wt_ax_damp} - \Delta bush_head_{wt_ax_damp} \quad (34)$$

where:

$\Delta bush_crank_{wt\ ax\ damp}$ is minimum gap between the lower pivot bushing extreme and the pivot base in case of also axial damping [m]

$\Delta bush_head_{wt\ ax\ damp}$ is minimum gap between the upper pivot bushing extreme and the pivot head in case of also axial damping [m]

If this is still not sufficient, the pivot diameter must be increased and the check must be repeated. The limits are linked to the material layer disposition into the bushing, but they do not take into account the tensioner application. In fact, there are other conditions to be fulfilled due to:

- loss of concentricity
- loss of parallelism

The loss of concentricity makes the pulley to rotate around a centre different from its geometrical one. This is a situation to be avoided since it is source of shocks, that are influencing negatively the tensioner life.

The loss of parallelism, instead, forces the pulley to work in a not aligned way. If this misalignment excesses a threshold value (that depends on the belt layout and on working conditions), the belt could move axially and fall from the tensioner support, with detrimental consequences on the engine. The loss of parallelism is induced by a not complete symmetry of the pivot bushing with respect to the belt. In fact, if the middle plane belt is not aligned with the pivot bushing one, a side of the pivot bushing itself will experience a higher load than the other one, bringing to a different wear between the two extremities as shown in the section of the pivot bushing in the figure 37.

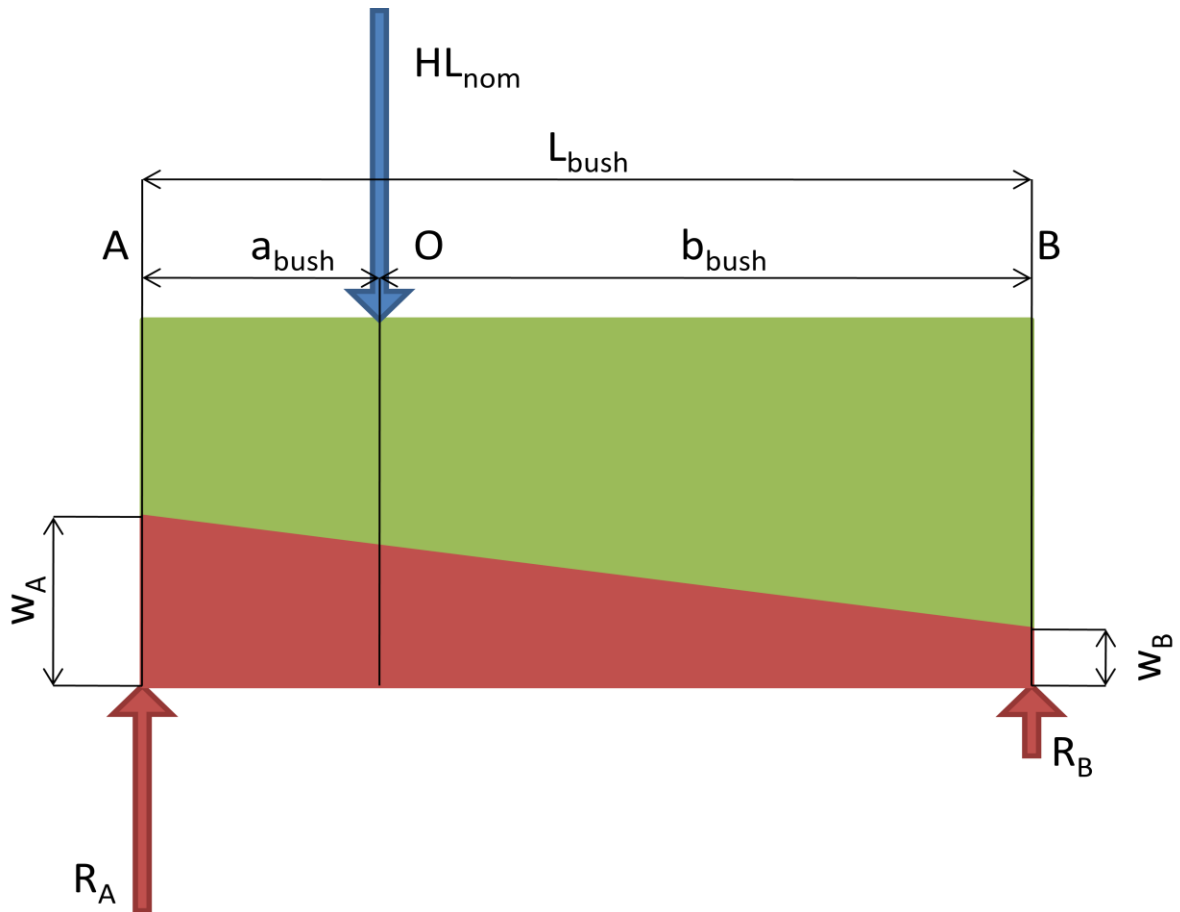


Figure 37. Pivot bushing wear model

In green the pivot bushing material section is depicted (which is a rectangle at new), while in red the worn out part is represented. As it can be seen, the red part has a trapezoidal shape, since the side with a bigger load has a higher thickness reduction with respect to the other one.

By considering the body translational equilibrium, equation 35 is retrieved:

$$HL_{nom} = R_A + R_B \quad (35)$$

where:

HL_{nom} is the nominal hubload [N]

R_A is the constraint reaction in A [N]

R_B is the constraint reaction in B [N]

Then, considering the rotational equilibrium, equations 36 and 37 can be obtained:

$$R_A = HL_{nom} \frac{b}{(a+b)} \quad (36)$$

$$R_B = HL_{nom} \frac{a}{(a+b)} \quad (37)$$

where:

a is the distance between the HL application point and the point A [m]

b is the distance between the HL application point and the point B [m]

At this point, the new pressure values can be computed in A and B points, according to equations 38 and 39:

$$p_{A \text{ bush}} = \frac{R_A}{\phi_{bush} * \frac{L_{bush}}{2}} \quad (38)$$

$$p_{B \text{ bush}} = \frac{R_B}{\phi_{bush} * \frac{L_{bush}}{2}} \quad (39)$$

By considering the Reye's hypothesis of an equal volume of worn out material for an equal friction forces work, the wear in A and B points can be computed through equations 40 and 41:

$$w_{A \text{ bush}} = \int k_{w \text{ bush}} * p_{A \text{ bush}} * v_{av \text{ bush}} \quad (40)$$

$$w_{B \text{ bush}} = \int k_{w \text{ bush}} * p_{B \text{ bush}} * v_{av \text{ bush}} \quad (41)$$

where:

$w_{A \text{ bush}}$ is the wear of the pivot bushing in point A [mm]

$w_{B \text{ bush}}$ is the wear of the pivot bushing in point B [mm]

$p_{A \text{ bush}}$ is the pressure on the pivot bushing surface in point A [N/m²]

$p_{B \text{ bush}}$ is the pressure on the pivot bushing surface in point B [N/m²]

$k_{w \text{ bush}}$ is the constant of wear of pivot bushing [mm*m*s/N]

$v_{av \text{ bush}}$ is the mean sliding speed of the pivot bushing [m/s]

Once the wear in the two extremities is known, the pulley parallelism can be computed through equation 42:

$$//_{pulley} = \phi_{pulley} * \frac{w_{B \text{ bush}} - w_{A \text{ bush}}}{L_{bush}} \quad (42)$$

where:

$//_{pulley}$ is the pulley parallelism [m]

ϕ_{pulley} is the pulley diameter [m]

The outputs of this stage are both in Excel and in Matlab. In the Excel output table the pivot bushing length is printed, as shown in the picture 38.

Pivot bushing length	[m]	0,016
----------------------	-----	-------

Figure 38. Flowchart section 5) output (1/3)

Besides this, two graphs are shown in Matlab environment:

- Pivot bushing average wear over time (see figure 39)
- Pulley parallelism over time (see figure 40)

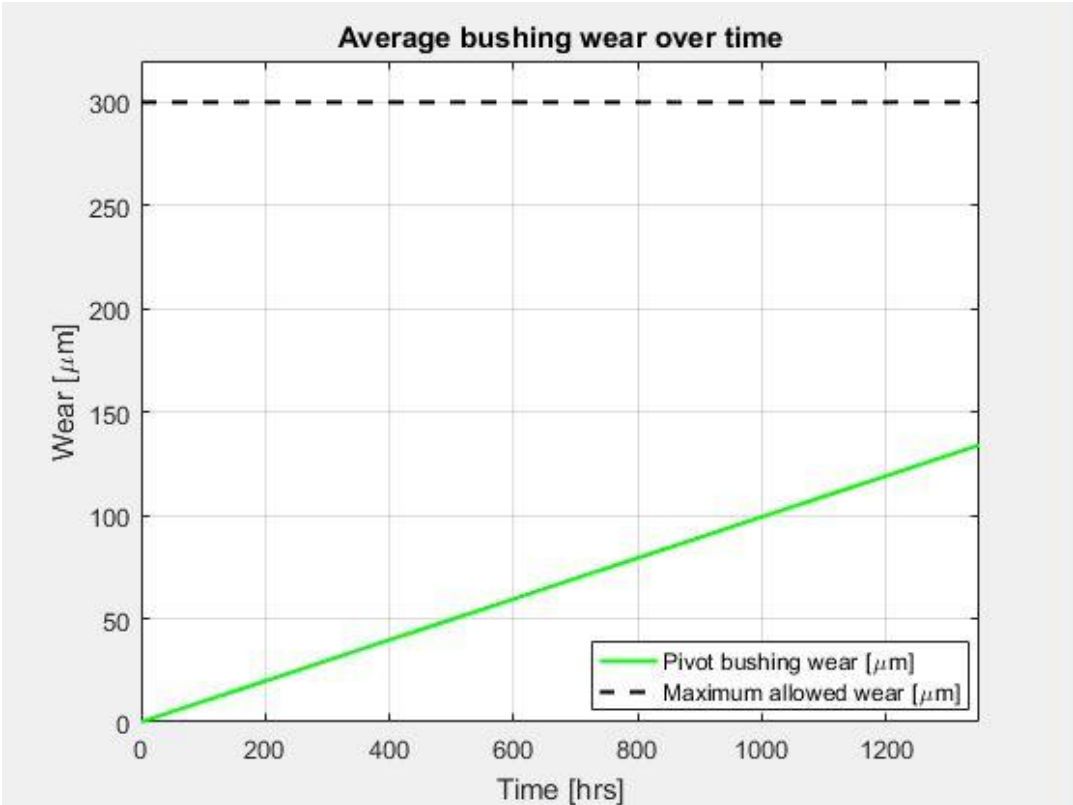


Figure 39. Flowchart section 5) output (2/3)

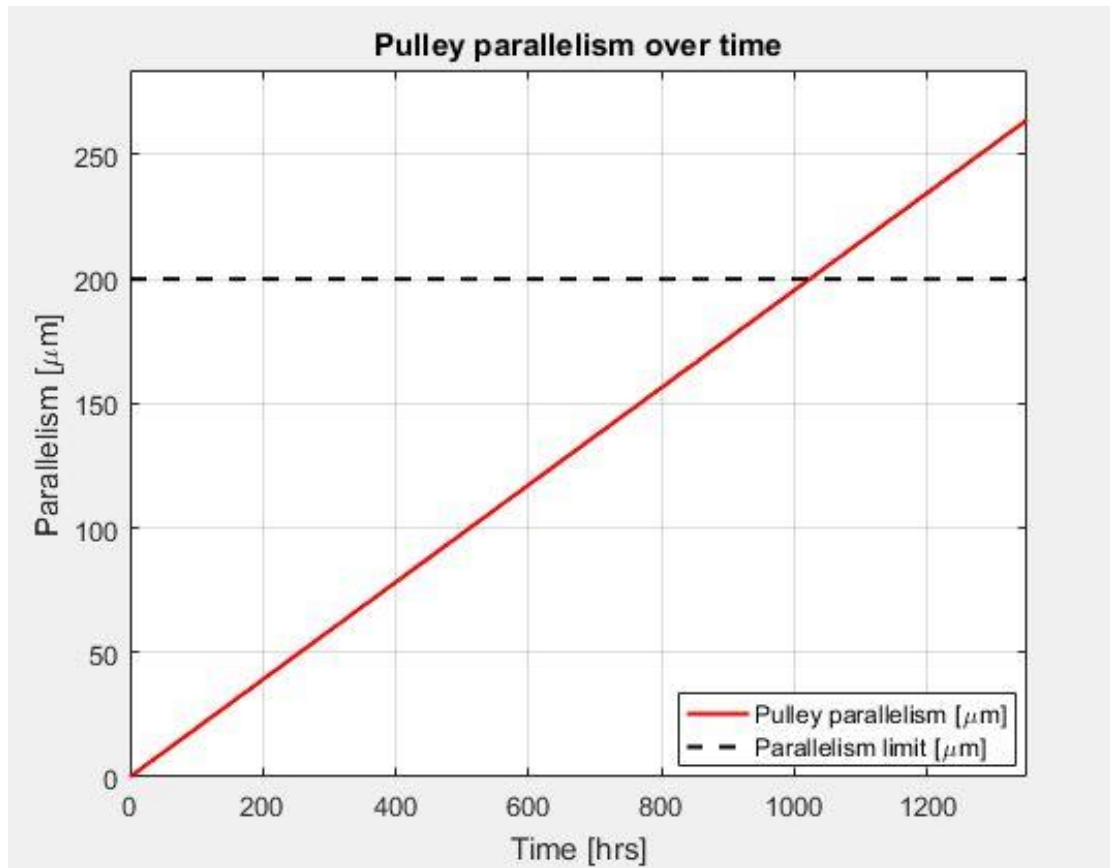


Figure 40. Flowchart section 5) output (3/3)

It is worth to notice that in figure 40, the graph line is in red in order to highlight the negative outcome.

5) Plastic friction element wear calculation

In a timing belt tensioner, the damping is obtained with the contribution of two phenomena: the friction that arises from the pivot rotation, the radial damping, and the friction due to the arm rotation, the axial damping. In this section the damping decay during the time will be investigated. The radial component is less dependent on time since, also in case of wear of the pivot bushing, being the radial force a function of external factors and being the materials always the same, the torque is quite constant. The axial damping component, instead, is heavily influenced by the time. In fact, this component is generated thanks to a cone spring that, exerting an axial force against the damper pad, compresses the axial stack-up of the tensioner. This compression generates a friction between the arm and the damper pad on one side and between the endcap spacer and the arm itself on the other side. The axial damping component can be expressed according to equation 9:

$$D_{AX} = F_{AX} * \phi_{plastic} * (R_{mdp} + R_{mes}) \quad (9)$$

where:

D_{AX} is the damping axial component [Nm]

F_{AX} is the axial force exerted by the cone spring [N]

R_{mdp} is the medium radius of the contact surface between the arm and the damper pad [m]

R_{mes} is the medium radius of the contact surface between the arm and the endcap spacer [m]

$\phi_{plastic}$ is the plastic friction coefficient [-]

The wear of the plastic elements generates an axial damping decay over time. This is due to the reduction of the thickness of these elements, that, in turn, brings to a lower force exerted by the cone spring, since the gap in which is positioned is growing in height. The axial damping component decreases until the cone spring detaches from the damper pad, exerting a null force on the axial stack-up. The wear of the plastic elements can be computed through equation 43:

$$w_{pfe} = w_{dp} + w_{es} \quad (43)$$

where:

w_{pfe} is the total wear of plastic friction elements [mm]

w_{dp} is the wear of the damper pad [mm]

w_{es} is the wear of the endcap spacer [mm]

The damper pad wear can be computed through equations 44, 45 and 46:

$$w_{dp} = \int k_{w\ plastic} * p_{dp}(w_{dp}) * v_{av\ dp} \quad (44)$$

$$p_{dp} = \frac{A_{c\ dp}}{F_{AX}} \quad (45)$$

$$v_{av\ dp} = (2 * \theta_{pp} * \pi * R_{m\ dp} * f) / 180 \quad (46)$$

where:

$k_{w\ plastic}$ is the constant of wear of plastic friction elements [mm*m*s/N]

p_{dp} is the pressure on the damper pad [N/m²]

v_{avdp} is the mean sliding speed of the damper pad [m/s]

$A_{c\ dp}$ is the area of the damper pad contact surface [m²]

θ_{pp} is the oscillation amplitude [deg]

f is the oscillation frequency [Hz]

Analogously, the endcap spacer wear can be computed thanks to equations 47, 48 and 49:

$$w_{es} = \int k_{w\ plastic} * p_{es}(w_{es}) * v_{av\ es} \quad (47)$$

where:

$$p_{es} = \frac{A_{c\ es}}{F_{AX}} \quad (48)$$

$$v_{av\ es} = (2 * \theta_{pp} * \pi * R_{m\ es} * f) / 180 \quad (49)$$

where:

p_{es} is the pressure on the endcap spacer [N/m²]

$v_{av\ es}$ is the mean sliding speed of the endcap spacer [m/s]

$A_{c\ es}$ is the area of the endcap spacer contact surface [m²]

The plastic friction elements dimensions are initialized as a function of the axial damping. Then, the simulation is run (the Simulink model is presented in picture 41). If the End Of Life (EOL) damping value is known, a check is performed in order to understand if this limit value is respected. If this is not the case and if the contact surfaces are not at maximum, these are incremented and simulation is run again. This step is repeated until the EOL damping value is respected, or until is possible to increase the contact surfaces. As an additional degree of freedom, the cone spring relaxation is introduced. In fact, the user has the possibility to introduce the setting losses, expressed in percentage of axial force lost and in how many hours it occurs. If the outcome of the simulation is positive, the plastic friction elements dimensions are printed in the excel file as outputs. Besides this, four graphs are produced in the Matlab environment (figures 42, 43, 44 and 45).

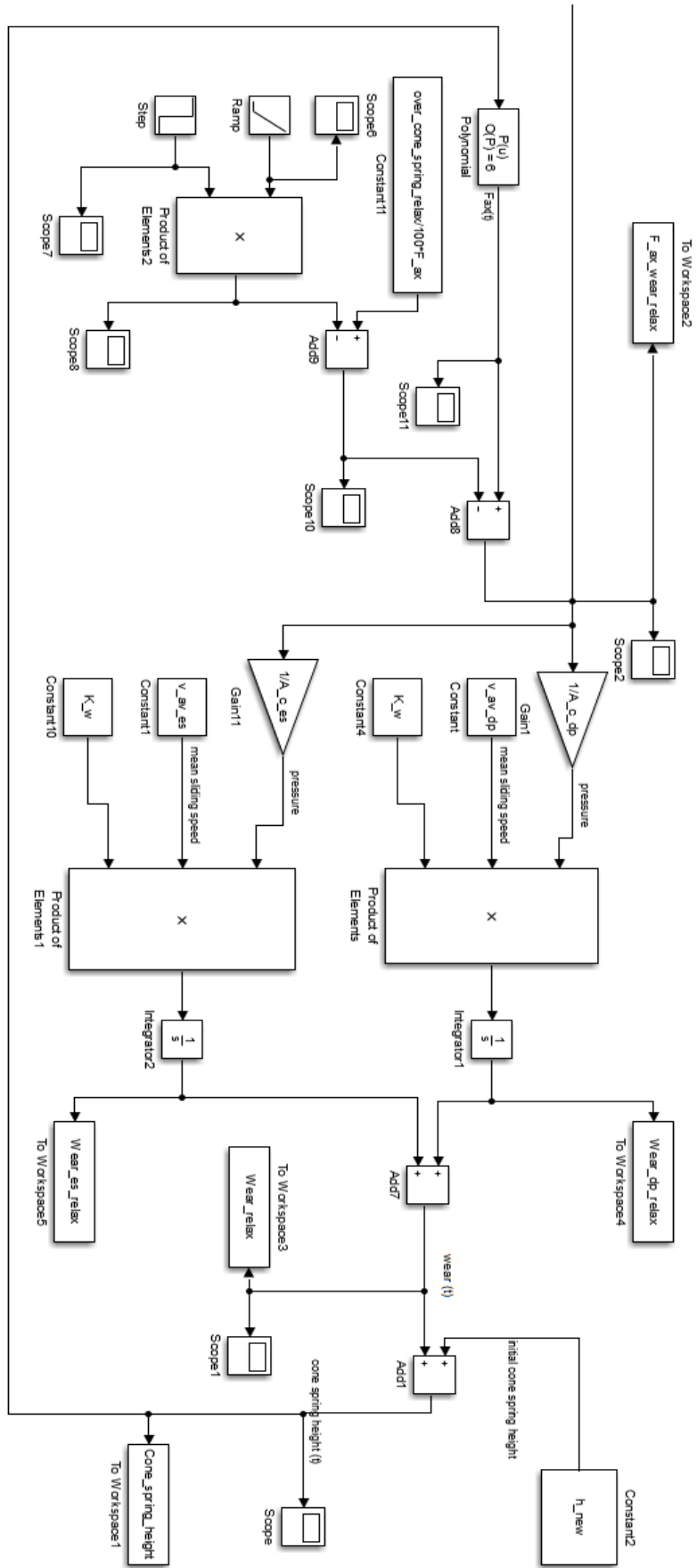


Figure 41. Plastic friction elements Simulink model

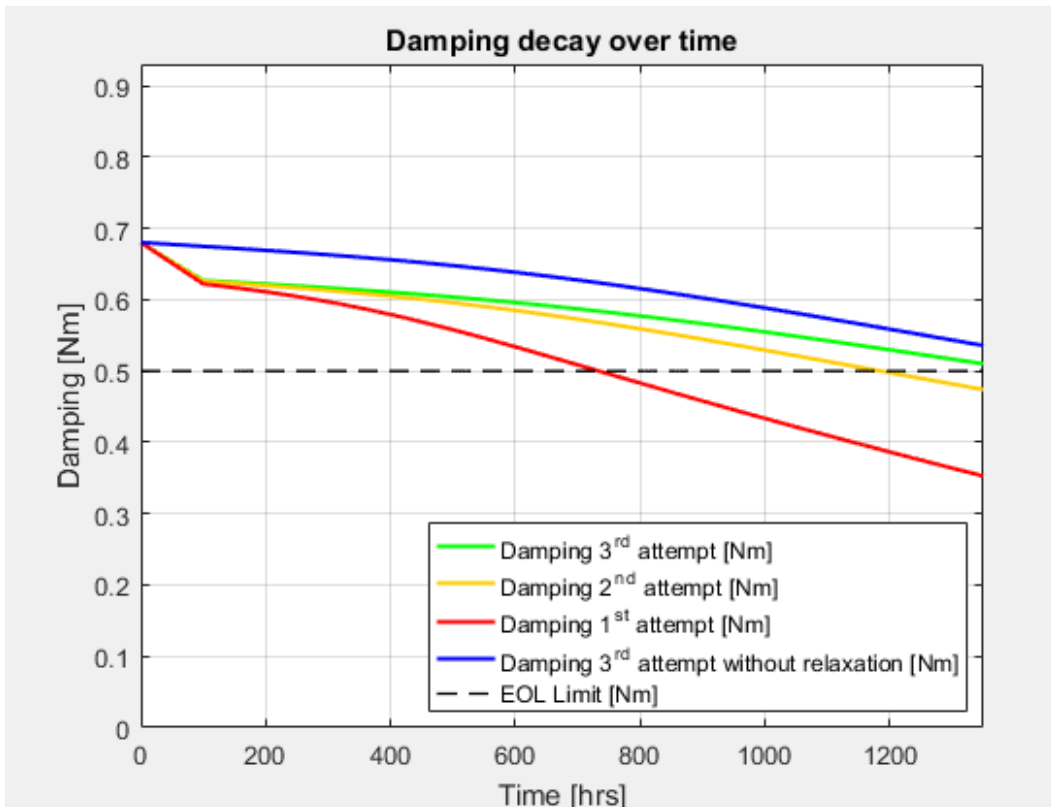


Figure 42. Flowchart section 6) output (1/5)

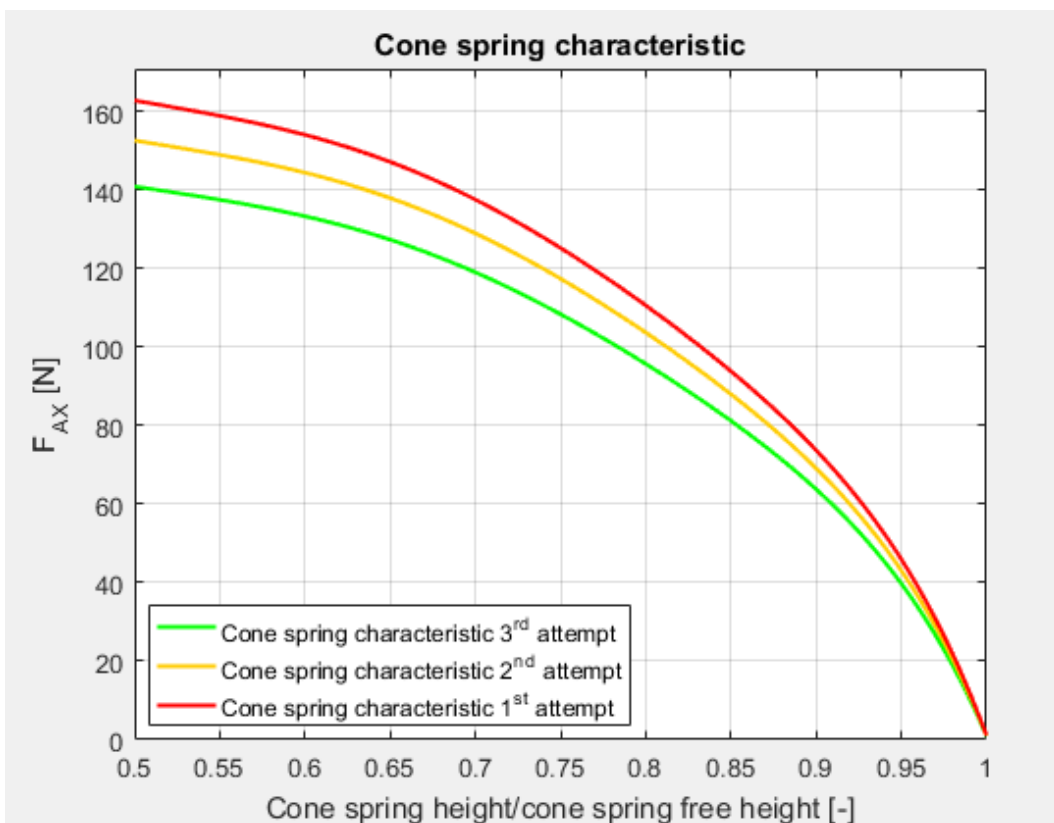


Figure 43. Flowchart section 6) output (2/5)

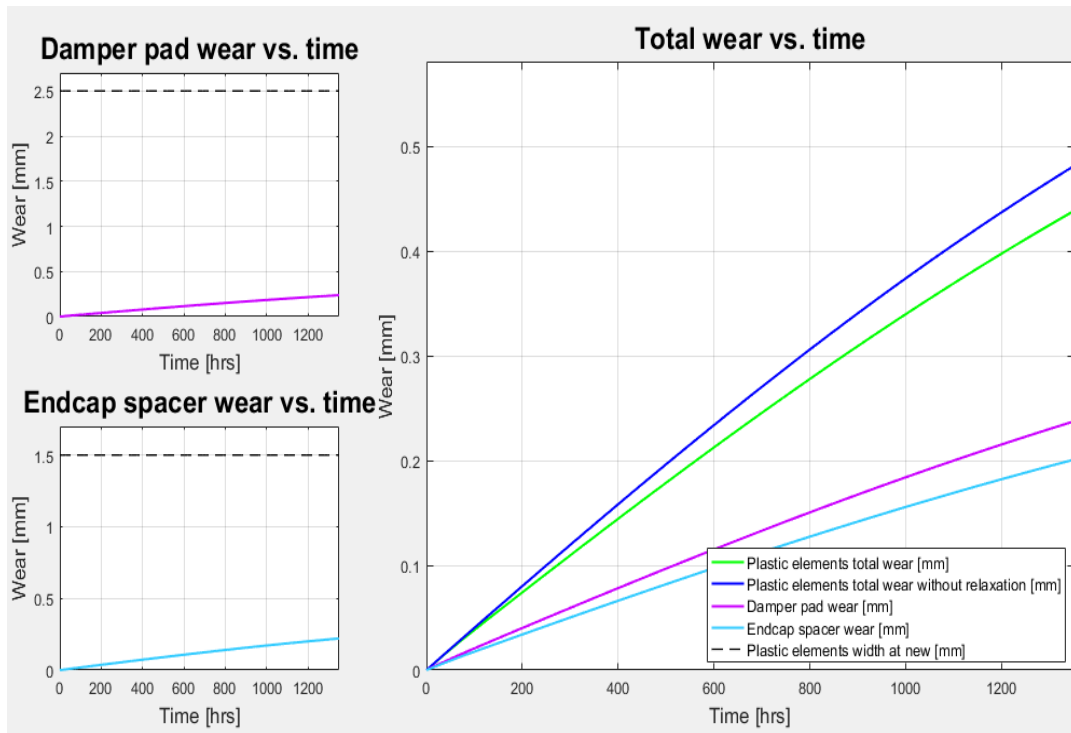


Figure 44. Flowchart section 6) output (3/5)

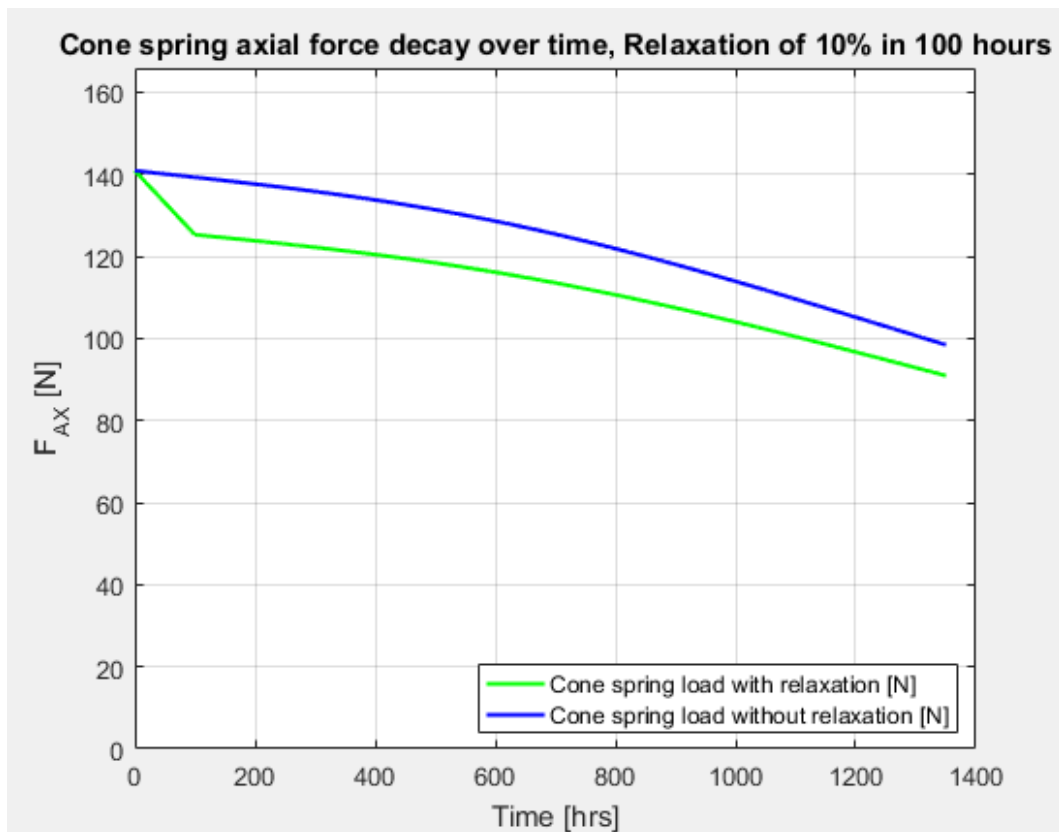


Figure 45. Flowchart section 6) output (4/5)

In the picture 42 the tensioner damping decay over time is represented. The curve depicted as 1st attempt is considering the plastic friction elements contact surfaces at minimum. Then, as explained above, they have been increased in two steps, reaching in this way the maximum contact surface. As it can be seen, either the 1st attempt, either the 2nd one, are resulting in an EOL damping below the threshold. The simulation corresponding to the 3rd attempt, instead, has a successful outcome, as it has been highlighted by the green colour. The blue line is representing the 3rd attempt simulation but neglecting the cone spring relaxation.

At this point, the attention can be moved to the following graph: here the cone spring characteristics are shown. By changing the plastic friction elements class, the medium radii of contact are changing, so, in order to obtain the same damping target, the cone spring axial force needs to be changed accordingly.

Then, the plastic friction elements wear has been considered. In fact, in the picture (44) the wear trend can be seen. In the subplots on the left there is the comparison between the width at new of the damper pad above and of the endcap spacer below with the wear during the test. In the subplot on the right, instead, the green line represents the total wear of the stack-up, which can be computed as the sum of the two contributions mentioned above, while the blue line represents the wear if the cone spring would experience a null relaxation. As a last graphical output of this section, the cone spring axial force decay over time can be seen. The blue curve is again taking into account the null cone spring relaxation. In fact, the force is decreasing in time only due to the spring gap growing in height due to wear. The green line, instead, shows the axial force trend accounting either for the effect just mentioned, either for the cone spring relaxation. Besides these graphical outputs, also plastic friction elements dimensions are computed and printed in the excel output column, as it is reported in the picture 46 represented here below.

Plastic friction elements		
Damper pad contact area	[mm ²]	460
Damper pad mean radius	[m]	0,013
Damper pad axial height	[mm]	3,5
Damper pad outern diameter	[mm]	31,5
Endcap spacer contact area	[mm ²]	490
Endcap spacer mean radius	[m]	0,014
Endcap spacer axial height	[mm]	1,5

Figure 46. Flowchart section 6) output (5/5)

6) Stack-up calculation (axial)

This step of the workflow is applied only to tensioners with axial damping. The cone spring axial force is a function of the cone spring gap height. The cone spring gap height can be computed as the pivot height, to which the endcap spacer, the arm and the damper pad heights must be subtracted. From an application to another one, the nominal value of these elements can change, but their tolerance with respect to the nominal value are fixed (shown in the table below), since they constitute a standard and they are represented in the table 6 here below:

Component	Tolerance [mm]
Pivot	± 0.07
Endcap spacer	± 0.05
Arm	± 0.05
Damper pad	± 0.05
Overall	± 0.22

Table 6. Tolerance value of cone spring gap height influencing elements

Since the cone spring gap height is the result of the tolerance chain between the above-mentioned elements, its tolerance is fixed too. The only degree of freedom is its nominal value. This degree of freedom is exploited by the cone spring supplier, in order to achieve the requested cone spring axial force.

7) Packaging constraints

In this workflow section the tensioner packaging issues are addressed. In fact, the constraints are considered, in order to detect the available space for each component of the tensioner. First of all, the middle plane belt height feasibility is checked. If a standard layout is considered, the maximum middle plane belt height must be compatible with the maximum pivot height (figure 47), respecting the condition stated by equation 50:

$$mpbh_{max} = h_{pivot_{max}} - \frac{w_{ballbearing}}{2} - h_{es} - h_e - h_{calking} \quad (50)$$

where

$mpbh_{max}$ is the maximum middle plane belt height [m]

$h_{pivot_{max}}$ is the maximum pivot height [m]

$w_{ballbearing}$ is the ball bearing width [m]

h_{es} is the endcap spacer height (if present) [m]

h_e is the endcap height [m]

$h_{calking}$ is the pivot height difference with respect to endcap needed to perform calking [m]

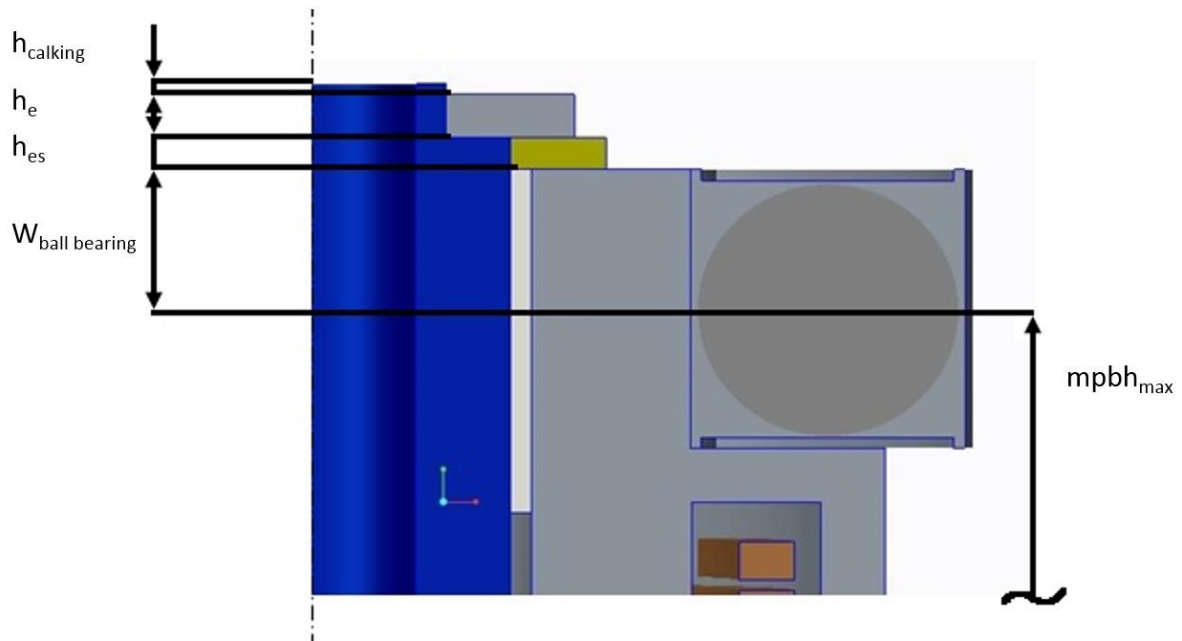


Figure 47. Maximum middle plane belt height definition (standard layout)

If the reverse layout is considered, instead, the minimum middle plane belt height must be investigated (figure 48), so the mathematical condition to be fulfilled becomes the equation 51:

$$mpbh_{min} = \frac{w_{ballbearing}}{2} + h_{es} + h_{pivot_{base}} \quad (51)$$

where:

$mpbh_{min}$ is the minimum middle plane belt height [m]

$h_{pivot\ base}$ is the height of the pivot base [m]

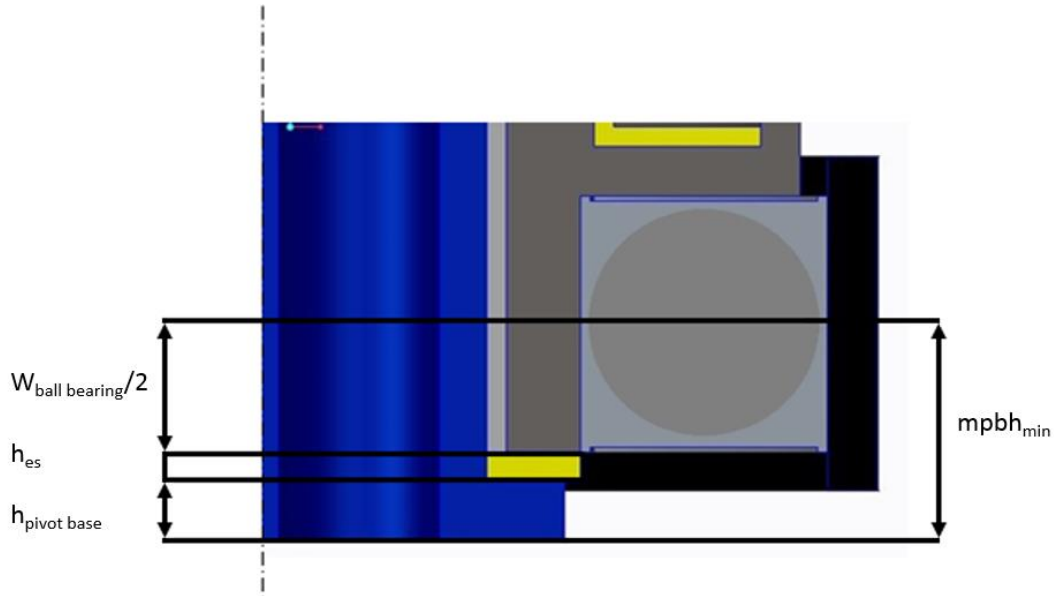


Figure 48. Minimum middle plane belt height definition (reversed layout)

Once the middle plane belt height feasibility has been confirmed, the spring housing dimensions are defined. In fact, its height, its external diameter and its internal diameter are evaluated. For what concerns the height, a distinction between standard and reverse layout must be performed again (as it can be seen in picture 49).

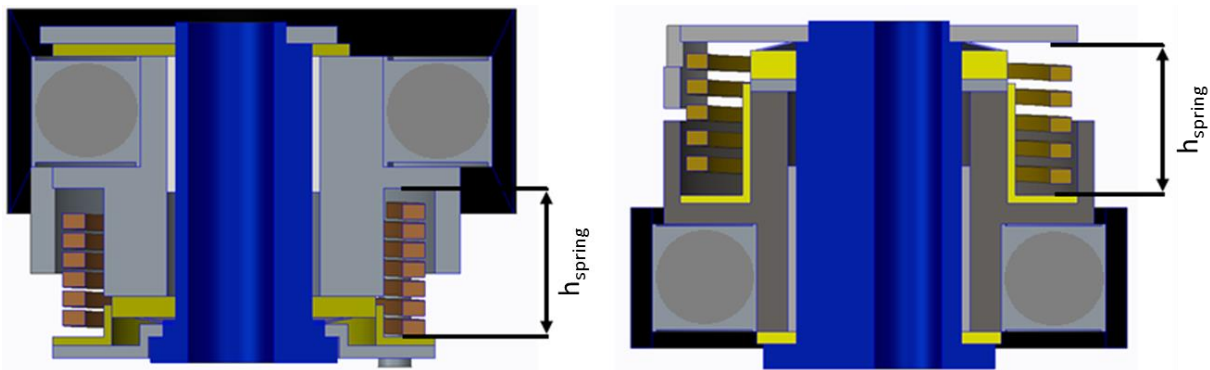


Figure 49. Spring housing height definition for standard (left) and reverse (right) layout

In case of standard layout, the spring cavity height can be computed through equation 52:

$$h_{spring} = mpbh - \frac{w_{ball\ bearing}}{2} - t_{arm} - t_{supp\ plate} - t_{spring\ bush} - \Delta_{crank-supp\ plate} \quad (52)$$

where

h_{spring} is the spring housing height [m]

$mpbh$ is the middle plane belt height [m]

t_{arm} is the axial thickness of the arm support of the ball bearing [m]

$t_{supp\ plate}$ is the support plate axial thickness [m]

$t_{spring\ bush}$ is the spring bushing axial thickness [m]

$\Delta_{crank-supp\ plate}$ is the gap between the crankcase and the support plate [m]

while, in case of reverse layout, the condition to be fulfilled is the equation 53:

$$h_{spring} = h_{pivot_{max}} - t_e - h_{calking} - t_{springbush} - mpbh - \frac{w_{ballbearing}}{2} - t_{arm} \quad (53)$$

where

t_e is the endcap thickness [m]

Once the axial spring housing dimension has been defined, the attention can be moved to its radial dimensions. In fact, its external and internal diameters must be evaluated.

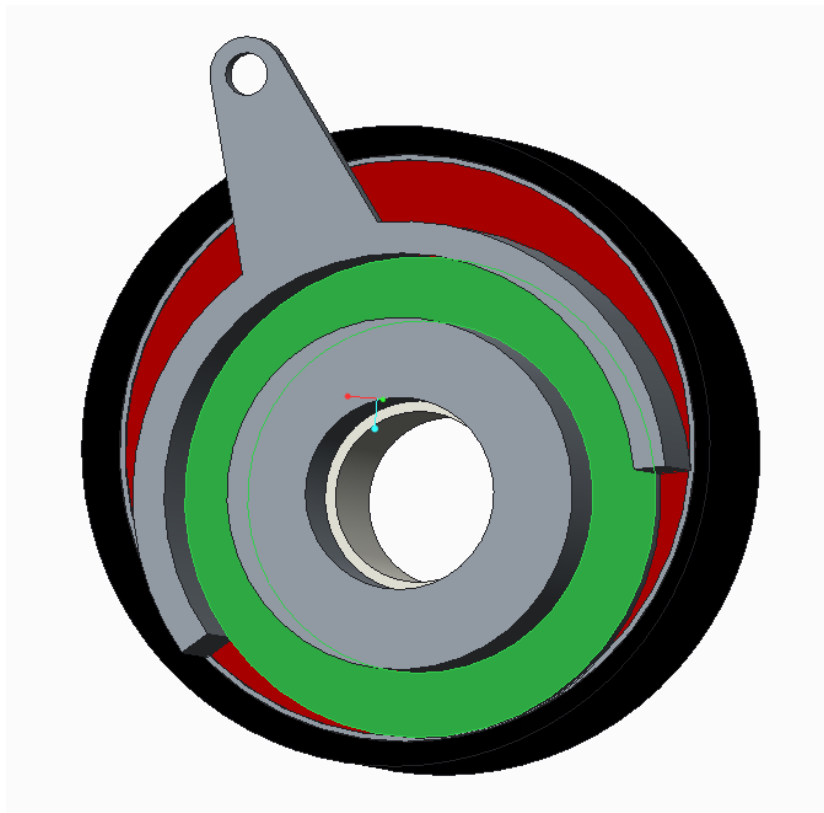


Figure 50. Spring housing (highlighted in green) radial constraints

The external diameter is computed according to equation 54:

$$\varnothing_{ext\ housing} = \varnothing_{ball\ bearing\ ext} - 2 * l_{arm} \tag{54}$$

where

$\varnothing_{ext\ housing}$ is the spring housing external diameter [m]

$\varnothing_{ball\ bearing\ ext}$ is the ball bearing external diameter [m]

l_{arm} is the working arm length [m]

The spring housing internal diameter, instead, has to provide a support for the spring itself in such a way that it is aligned with the lower constraints. The aim is to maintain the spring axis aligned with the tensioner one. This aspect is translated into an internal diameter equal to the spring bushing upper part external one, as it can be seen in the figure 51 here below (the main spring has been removed for clarity).

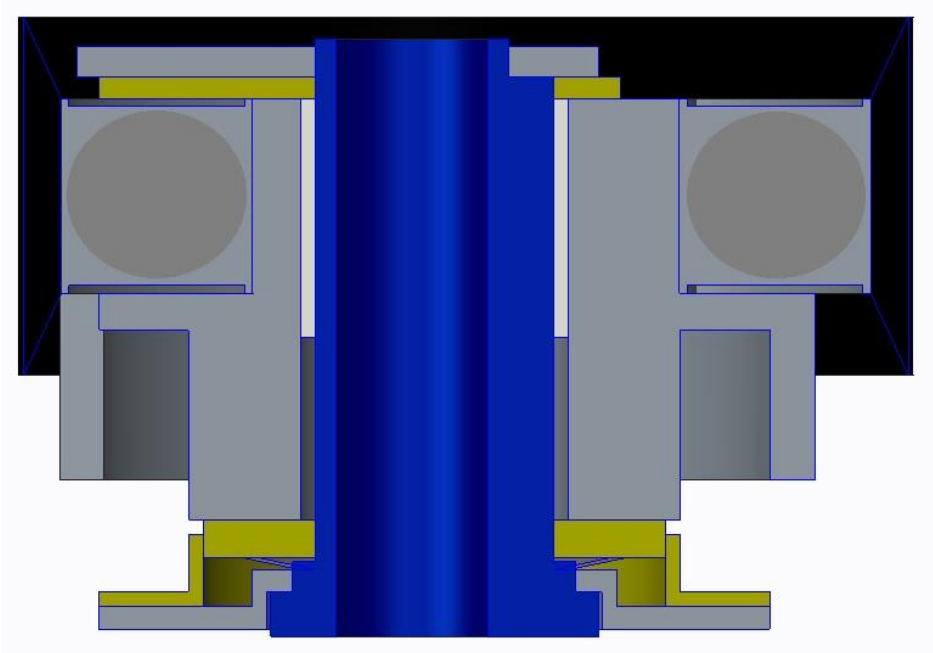


Figure 51. Section of a timing belt tensioner

8) Cone spring calculation

This step of the workflow is applied only to tensioners with axial damping.

As explained above, in order to introduce the axial damping a cone spring is implemented. This solution is preferable, since it is possible to reach quite high loads with a limited working space. Besides this, another advantage of this solution is the possibility to choose the spring characteristic. In fact, it can be linear, or regressive; in this last case the curvature of the spring characteristic can be modified acting on the spring dimensions (see picture 52). Finally, the shape of the spring (a cone, as the name suggests) forces the load transmission to be concentric.

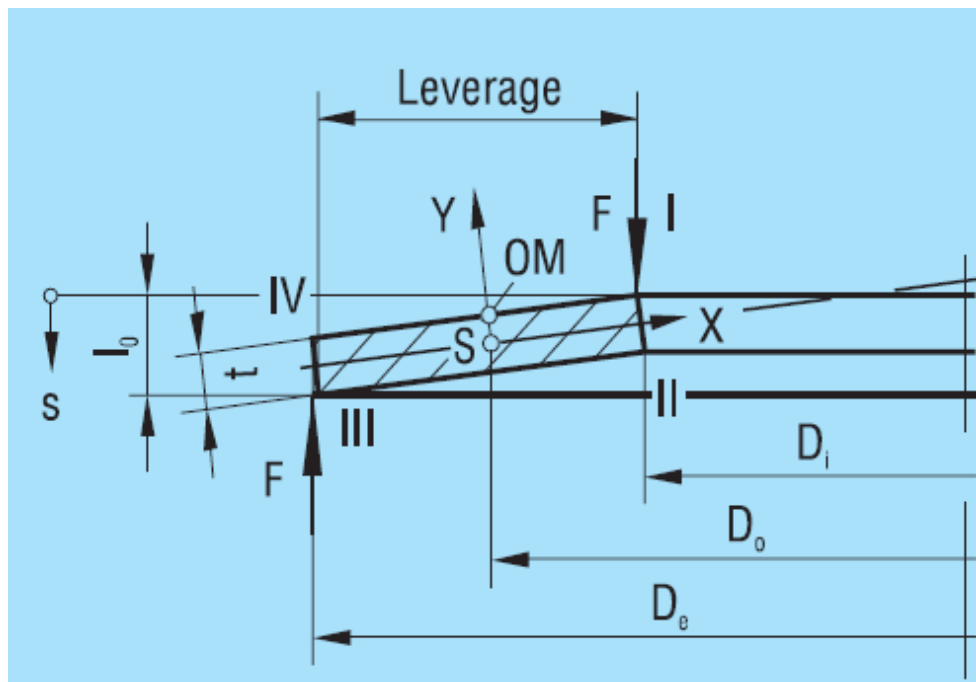


Figure 52. Section of a cone spring

Three fundamental parameters have to be considered, expressed in equations 55, 56 and 57:

$$\delta = \frac{D_e}{D_i} \quad (55)$$

where

δ is the cone spring diameter ratio [-]

D_e is the cone spring external diameter [m]

D_i is the cone spring internal diameter [m]

$$\zeta = \frac{h_0}{t} = \frac{l_0 - t}{t} \quad (56)$$

where

ζ is the cone spring aspect ratio [-]

h_0 is the unloaded cone spring cone height [m]

t is the cone spring thickness [m]

l_0 is the unloaded cone spring height [m]

$$th_{CS} = \frac{D_e}{t} \quad (57)$$

where

th_{CS} is the cone spring thinness [-]

Cone spring supplier experience permits to individuate a range containing optimal values for each of the above listed three parameters; they are shown in the table 7.

Parameter	Optimal range	
	From	To
δ [-]	1.8	2.4
h_0/t [-]	0.45	1.2
D_e/t [-]	18	42

Table 7. Cone spring fundamental parameters optimal range

Defined as F_c the axial force that the cone spring is exerting at a deflection equal to its initial cone height, the h_0/t parameter influence on the cone spring characteristic can be seen in the picture 53, shown here below.

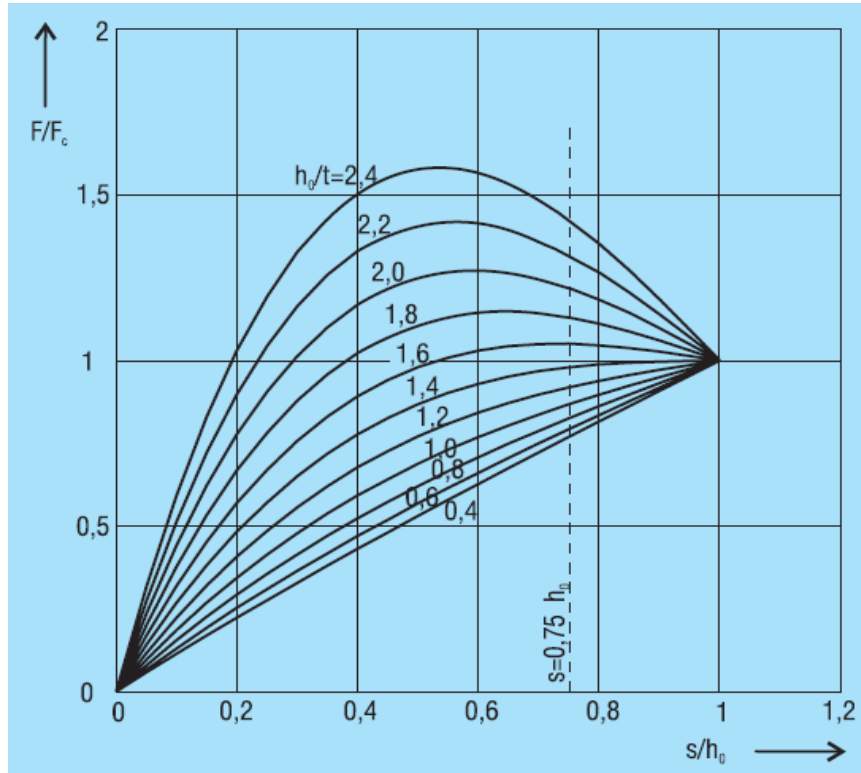


Figure 53. Cone spring characteristic as a function of h_0/t

Some values of the h_0/t ratio bring to particular cone spring characteristic. In fact, if the ratio assumes a value equal to 0,4, the spring presents a linear characteristic. Then, for a ratio equal to $\sqrt{2}$, the force vs. displacement curve approaches the complete spring deflection with a horizontal tangent. This particular situation is quite desirable if the goal is to obtain an as constant as possible load for a given working height variation (this type of spring is implemented in the timing belt tensioners to obtain a constant damping value at new). For growing h_0/t ratios, the cone spring characteristic is more and more regressive.

The influence of the h_0/t value on the tensioner damping decay over time has been investigated through a durability test simulation. Five different cone springs have been simulated. They have been modelled in order to obtain the same free height and the same force value when the spring deflection is equal to the initial cone height (figure 54). In this way the five cone springs characteristics present equal starting and ending points. Only the curvature between these two conditions is changing, replying in this way the situation depicted in figure 53 presented above. The five cone springs have:

- $h_0/t = 0,4$ (to obtain a linear characteristic)
- $h_0/t = 1,0$ (regressive characteristic with positive derivative for $s=h_0$)
- $h_0/t = 1,4$ (regressive characteristic with null derivative for $s=h_0$)
- $h_0/t = 1,8$ (regressive characteristic with negative derivative for $s=h_0$)
- $h_0/t = 2,2$ (regressive characteristic with negative derivative for $s=h_0$)

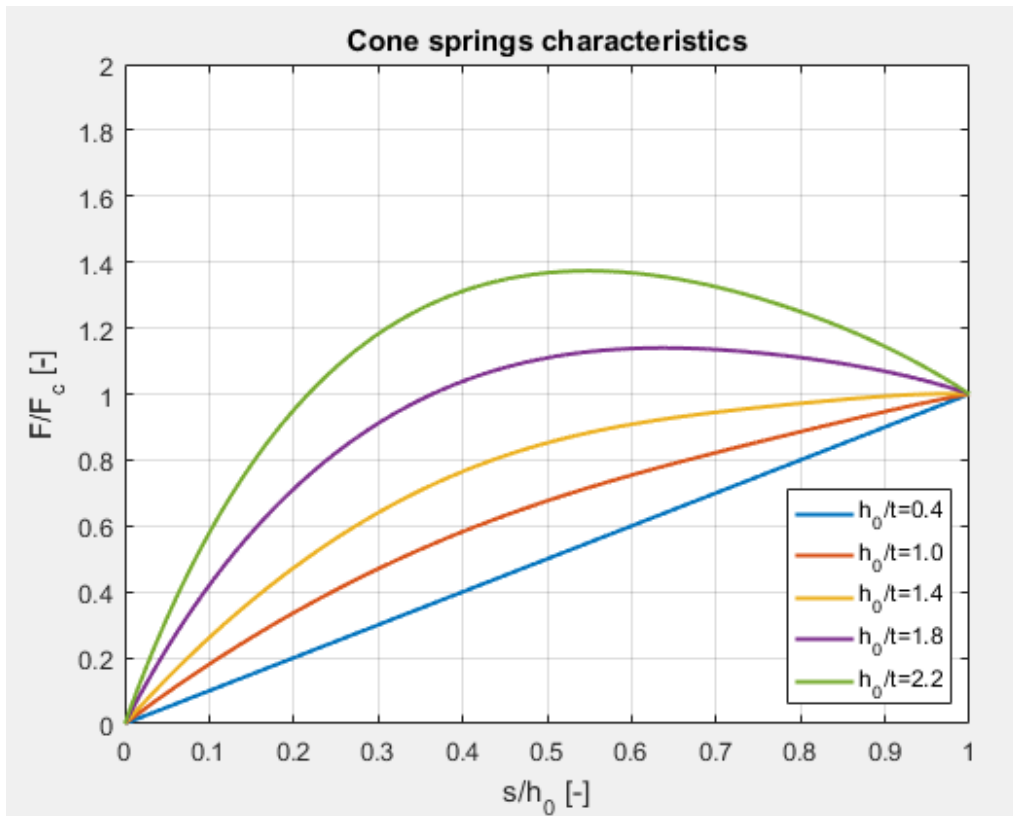


Figure 54. Cone spring characteristics considered in the simulation

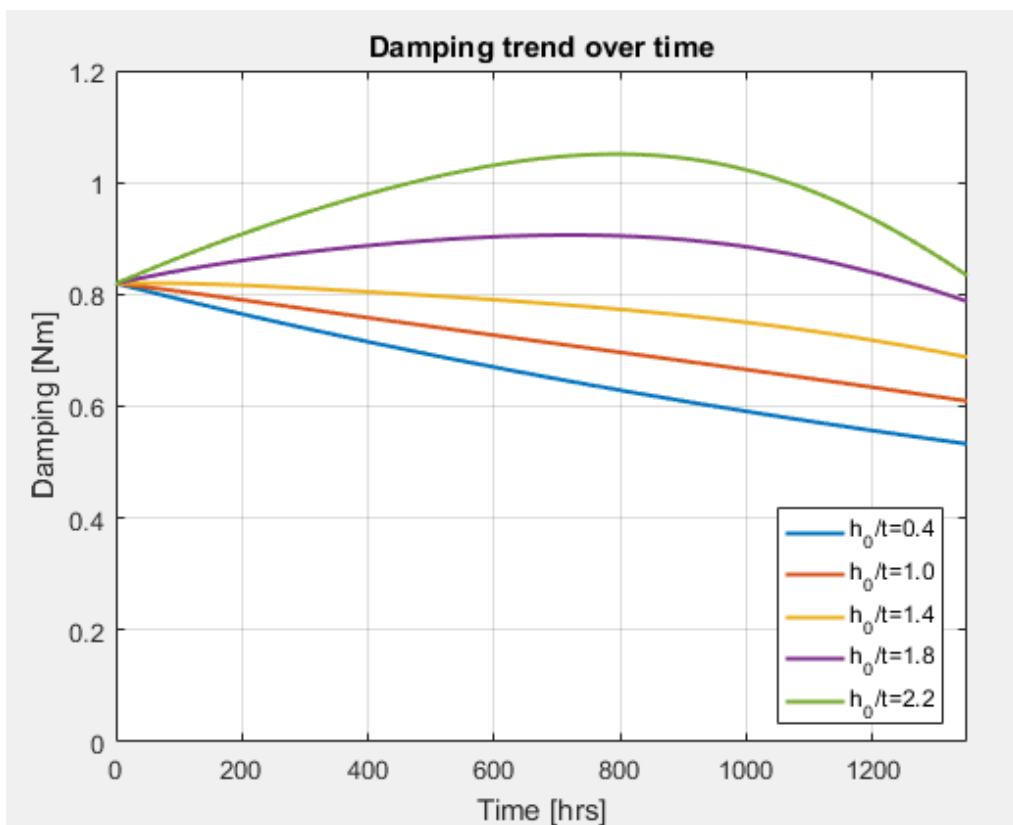


Figure 55. Damping trend over time as a function of the h_0/t parameter

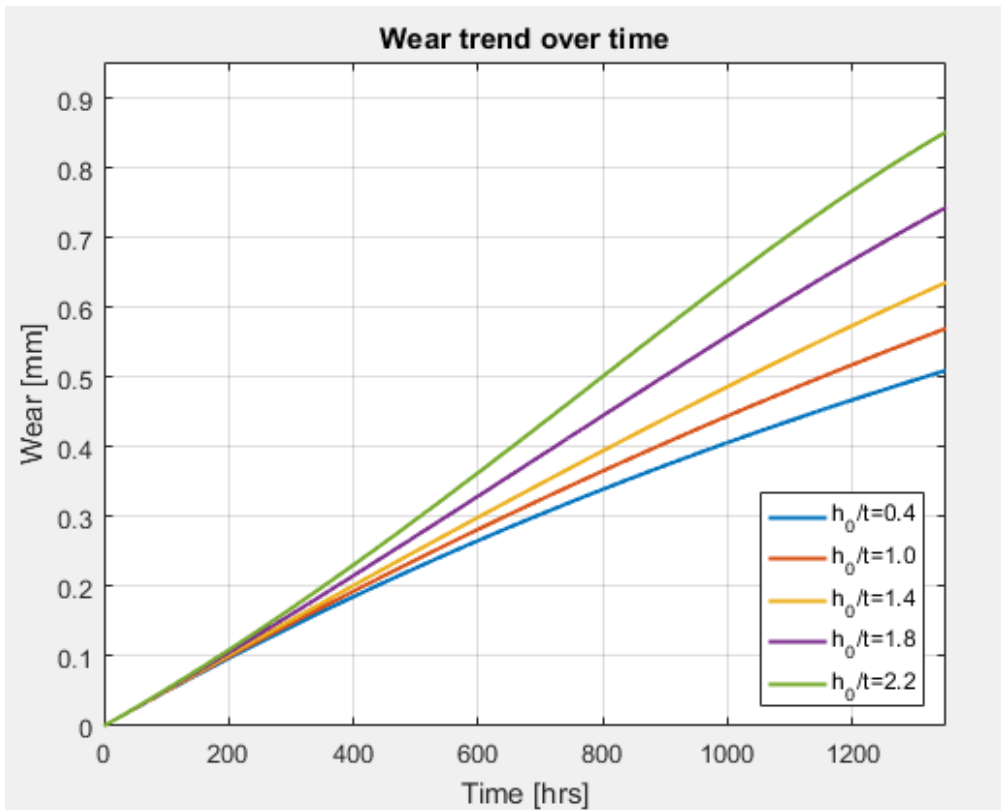


Figure 56. Wear trend over time as a function of the h_0/t parameter

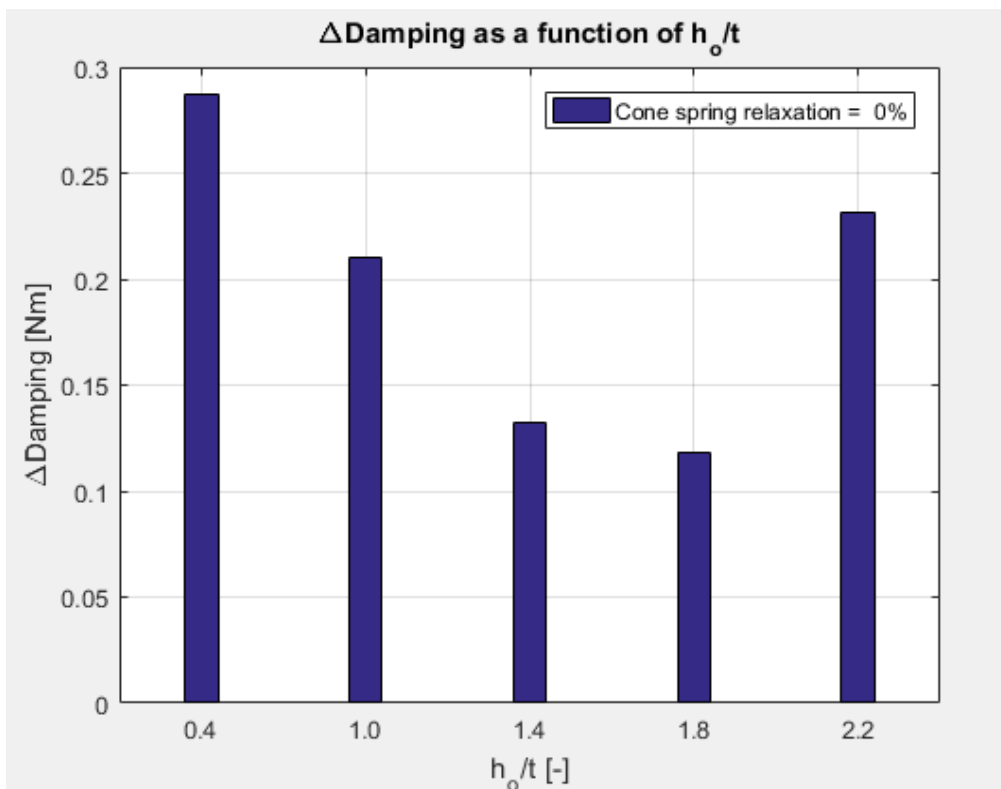


Figure 57. Damping variation during durability test simulation as a function of cone spring aspect ratio

From the picture 56, it can be seen that there is a substantial difference in terms of wear at the end of the durability test, if a different cone spring characteristic is implemented. In particular, for h_0/t equal to 2.2, the total wear (damper pad plus endcap spacer) at 1250 hrs is almost twice the value reached by considering the linear characteristic. This is due to the higher average force experienced by the cone spring, which is in turn translated in higher average pressures on plastic friction elements. Moving the attention to the picture 55, it can be seen that, despite the highest wear, the h_0/t equal to 2.2 permits to reach the higher tensioner damping value at the end of the durability test simulation (very similar to starting value). This beneficial aspect is counteracted by a high damping variation (which can be appreciated in picture 57, introducing in this way the need for a narrower damping tolerance in production. By considering, instead, the cone spring with aspect ratio equal to 0.4, the lowest wear is obtained. Besides this, the highest tensioner damping variation is obtained as well. This solution is, then, the worst.

Moving the attention to the cone spring with aspect ratio equal to 1,4, it is worth to notice the horizontal tangent of the force/displacement characteristic in correspondence of maximum deflection (friction plastic elements at maximum width). This situation represents the tensioner at new and brings to the lowest damping variation (almost null) in the first 100 hours of the durability test. Since the goal is to reach an as stable as possible tensioner damping over time, looking again at the figure 57, the outcome of the simulation is that the best solution is the cone spring with an aspect ratio equal to 1,8 in case of a cone spring that does not experience relaxation.

In order to account for the cone spring relaxation effect, it has been introduced in the simulation with two different values:

- 5% in 100 hours
- 10% in 100 hours

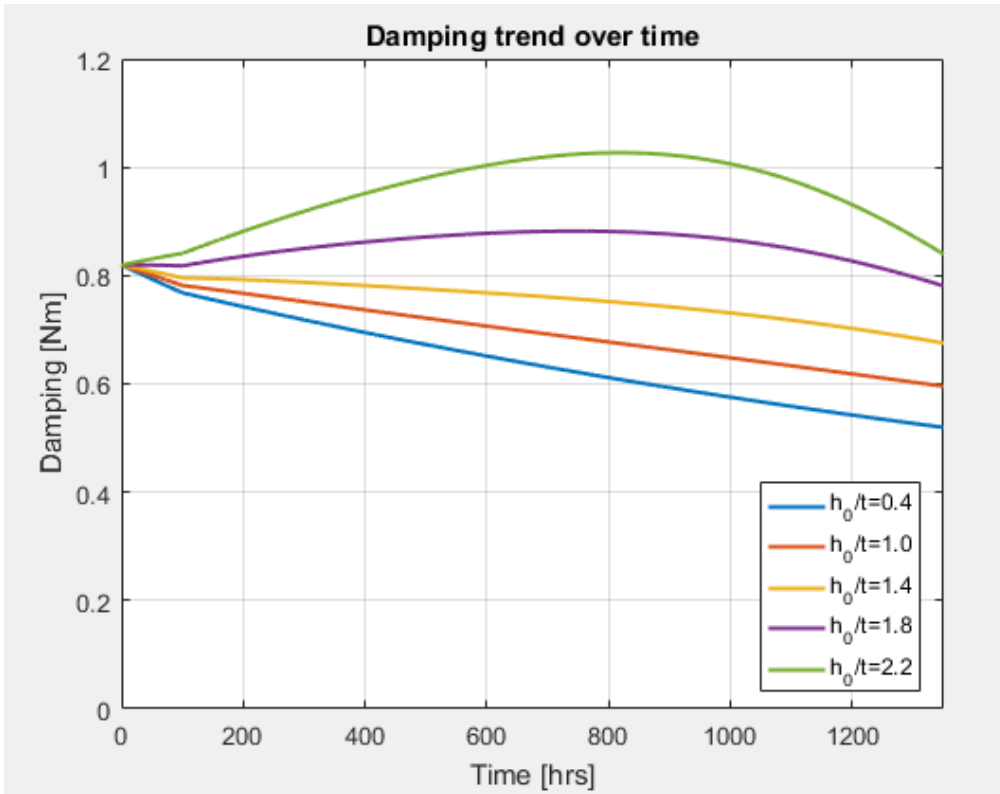


Figure 58. Damping trend over time as a function of the h_0/t parameter (cone spring relaxation: 5% in 100hrs)

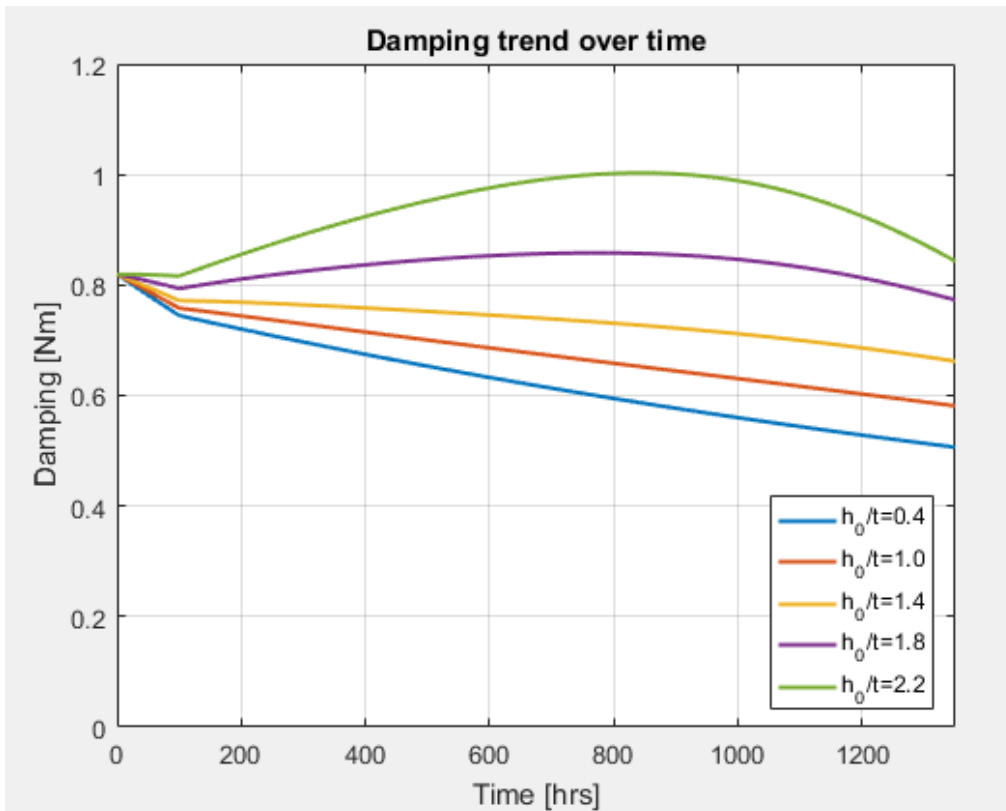


Figure 59. Damping trend over time as a function of the h_0/t parameter (cone spring relaxation: 10% in 100hrs)

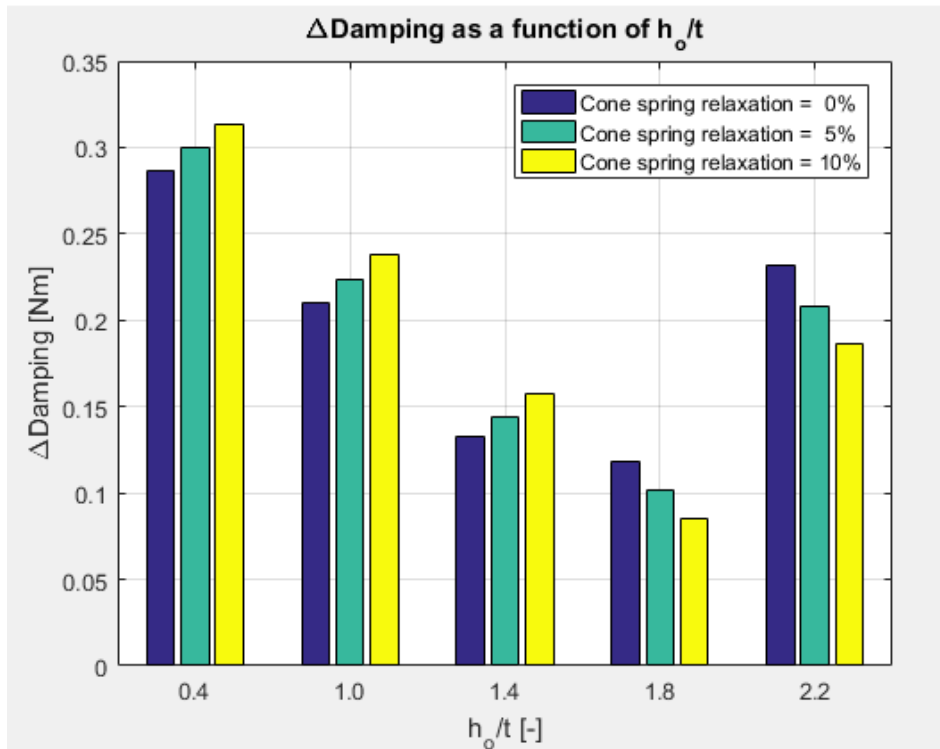


Figure 60. Damping variation during durability test simulation as a function of cone spring aspect ratio

Graphs showing cone springs characteristics and wear trend over time with 5% and 10% cone spring relaxation have not been represented since there are no appreciable differences with ones neglecting the relaxation. By looking at figure 58, it can be seen that the 5% cone spring relaxation is balanced by the cone spring characteristic with aspect ratio 1.8. The same phenomenon occurs with the 10% cone spring relaxation, but the balance is achieved with a h_0/t ratio equal to 2.2 (see figure 59).

The summary of the outcomes of the simulations can be found in picture 60. Here the maximum damping variation during the durability test simulation has been plotted as a function of the cone spring aspect ratio. As it can be seen, the cone spring with aspect ratio 1.8 results to be the best solution, bringing to the lowest damping variation over time. This is true for all cone spring relaxation levels considered. In particular, the cone spring setting losses have a beneficial influence on the tensioner damping variation for aspect ratios equal to 1.8 or bigger. Comments done until now hold for plastic friction elements made in PPA+10%CF+10%AR+PTFE, arm in die casted aluminium and endcap in nickel coated steel. Under the hypothesis of changing plastic friction elements material, the simulations have been repeated. In fact, two different materials have been introduced for the damper pad and for the endcap spacer:

- Material more resistant to wear (constant of wear equal to the half of the current one)
- Material less resistant to wear (constant of wear equal to twice the current one)

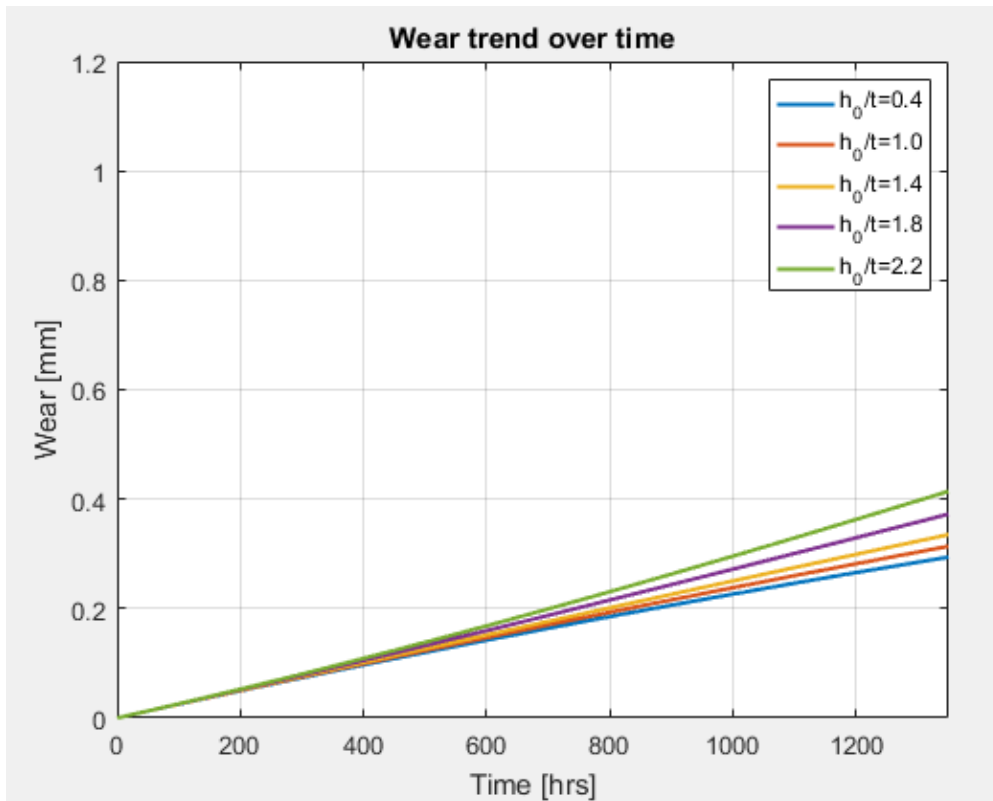


Figure 61. Wear trend over time as a function of the h_0/t parameter ($\frac{1}{2} * K_w plastic$)

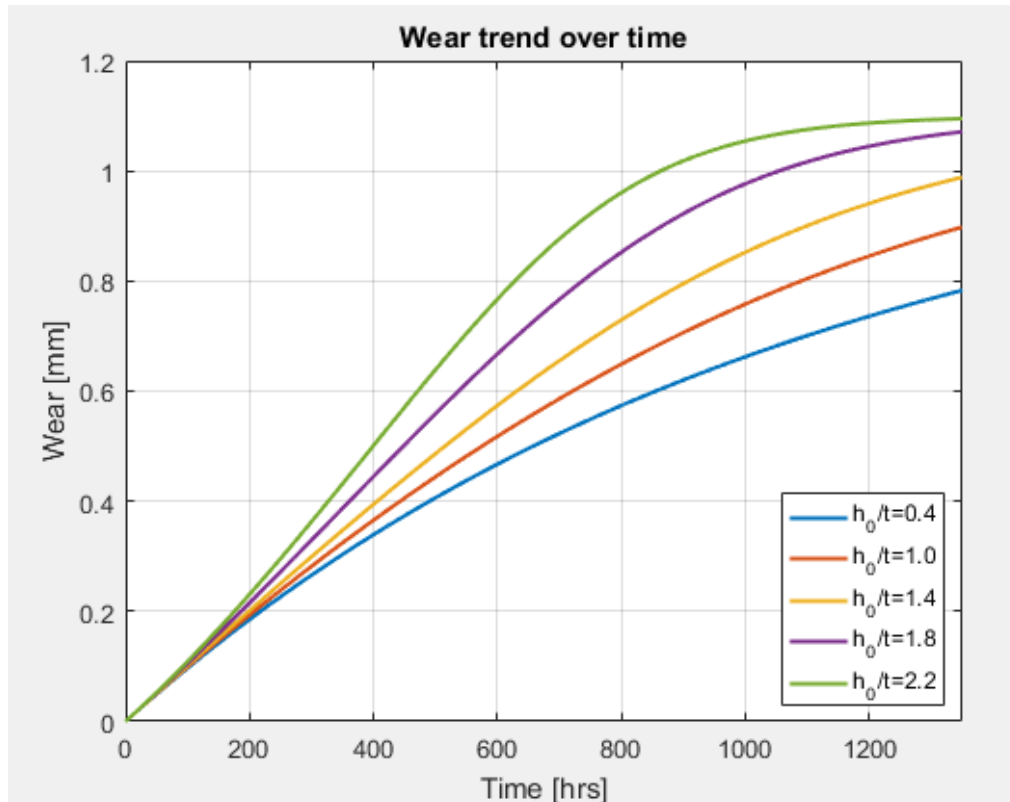


Figure 62. Wear trend over time as a function of the h_0/t parameter ($2 * K_w plastic$)

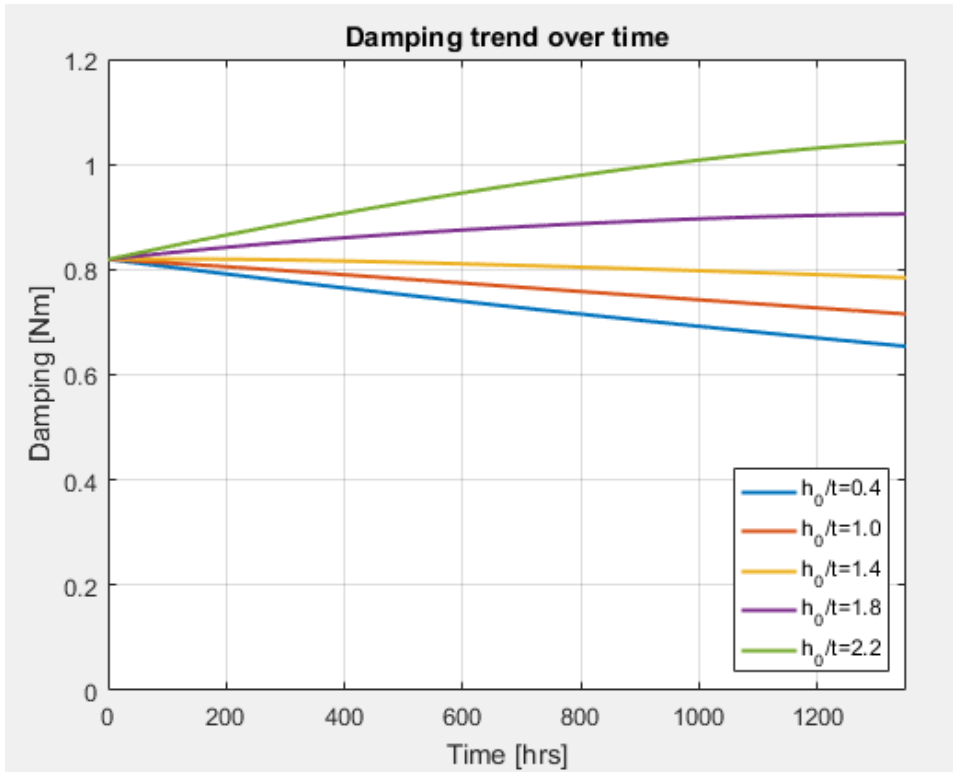


Figure 63. Damping trend over time as a function of the h_0/t parameter (cone spring relaxation: 0%, $\frac{1}{2} * K_w plastic$)

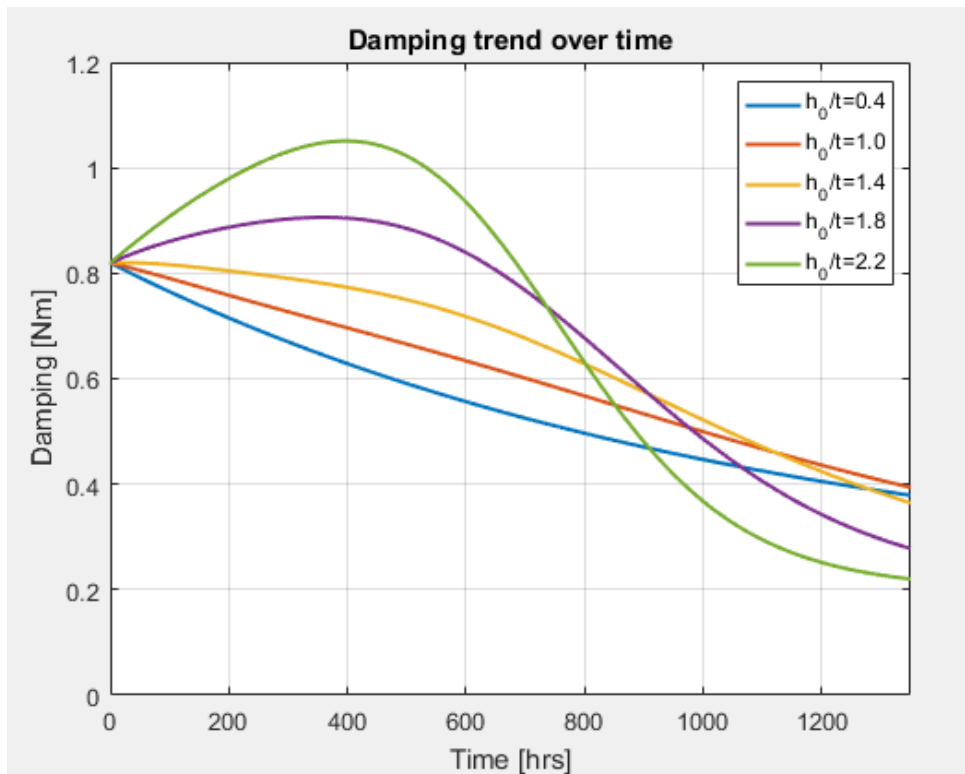


Figure 64. Damping trend over time as a function of the h_0/t parameter (cone spring relaxation: 0%, $2 * K_w plastic$)

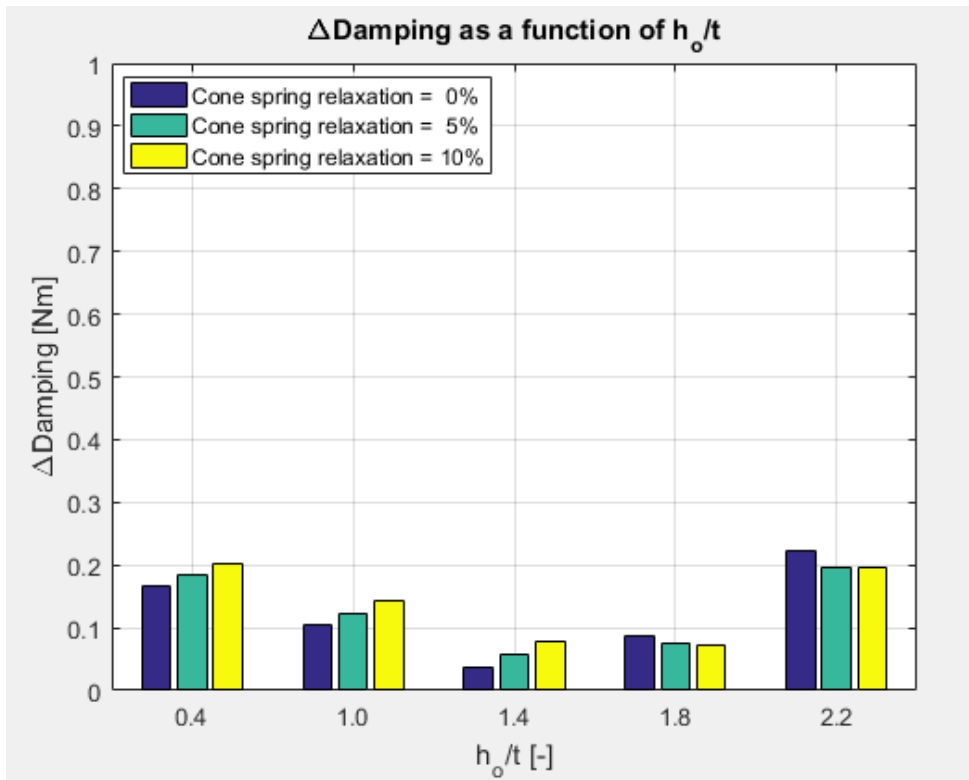


Figure 65. Damping variation during durability test simulation as a function of cone spring aspect ratio ($\frac{1}{2} * K_w$ plastic)

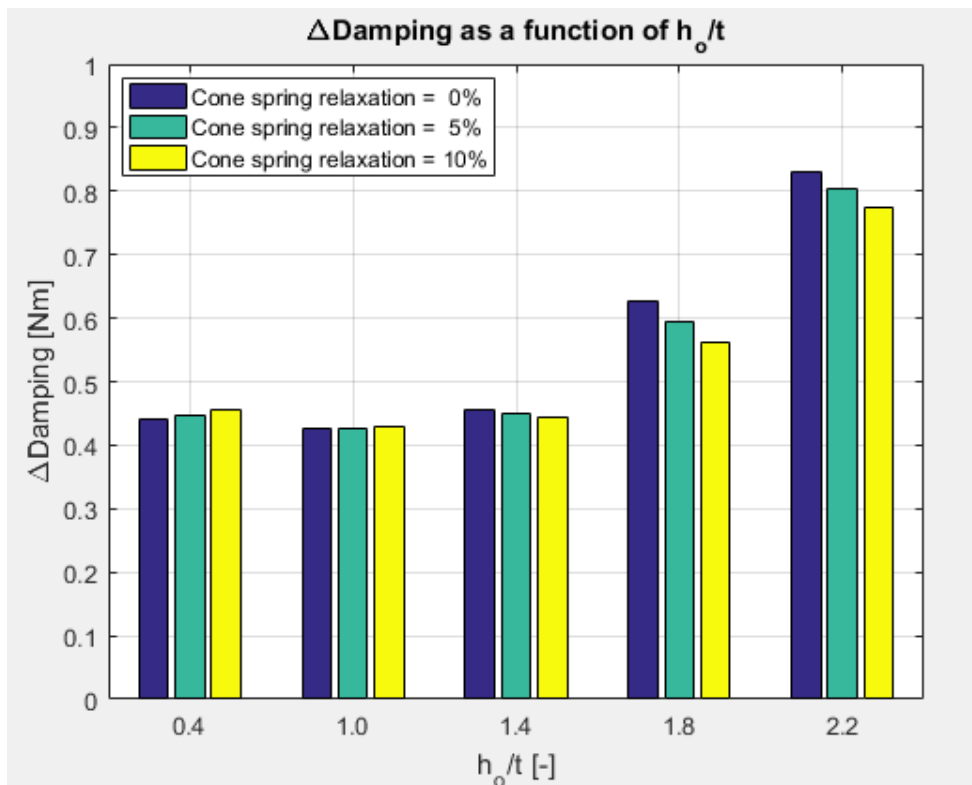


Figure 66. Damping variation during durability test simulation as a function of cone spring aspect ratio ($2 * K_w$ plastic)

The first result that comes out from the simulation is the different wear level. As it can be seen from picture 61, the harder material wear is slightly influenced by the cone spring characteristic. For the softer material (figure 62), instead, besides the higher wear average value (as it was expected), is interesting to notice the asymptote highlighted by the most regressive spring. This situation occurs since the cone spring is exerting a very low force on plastic elements. This means that the axial damping of the tensioner is near to the null value. This is confirmed by picture 64, in which a damping asymptote can be identified as well. The asymptote value corresponds to the radial damping of the tensioner itself. Since it is depending on tensioner geometrical data, it is independent from the cone spring aspect ratio. In fact, this parameter influences only the time at which it is approached. Then, the picture 65 and 66 are presented. They have the same scale in order to highlight the remarkable damping difference. The final outcome of this simulation is that, in order to achieve a more stable tensioner damping over time, is better to implement a more wear resistant material for plastic friction components. For the softer material, the most advantageous aspect ratio is the one equal to 1.0, independently from the cone spring relaxation (see figure 66), while, for the harder material, the most advantageous aspect ratio choice is 1.4 for cone spring relaxation equal to 0% or 5%. If the cone spring relaxation is equal to 10%, instead, a h_0/t equal to 1.8 has to be selected (see figure 65). Particular care must be taken to the stress level. In fact, as it grows, the cone spring experiences setting losses always more and more evident. The stress level in the material can be computed analytically, thanks to the Almen and László theory. This theory assumes that the cone spring deflection occurs due to the rotation of the element around a diameter D_0 , which can be computed according to equation 58:

$$D_0 = \frac{D_e - D_i}{\ln \frac{D_e}{D_i}} \quad (58)$$

The assumptions of this theory are:

- linear Young's modulus
- rectangular cross-section
- deflection remaining in one plane during the complete stroke

The reference stress value can be computed as a function of the cone spring dimensional feature, through equations 59, 60, 61, 62 and 63:

$$\sigma_{OM} = - \frac{4E}{1-\mu^2} * \frac{t^2}{K_1 * D_e^2} * K_4 * \frac{s}{t} * \frac{3}{\pi} \quad (59)$$

where:

$$K_1 = \frac{1}{\pi} * \frac{\left(\frac{\delta-1}{\delta}\right)^2}{\frac{\delta+1}{\delta-1} \frac{2}{\ln\delta}} \quad (60)$$

$$K_4 = \sqrt{-\frac{C_1}{2} + \sqrt{\left(\frac{C_1}{2}\right)^2 + C_2}} \quad (61)$$

where:

$$C_1 = \frac{\left(\frac{t'}{t}\right)^2}{\left(\frac{1}{4} * \frac{l_0}{t} - \frac{t'}{t} + \frac{3}{4}\right) \left(\frac{5}{8} * \frac{l_0}{t} - \frac{t'}{t} + \frac{3}{8}\right)} \quad (62)$$

$$C_2 = \frac{C_1}{\left(\frac{t'}{t}\right)^3} * \left[\frac{5}{32} \left(\frac{l_0}{t} - 1\right)^2 + 1 \right] \quad (63)$$

where:

σ_{OM} is the reference stress [MPa]

E is the Young's Modulus [MPa]

μ is the Poisson's ratio [-]

s is the spring deflection [mm]

t' is the reduced thickness (contact flats springs) [mm]

In order to avoid any lateral movement of the cone spring, a guide element must be present. In a timing belt tensioner this function is accomplished by the pivot. A prescribed clearance has to be respected between the pivot outer diameter and the cone spring inner diameter (shown in table 8), in order to avoid the cone spring jamming.

Internal diameter [mm]	Clearance
< 18	0.2
18 ≤ D _i < 22	0.3
22 ≤ D _i < 28	0.4

Table 8. Cone spring-pivot clearance

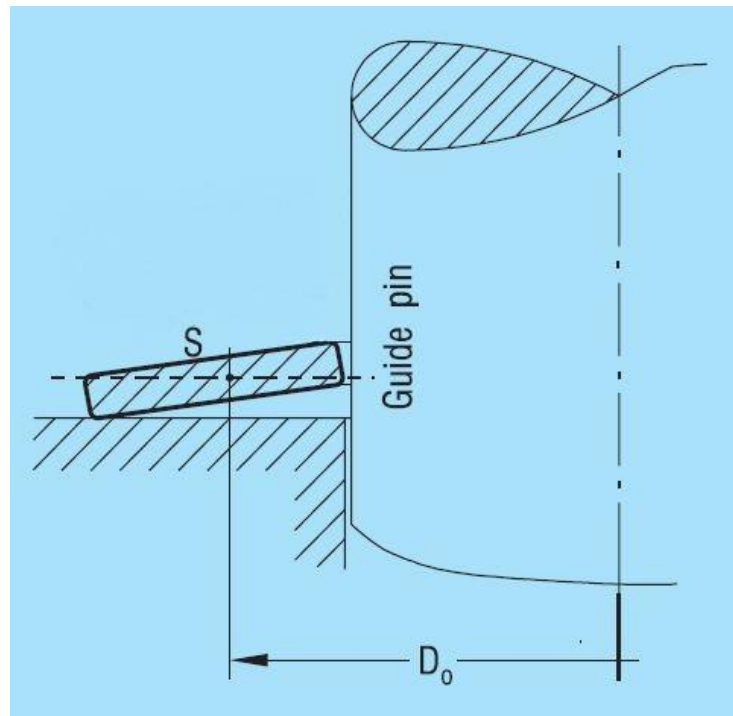


Figure 67. Cone spring-guide pin coupling scheme

In the picture 67, the rotation point of the cone spring during its deflection can be found (indicated with S). The dashed horizontal line passing through this point is needed in order to understand if a reduction in inner diameter occurs. In fact, if in the unloaded condition the corner of the cone spring section nearer to the guide is below this horizontal line, the inner diameter reduction is avoided, while, on the contrary, if it is above, an inner diameter reduction occurs. In this way, the key role of the guide clearance tolerances can be understood.

Aspects observed show the importance to leave the cone spring height degree of freedom to the cone spring supplier, but not its tolerance. In fact, as explained in point 6 of the dimensioning flowchart, the cone spring gap height tolerance is fixed. At this point the damping tolerance, coming from the system calculation, can be considered too. From the combination of these two tolerances, the one of the cone spring can be set. In fact:

- the upper damping tolerance limit must not be overcome, even in case of maximum material conditions (lower cone spring gap height tolerance limit)
- the lower damping tolerance limit must be assured, even in case of minimum material conditions (upper cone spring gap height tolerance limit)

Since the plastic friction elements dimensions have been set at point 5 of the workflow, it is possible to translate the upper and lower damping limit into axial force values. Thanks to this last passage, the graph here below represented can be built. This will be the input for the cone spring supplier, who has to adapt the cone spring characteristics to it.

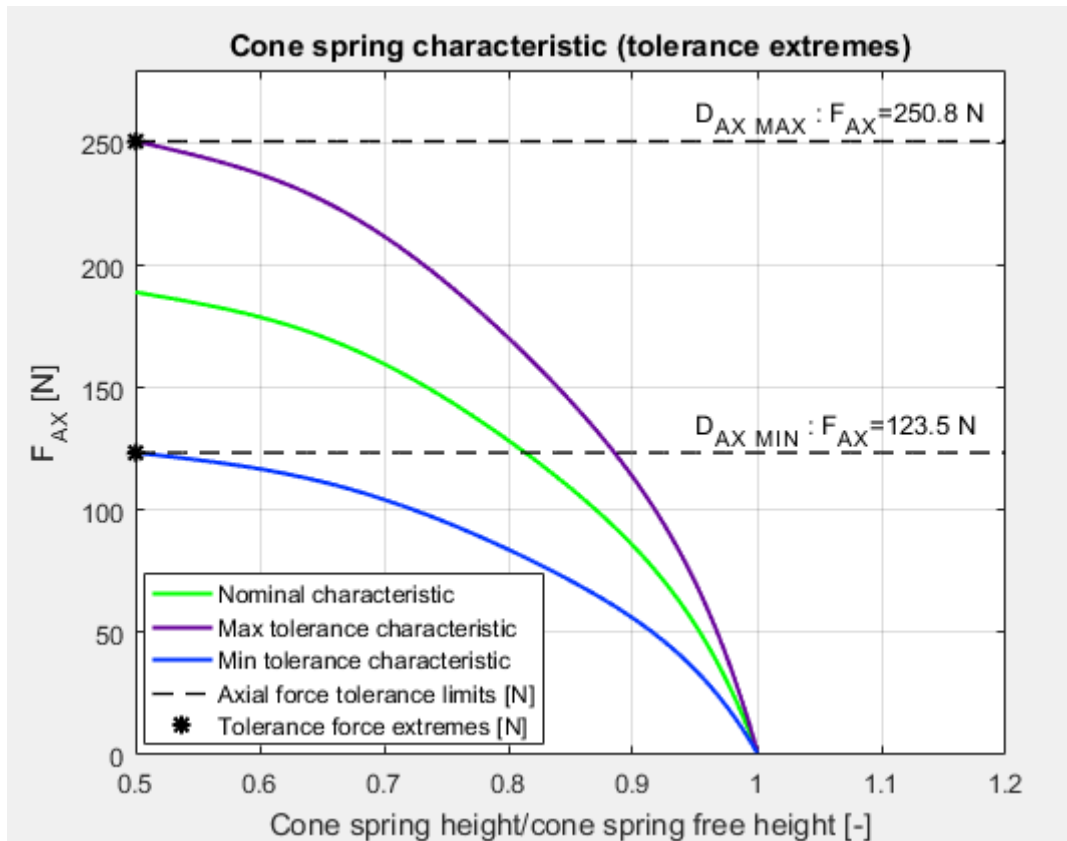


Figure 68. Flowchart section 8) output (1/2)

This is not the only output of this stage. Besides this, in fact, the cone spring dimensional features are specified (see figure 69). The inner diameter is computed considering the pivot outer diameter and the guide clearance according to table 8. Since the cone spring exerts the axial force on the damper pad, the outer diameter, instead, has to provide a proper contact with the plastic friction element, even in case of total compression. For this reason, it has been set as 1mm less than the outer damper pad diameter.

Cone spring		
F_{ax} max tolerance	[N]	250,8
F_{ax} min tolerance	[N]	123,5
Minimum internal diameter	[mm]	16,2
Maximum external diameter	[mm]	30,5

Figure 69. Flowchart section 8) output (2/2)

9) Main spring calculation

The main spring of a timing belt tensioner is of the helical type. Its main tasks are:

- exchange a torque
- absorb/discharge energy

It can work in two different conditions:

- winding
- un-winding

In most cases, in timing belt tensioners the main spring set to work in winding conditions. In fact, springs implemented are usually quite slender, so with a high mean body diameter to wire dimension ratio. This brings to a heavier task for the spring itself. Due to this aspect, fatigue issue is a crucial one: cracks start from the external surface of the coils. During the formation of a winding helical spring, the wire is wound at an angle bigger than the free state one, in order to get the desired value when the spring hooks are released. Due to this phenomenon, called presetting, when the spring is unloaded, the external side of the coils are put in compression. It is beneficial from the stress level point of view, like it is schematized in the picture below.

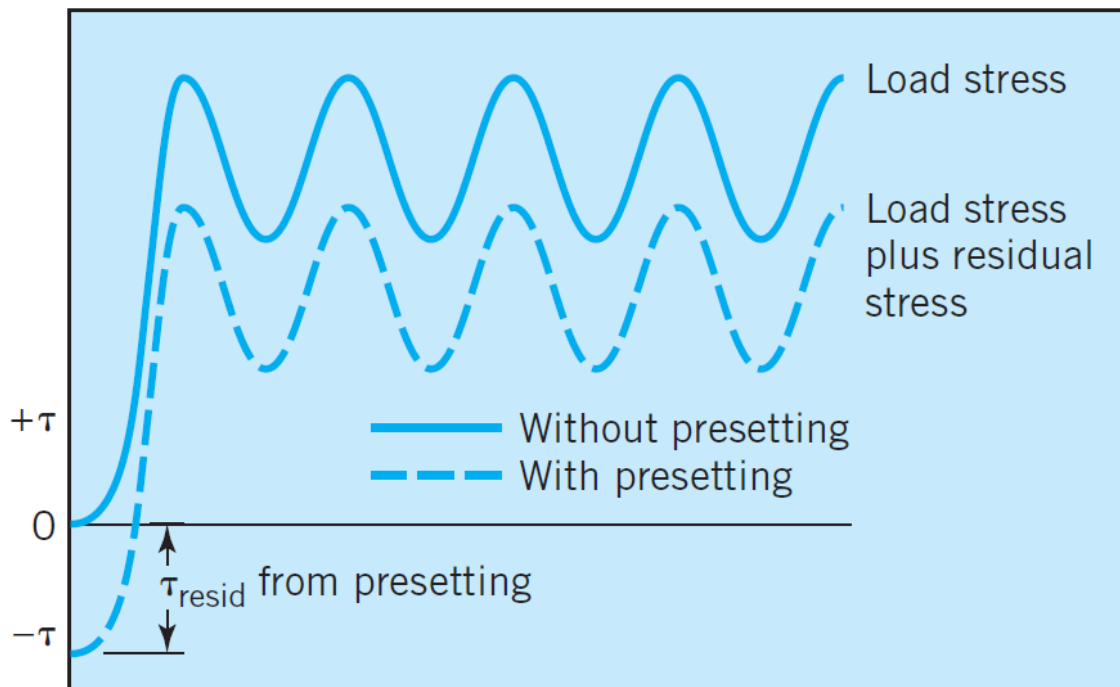


Figure 70. Spring stress level comparison as a function of presetting

As it can be seen from the figure 70, this procedure is very similar to a shot-peening, since the beneficial effects of implementing a winding main spring for a timing belt tensioner are reached either for the fatigue aspect, either for the maximum stress of the material.

Besides this, another choice that the designer has to take in charge is what type of wire to implement:

- round wire
- rectangular/square wire

Round wire is preferred due to the lower cost, but it is a less efficient choice at the same time. In fact, if it is not sufficient, the rectangular wire is implemented.

In a timing belt tensioner, the spring stiffness and the torque at nominal position are defined as a function of the belt tension required and as a function of the tensioner geometrical characteristics (e.g. the working arm length). First of all, in order to achieve the torsional stiffness required, the number of active coils has to be defined. If the spring is of a round wire type, this is done according to equation 64:

$$n_a = \frac{E * d_{wire}^4 * \pi}{180 * 64 * k_t * mbd} \quad (64)$$

where:

n_a is the number of active coils in free state condition [-]

E is the Young's modulus [MPa]

d_{wire} is the diameter of the wire section [m]

k_t is the torsional stiffness [Nm/deg]

mbd is the mean body diameter in free state condition [m]

If, instead, the spring wire section is rectangular, this is done according to equation 65:

$$n_a = \frac{E * b_{wire} * h_{wire}^3}{180 * 12 * k_t * mbd} \quad (65)$$

where:

b_{wire} is the section side parallel to spring axis revolution [m]

h_{wire} is the section side orthogonal to spring axis revolution [m]

Then, it is possible to compute the spring working angle in several working conditions. The nominal angle is computed according to equation 66:

$$\theta_{nom} = \frac{T_{nom} + T_{tol\%} * T_{nom}}{k_t} \quad (66)$$

where:

ϑ_{nom} is the angle between spring hooks at nominal torque [deg]

T_{nom} is the spring nominal torque [Nm]

$T_{tol\%}$ is the spring torque tolerance percentage [-]

In an analogous way the working oscillation angles can be computed through equations 67 and 68:

$$\theta_{nom+} = \theta_{nom} + \frac{1}{2} * \theta_{pp} \quad (67)$$

$$\theta_{nom-} = \theta_{nom} - \frac{1}{2} * \theta_{pp} \quad (68)$$

where:

ϑ_{nom+} is the angle between spring hooks at nominal torque plus half oscillation amplitude [deg]

ϑ_{nom-} is the angle between spring hooks at nominal torque minus half oscillation amplitude [deg]

ϑ_{pp} is the oscillation amplitude [deg]

Then, the two extreme working conditions angles can be computed according to equations 69 and 70:

$$\theta_{inst} = \theta_{nom} + \Delta\theta_{inst-nom} \quad (69)$$

$$\theta_{free\ arm} = \theta_{nom} - \Delta\theta_{nom-free\ arm} \quad (70)$$

where

ϑ_{inst} is the angle between spring hooks in installation condition [deg]

$\Delta\vartheta_{inst-nom}$ is the angle between installation and nominal conditions [deg]

$\vartheta_{free\ arm}$ is the angle between spring hooks in free arm condition [deg]

$\Delta\vartheta_{nom-free\ arm}$ is the angle between nominal and free arm conditions [deg]

At this stage is possible to compute the torque in each of the above-mentioned condition through equation 71:

$$T_i = \theta_i * k_t \quad (71)$$

where:

T_i is the torque in the investigated condition [Nm]

ϑ_i is the angle between spring hooks in the investigated condition [deg]

By knowing the torque exerted by the helical spring, the level of stress can be computed as well. The spring wire must not yield, also in the worst working condition, which is the installation position, so the condition stated by equation 72 must be fulfilled:

$$\sigma_{inst} < \sigma_{YS} \quad (72)$$

where, in case of round wire, stress level in the spring for the different working conditions are computed according to equations 73, 74 and 75:

$$\sigma_i = k_f \frac{32 * T_i}{\pi * d_{wire}^3} \quad (73)$$

where:

$$k_f = \frac{4c^2 - c - 1}{4c(c - 1)} \quad (74)$$

where:

$$c = \frac{m * b * d}{d_{wire}} \quad (75)$$

where:

σ_{inst} is the spring stress in installation position [MPa]

σ_{YS} is the yield strength of the spring wire [MPa]

σ_i is the stress level due to T_i [MPa]

k_f is the curvature correction factor [-]

c is the spring index [-]

In case of rectangular wire, instead, stress level in the spring for the different working conditions are computed according to equations 74, 76 and 77:

$$\sigma_i = k_f \frac{6 * T_i}{b_{wire} * h_{wire}^2} \quad (76)$$

where k_f is computed through equation num and the spring index is equal to:

$$c = \frac{m * b * d}{\left(\frac{16}{3} * b_{wire} * h_{wire}^2\right)^{\frac{1}{3}}} \quad (77)$$

Then, the number of active coils in each working condition can be obtained. If the spring is of the winding type, this is done thanks to equation 78:

$$n_i = n_a + \frac{\theta_i}{360} \quad (78)$$

while, if it is working in unwinding conditions, it is performed through equation 79:

$$n_i = n_a - \frac{\theta_i}{360} \quad (79)$$

where

n_i is the number of active coils in the investigated condition [-]

Once this is known, through equation 80, it is possible to define the mean body diameter of the spring in the different conditions:

$$mbd_i = mbd * \frac{n_a}{n_i} \quad (80)$$

where

mbd_i is the mean body diameter in the investigated condition [mm]

At this point the attention can be moved to the packaging issues. In the radial direction the critical issue is the contact between the spring and the housing. It is worth to notice that, in case of winding springs, a contact between the two in the external side must be avoided between, while a contact on the internal side is fundamental for the forces and moment equilibrium. However, a contact in a wider area also on the internal side must be avoided as well. In fact, this would bring the spring to lock and to decrease its number of active coils, so its stiffness would increase, with negative effect on the tensioner performances. The same holds for unwinding springs, but with internal and external contacts considerations interchanged.

In order to successfully evaluate the external contact, the condition stated by equation 81 must be met:

$$D_{ext\ spring\ max} < D_{ext\ housing\ min} \quad (81)$$

where

$$D_{ext\ housing\ min} = D_{ext\ housing\ nom} - D_{ext\ housing\ tol} \quad (82)$$

and, in case of round wire

$$D_{ext\ spring\ max} = mbd_{max\ nom} + mbd_{tol} + (d_{wire} + d_{wire\ tol}) \quad (83)$$

or, in case of rectangular wire

$$D_{ext\ spring\ max} = mbd_{max\ nom} + mbd_{tol} + (h_{wire} + h_{wire\ tol}) \quad (84)$$

where

$D_{spring\ max}$ is the maximum external diameter of the spring [m]

$D_{exthousing\ min}$ is the minimum external diameter of the housing [m]

$D_{ext\ housing\ nom}$ is the nominal external diameter of the housing [m]

$D_{ext\ housing\ tol}$ is the housing external diameter tolerance [m]

$mbd_{max\ nom}$ is the maximum nominal mean body diameter of the spring [m]

mbd_{tol} is the spring mean body diameter tolerance [m]

$d_{wire\ tol}$ is the tolerance on the wire section diameter [m]

$h_{wire\ tol}$ is the tolerance on the section side orthogonal to spring axis revolution [m]

It is worth to notice that the mean body diameter of the spring is a function of the spring working condition. In fact, regarding the external side contact, if a winding spring is implemented, the worst case is represented by the free arm position, while if an unwinding spring is considered, the worst case is represented by the installation position. This holds for the working range, but also the tensioner assembling operation has to be taken into account. In this case, for the winding spring only, the free state position instead of the free arm one has to be considered, in order to avoid the interference between the housing and the spring.

In order to successfully evaluate the internal contact, instead, the condition stated by equation 85 must be met:

$$D_{int\ spring\ min} < D_{int\ housing\ max} \quad (85)$$

where

$$D_{int\ housing\ max} = D_{int\ housing\ nom} + D_{int\ housing\ tol} \quad (86)$$

and, in case of round wire

$$D_{int\ spring\ min} = mbd_{min\ nom} - mbd_{tol} - (d_{wire} + d_{wire\ tol}) \quad (87)$$

or, in case of rectangular wire

$$D_{int\ spring\ min} = mbd_{min\ nom} - mbd_{tol} - (h_{wire} + h_{wire\ tol}) \quad (88)$$

where

$D_{int\ spring\ min}$ is the minimum internal diameter of the spring [m]

$D_{int\ housing\ max}$ is the maximum internal diameter of the housing [m]

$D_{int\ housing\ nom}$ is the nominal internal diameter of the housing [m]

$D_{int\ housing\ tol}$ is the housing internal diameter tolerance [m]

$mbd_{min\ nom}$ is the minimum nominal mean body diameter of the spring [m]

mbd_{tol} is the spring mean body diameter tolerance [m]

$d_{wire\ tol}$ is the tolerance on the wire section diameter [m]

$h_{wire\ tol}$ is the tolerance on the section side orthogonal to spring axis revolution [m]

It is worth to notice that the mean body diameter of the spring is a function of the spring working condition. In fact, regarding the internal side contact, if a winding spring is implemented, the worst case is represented by the installation position, while if an unwinding spring is considered, the worst case is represented by the free arm position. This holds for the working range, but also the tensioner assembling operation has to be taken into account. In this case, for the unwinding spring only, the free state position instead of the free arm one has to be considered, in order to avoid the interference between the housing and the spring.

Once the checks on the radial contacts have been performed, the attention can be moved to the axial issues. In fact, the contact between the coils must be avoided, also in the worst working condition. In order to assure this, the relation described by equation 89 has to be fulfilled.

$$g_{spring\ wc} > 0 \quad (89)$$

where, in case of round wire

$$g_{spring\ i} = p_{spring\ i} - d_{wire} \quad (90)$$

or, in case of rectangular wire

$$g_{spring\ i} = p_{spring\ i} - h_{wire} \quad (91)$$

where, in case of round wire

$$p_{spring\ i} = \frac{H_{spring\ i} - d_{wire}}{n_i} \quad (92)$$

or, in case of rectangular wire

$$p_{spring\ i} = \frac{H_{spring\ i} - h_{wire}}{n_i} \quad (93)$$

where

$g_{spring\ wc}$ is the spring coil spacing in the worst working condition [m]

$g_{springi}$ is the spring coil spacing in the investigated condition [m]

$p_{springi}$ is the spring pitch in the investigated condition [m]

$H_{springi}$ is the spring height in the investigated condition [m]

It is worth to notice that in free condition, the spring height corresponds to its free height (without any axial load applied on it), while in free state, nominal, and all intermediate conditions, the spring height is equal to the tensioner spring housing one.

Once these static verifications have been performed, the attention can be moved to the fatigue verification. This is done through the Smith-Goodman diagram (figure 71). In order to build it, the material characteristics have to be considered (tensile and yield strength). Then, the application is identified (green segment in figure 71). At this point is possible to compute the safety factor, which corresponds to the ratio between the length of the segment which connects the graph origin and the upper working range and the length of the segment with the same slope, but which connects the origin of the diagram itself and the upper delimiting line (blue in figure 71).

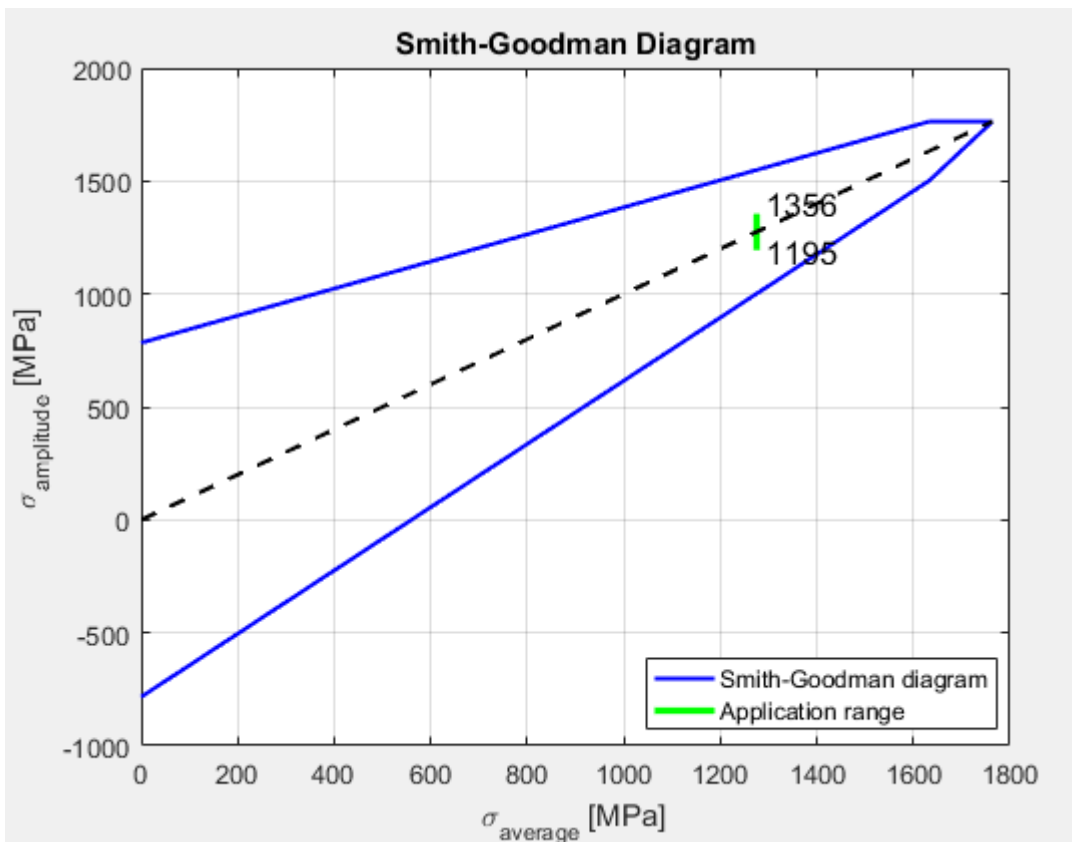


Figure 71. Flowchart section 9) output (1/2)

Besides this, in the Excel outputs table, the main numerical outputs of the spring are summarized (figure 72). After the safety factor and the spring stresses in the main working conditions, also material, working conditions, wire section typology and sizes, number of active coils at free state and mean body diameter are summarized.

Main spring		
Spring safety factor	[-]	1,40
Spring σ_a max	[MPa]	1356
Spring σ_a min	[MPa]	1195
Spring σ_{inst}	[MPa]	1651
Spring material	[-]	VDSiCr
Working condition	[-]	Winding
Wire section type	[-]	Flat wire
Wire section sizes	[mm x mm]	1.8 x 2.6
Number of active coils	[-]	4,088
Mean winding diameter	[mm]	41,000

Figure 72. Flowchart section 9) output (2/2)

10) Tilting-Sliding verification

Timing belt tensioner is fixed on the engine crankcase through a bolt. In most cases it is a M8 bolt, hosted in an 8,2mm diameter hole. If it is not sufficient a M10 bolt is used. In this case a 10,2mm diameter hole is needed.

Bolt has to deny:

- tensioner tilting
- tensioner sliding

The aim of this section is to identify the correct tightening torque of the screw in order to achieve the prescribed safety factor (chosen by the user) either on tilting, either on sliding.

Tensioner tilting occurs due to the hubload offset. In fact, due to functional requirements, the middle plane of the belt is positioned at a given distance from the engine crankcase. Due to this aspect, by referring to the pivot base, the hubload presents an arm different from zero. This brings the contact pressure to have a sinusoidal law as a function of the contact angle. This sine wave average value is equal to the average contact pressure (which corresponds to the pressure achieved by tightening the screw, without the hubload application). Then, the sine wave amplitude permits to identify a maximum and a minimum contact pressure point. These are located on the same pivot base diameter, since they are located at 180° from each other. The critical point is the one characterized by the lowest contact pressure. In fact, it must not reach the null value, otherwise the pivot base detaches from the engine surface and the tensioner tilts. If this happens, the tensioner is no more able to work, with detrimental consequences on the engine belt-drive.

In order to consider the proper safety factor, the reference hubload can be computed through the equation 94:

$$HL_{tilting} = HL_{nom} * SF_{min\ tilting} \quad (94)$$

where:

$HL_{tilting}$ is the tilting safety factor reference hubload [N]

$SF_{min\ tilting}$ is the tilting minimum safety factor [-]

HL_{nom} is the nominal hubload [N]

So, the tilting torque computed through equation 95:

$$T_{tilting} = HL_{tilting} * (h_{middle\ plane\ belt} + h_{middle\ plane\ belt\ tol}) \quad (95)$$

where:

$T_{tilting}$ is the tilting torque due to belt offset [Nm]

$h_{middle\ plane\ belt}$ is the belt offset [m]

$h_{middle\ plane\ belt\ tol}$ is the belt offset tolerance [m]

The belt offset tolerance has been considered in order to analyse the worst case condition, in such a way to assure the requirement fulfilment also in this extreme conditions. Then, the minimum average contact pressure needed can be computed through equation 96:

$$\sigma_{contact\ avg} = \frac{360}{\theta_{contact}} * T_{tilting} * \frac{64}{\pi(d_{ext\ pivot\ base}^4 - d_{int\ pivot\ base}^4)} * \frac{d_{ext\ pivot\ base}}{2} \quad (96)$$

where:

$\sigma_{contact\ avg}$ is the average contact pressure of the pivot base on the crankcase [MPa]

$\theta_{contact}$ is the contact angle of the pivot base on the crankcase [deg]

d_{ext} is the pivot base contact external diameter [m]

d_{int} is the pivot base contact internal diameter [m]

So, the minimum bolt axial force to assure the required tilting safety factor is defined by equation 97:

$$F_{ax\ bolt\ tilting} = \sigma_{contact\ avg} * A_{pivot\ base} \quad (97)$$

where:

$F_{ax\ bolt\ tilting}$ is the minimum bolt axial force needed to assure the tilting safety factor [N]

$A_{pivot\ base}$ is the pivot contact area on the crankcase [m²]

Once the minimum force that has to be assured for the tensioner tilting safety factor fulfilment has been evaluated, the attention can be moved to the tensioner sliding. It occurs due to the hubload direction. In fact, it is parallel to the engine crankcase and it makes the tensioner to move on the surface if not correctly faced. This would be a great problem, since bolts are not designed to be subjected to shear forces. So the bolt axial force must ensure a friction force on the pivot base in such a way to avoid it. As for the tilting issue, through equation 98 a sliding safety factor is considered too:

$$HL_{sliding} = HL_{nom} * SF_{min\ sliding} \quad (98)$$

where:

$HL_{sliding}$ is the sliding safety factor reference hubload [N]

$SF_{min\ sliding}$ is the sliding minimum safety factor [-]

HL_{nom} is the nominal hubload [N]

Then, the minimum bolt axial force to assure the required sliding safety factor is defined by equation 99:

$$F_{ax\ bolt\ sliding} = \frac{HL_{sliding}}{f_{friction\ crankcase}} \quad (99)$$

where:

$F_{ax\ boltsliding}$ is the minimum bolt axial force needed to assure the sliding safety factor [N]

$f_{friction\ crankcase}$ is the pivot base-crankcase friction coefficient [-]

At this stage, the minimum bolt axial force that has to be assured to cope with the application requirements can be retrieved:

$$F_{ax\ bolt} = \max(F_{ax\ bolt\ tilting}, F_{ax\ bolt\ sliding}) \quad (100)$$

Once the bolt axial force is known, the screw dimensioning can start. As a first attempt, the M8x1,25 is considered. By knowing the format of the screw, the tightening torque needed to achieve the target axial force can be computed through equation 101:

$$T_{bolt} = \frac{F_{ax\ bolt}}{2} * \left(\frac{p_{bolt}}{\pi} + d_{m\ bolt} \frac{\tan(\varphi)}{\cos(\beta)} + d_{t\ bolt} * \tan(\varphi_s) \right) \quad (101)$$

where

$$d_{m\ bolt} = d_{nom\ bolt} - 0.6495 * p_{bolt} \quad (102)$$

where

T_{bolt} is the bolt tightening torque [Nm]

p_{bolt} is the bolt pitch [m]

$d_{nom\ bolt}$ is the nominal bolt diameter [m]

$d_{m\ bolt}$ is the thread mean diameter [m]

$d_{t\ bolt}$ is the bolt head-clamped member interface mean diameter [m]

φ is the thread friction coefficient [-]

φ_s is the bolt head-clamped member interface friction coefficient [-]

β is the thread semi-angle [deg]

Then, the bolt normal stress can be computed through equation 103:

$$\sigma_{ax\ bolt} = \frac{4 * F_{ax\ bolt}}{\pi * d_{n\ bolt}^2} \quad (103)$$

where

$$d_{n\ bolt} = d_{nom\ bolt} - 1.2268 * p_{bolt} \quad (104)$$

where

$\sigma_{ax\ bolt}$ is the bolt normal stress [MPa]

$d_{n\ bolt}$ is the bolt core diameter [m]

and the bolt tangential stress can be computed through equation 105:

$$\tau_{bolt} = \frac{16 * T_{bolt\ thread}}{\pi * d_{n\ bolt}^3} \quad (105)$$

where:

$$T_{bolt\ thread} = \frac{F_{ax\ bolt}}{2} * \left(\frac{p_{bolt}}{\pi} + d_{m\ bolt} \frac{\tan(\varphi)}{\cos(\beta)} \right) \quad (106)$$

where

$T_{bolt\ thread}$ is the tightening torque due to thread(s) [Nm]

This is needed in order to be able to compute the equivalent stress, through the hypothesis of Von Mises, as defined in equation 107:

$$\sigma_{Von\ Mises} = \sqrt{\sigma_{ax\ bolt}^2 + 3 * \tau_{bolt}^2} \quad (107)$$

where:

$\sigma_{Von\ Mises}$ is the bolt equivalent stress [MPa]

This output is needed in order to detect the correct bolt material class, in such a way to avoid overcoming the yield limit. If the equivalent stress level overcomes the yield limit of the maximum bolt material class, the bolt format is increased and the calculations above mentioned have to be performed again. Else, the attention can be moved to the clamped members material stress. In fact, the under-bolt head stress level is investigated, through equation 108:

$$\sigma_{head\ bolt} = \frac{F_{ax\ bolt}}{A_{head\ bolt}} \quad (108)$$

where:

$$A_{head\ bolt} = \frac{\pi * (d_{ext\ head\ bolt}^2 - d_{int\ pivot\ base}^2)}{4} \quad (109)$$

where:

$\sigma_{head\ bolt}$ is the under-bolt head stress [MPa]

$A_{head\ bolt}$ is the under-bolt head contact area [m²]

$d_{\text{ext head bolt}}$ is the external bolt head contact diameter [m]

Besides this, the average stress on the threads is investigated as well, with law stated in equation 110:

$$\sigma_{\text{thread}} = \frac{F_{\text{ax bolt}}}{A_{\text{thread}} * n_{\text{thread}}} \quad (110)$$

where:

$$A_{\text{thread}} = \frac{\pi * (d_{\text{nom bolt}}^2 - d_{\text{bolt}}^2)}{4} \quad (111)$$

where:

σ_{thread} is the bolt thread stress [MPa]

A_{thread} is the bolt thread projected area [m²]

n_{thread} is the number of active threads [-]

These outputs are then compared with the clamped members material strength. If the bolt under-head contact stress is resulting higher than material compression strength, a warning is shown and a minimum bolt head contact external diameter is suggested in order to solve the issue. An analogue procedure has to be considered for the clamped members tractive strength, for which, if needed, a minimum number of active threads is suggested.

If the bolt is verified, the main numerical results of this stage are summarized in the Excel output table, as it can be seen in figure 73 here below.

Bolt		
T_{bolt}	[Nm]	19,43
$F_{\text{ax bolt}}$	[N]	14003
σ_{bolt}	[MPa]	381,43
T_{bolt}	[MPa]	183,88
$\sigma_{\text{eqv bolt}}$	[MPa]	496,91
$\sigma_{\text{under bolt head}}$	[MPa]	117,45
σ_{thread}	[MPa]	381,88
Bolt format	[-]	M8 x 1,25
Bolt material class	[-]	8,8
Tilting - Sliding verification		
Pivot base contact surface	[mm ²]	327,32
Contact surface pressure	[MPa]	42,78
Tilting safety factor	[-]	3,00
Sliding safety factor	[-]	3,02

Figure 73. Flowchart section 10) output (1/2)

Besides this, also a graphical output is obtained (figure 74). It represents the pivot base contact pressure as a function of the contact angle. As it can be seen it has a sinusoidal trend, whose minimum has to be always higher than zero in order to obtain the tilting verification. The blue line represents the nominal curve, while the green line represents the worst condition (the colour highlights the positive outcome of the evaluation).

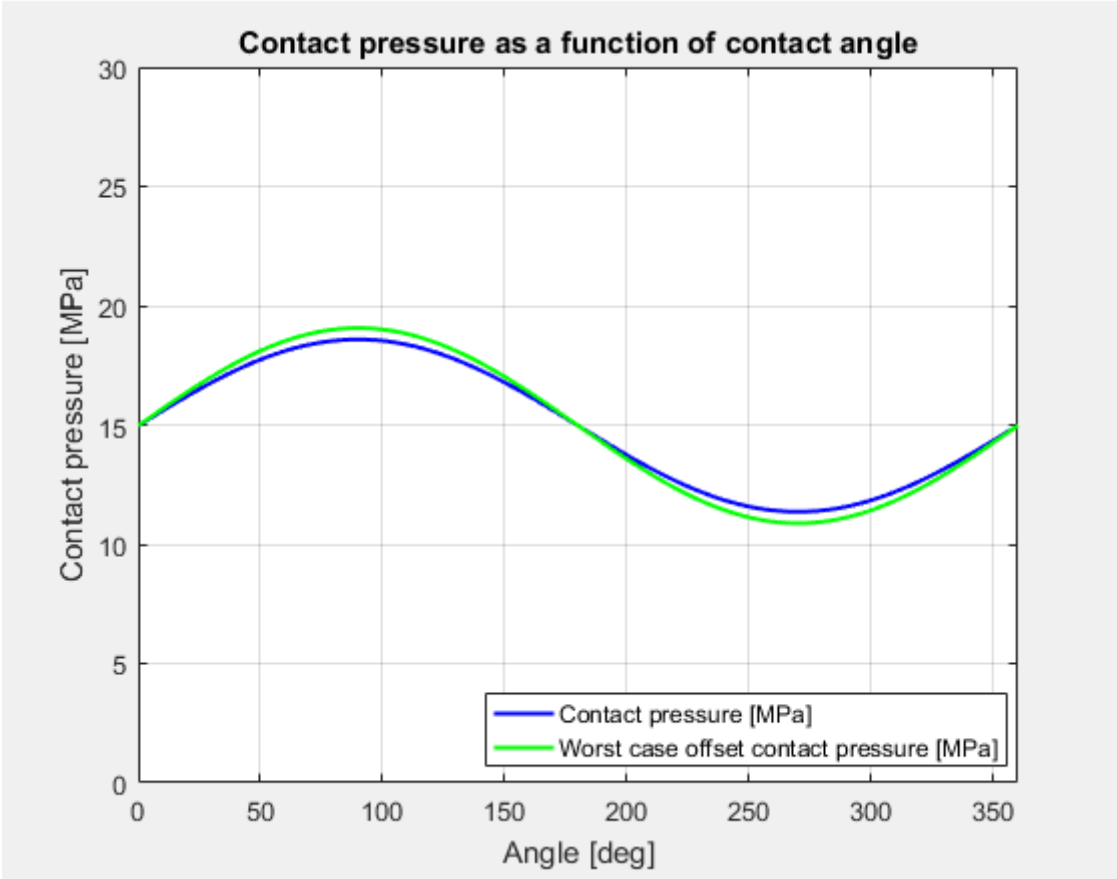


Figure 74. Flowchart section 10) output (2/2)

11) 3D CAD Parametric model

At the end of the dimensioning flowchart, all the outputs described above are obtained. This means that several data summarized in the Excel output table, together with several graphs in Matlab environment are available. In order to figure out the result of this procedure, the user would have to pass to a 3D CAD environment, and, inserting the values available at this stage, he would build a simplified 3D model, from which he could then start a progressive refinement, until the first verified revision can be send to the testing department. This last step requires the user know-how, together with the needed customization in order to cope with the application requisites, changing from one to another. As a consequence, this cannot be automated.

This is not valid for the simplified model: it can be generated automatically from the system. To do this, for each product family a generic model is needed. Its dimensions and features are then updated as a function of the inputs, coming from Matlab environment, summarized in a table.

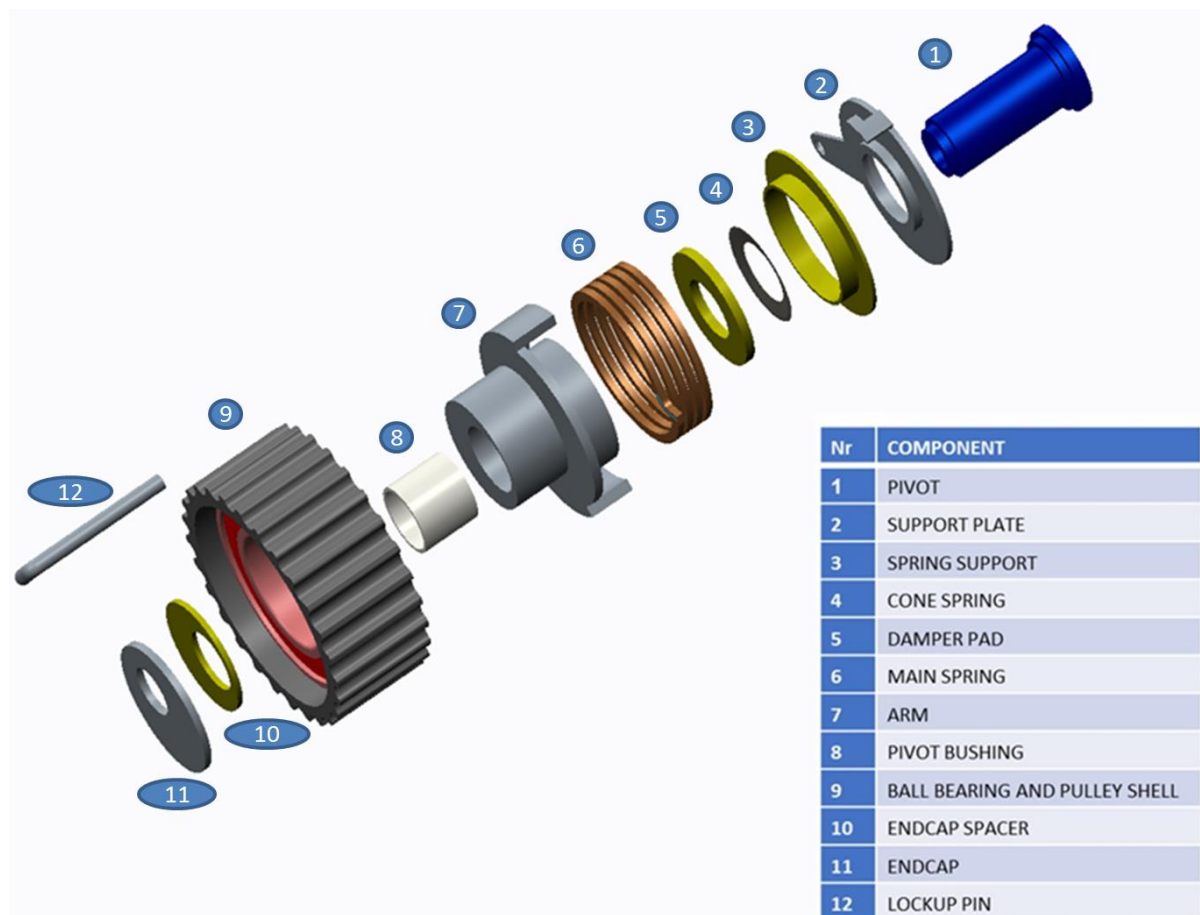


Figure 75. Exploded view of a simplified 3D model

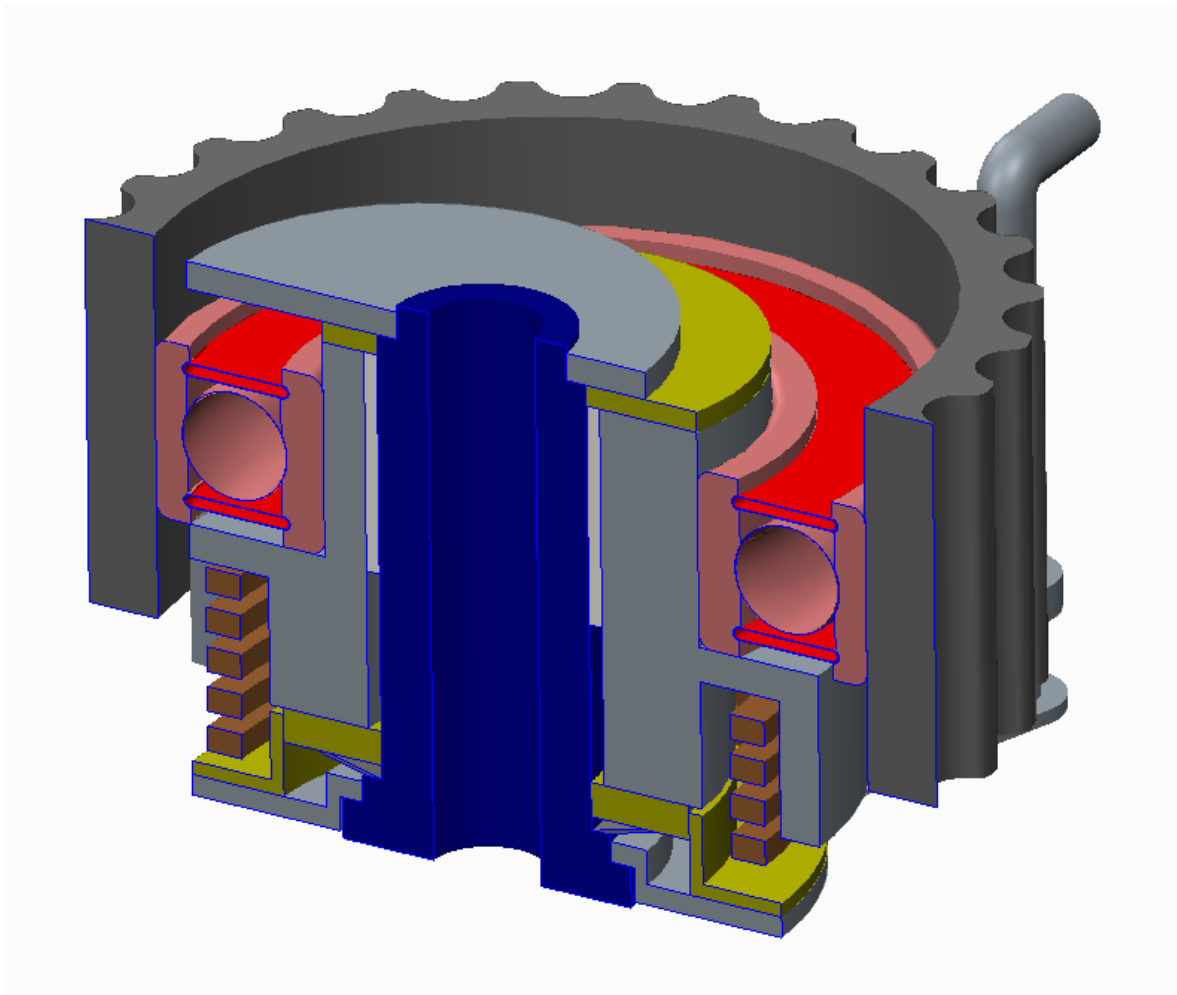


Figure 76. Section view of a simplified 3D model

As it can be seen from the pictures 75 and 76, the model is very simple. In fact, almost no chamfers or rounds are present. At the same time, it permits to evaluate the timing belt tensioner verification, by containing all the components present in a real assembly. The most important output of this stage, besides being the starting point for the final modelling, is the visual check of the packaging constraints. Another crucial aspect that has to be emphasised is that, starting from the same 3D CAD model, permit to achieve a strong standardization among products of the same typology.

Comparison with real tensioners

In this section some real applications are considered. This is done in order to evaluate the automatic design flowchart performances. This procedure consists on inserting the same design inputs as the real cases and then analyse the outputs, highlighting the differences between the 3D model and the real tensioner.

The first case study has a standard layout. It is a Belt In Oil application with axial damping system (picture 78). Due to the system layout, it is positioned in the internal side of the timing belt, this is the reason why it presents a toothed pulley (as it can be seen from picture 77).

The second case study has a reverse layout. It is a Belt In Oil application as well and, as the previous one, it is provided of axial damping system (section view in figure 89). It contacts the belt in its external side, so the tensioner pulley is flat (it can be seen in figure 88).

The last case study has a standard layout. It is a “Dry” application, this means that the belt drive system is not in contact with engine oil, but it is in free air (protected by a proper carter). As most dry applications, due to higher friction coefficients, the radial damping is sufficient to cope with tensioner specifications, so the axial damping system is not present, as it can be seen from the section view in figure 100. This brings to a more compact layout, as it can be seen from picture 99.

Case study nr. 1

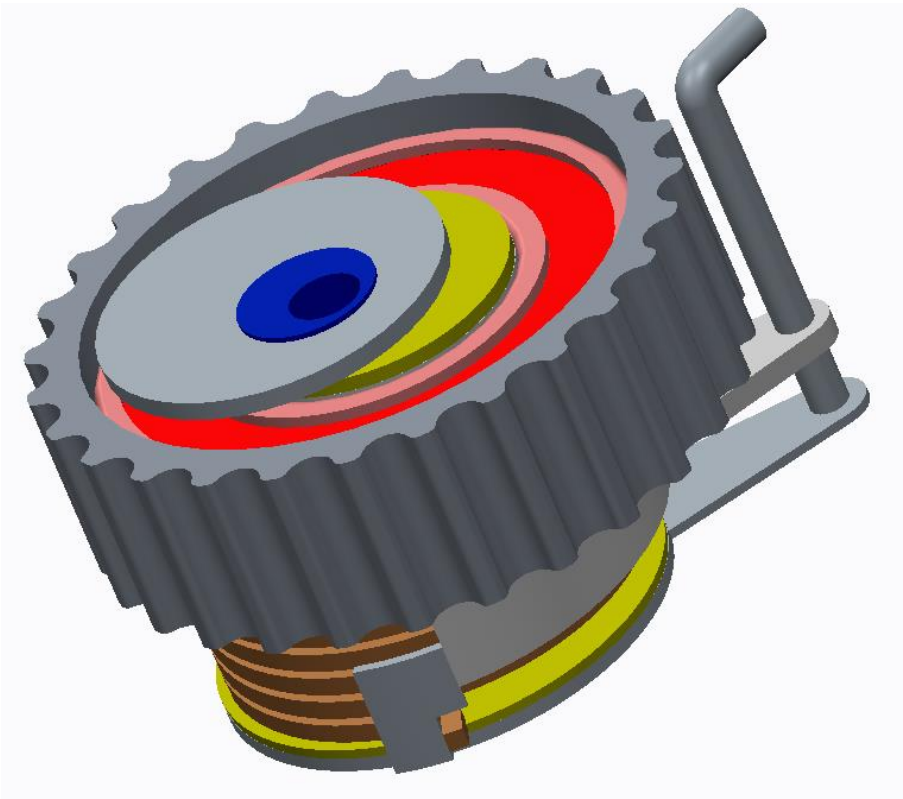


Figure 77. 1st case study 3D model

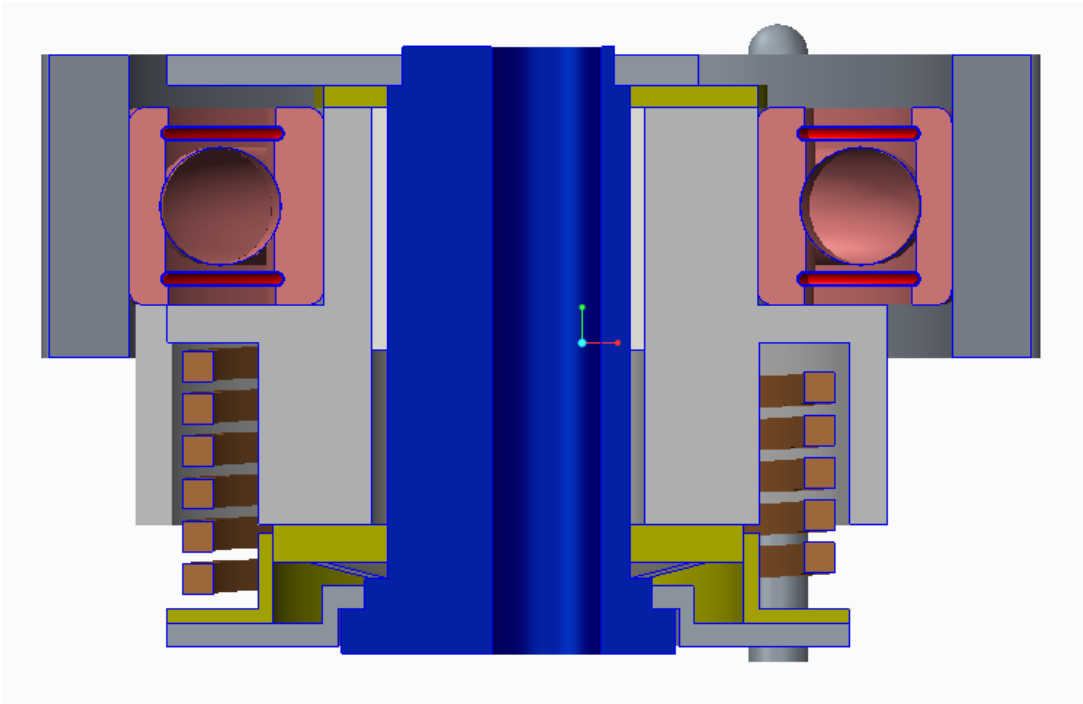


Figure 78. 1st case study 3D model (section view)

Input list

Engine application		
Application type	[-]	Belt In Oil
Engine fuel	[-]	Gasoline
Pulley		
Pulley shell type	[-]	Toothed
Pulley diameter	[mm]	66
Pulley max parallelism EOL	[mm]	0.3
Tensioner geometrical data		
Belt loading type	[-]	Double eccentric
Working arm length	[mm]	5.0
Loading arm length	[mm]	2.5
Differential angle	[deg]	85
Wrap angle	[deg]	69.2
Nom arm angle with respect to H.E.R.	[deg]	136.7
Belt		
Belt width	[mm]	16
Middle plane belt height	[mm]	29.5
Middle plane belt height increment (worst case)	[mm]	2
Lock-up pin		
Lock-up pin position radius	[mm]	33
Lock-up pin angular position	[deg]	127
Lock-up pin diameter	[mm]	4
Space constraints		
Max pivot height	[mm]	40
Max axial displacement	[mm]	42
Pivot		
Pivot class diameter	[mm]	16
Pivot bushing radial thickness	[mm]	1
Durability test		
Theta peak-to-peak	[deg]	16
Frequency	[Hz]	50
Duration	[hrs]	1200
Tensioner specifications		
Calculated torque target	[Nm]	3.25
Damping target	[Nm]	2.00
Damping tolerance	[Nm]	0.30
Damping EOLife limit	[Nm]	1.50
Main spring		
Spring stiffness	[Nm/deg]	0.018
Spring torque tolerance	[%]	4%
Bolt		
Tilting safety factor	[-]	3.50
Sliding safety factor	[-]	3.50
Fixation dimensional features		
Engine support internal diameter	[mm]	8.2
Engine support external diameter	[mm]	25.0
Contact angle	[deg]	360
Bolt head contact external diameter	[mm]	11

Number of active threads	[-]	2.6
σ_{YS} support (compression)	[MPa]	400
σ_{YS} support (traction)	[MPa]	400

Table 9. 1st case study design input

Output list			
		<u>Automatic design tool</u>	<u>Real tensioner</u>
Tensioner architecture			
Tensioner architecture typology	[-]	Rotary, Standard	Rotary, Standard
Pulley			
Pulley width	[mm]	20	20
Ball bearing			
Ball bearing typology	[-]	6006	6006
Pivot			
Pivot diameter	[mm]	16	16
Pivot bushing length	[mm]	16	18
Tensioner characterization			
Axial damping	[Y/N]	Yes	Yes
Axial damping	[Nm]	1.71	N/A
Radial damping	[Nm]	0.29	N/A
Spring torque @ nominal position	[Nm]	3.07	2.92
Plastic friction elements			
Damper pad contact area	[mm ²]	460	350
Damper pad mean radius	[mm]	12.5	11.0
Damper pad axial height	[mm]	3.5	2.5
Damper pad outer diameter	[mm]	31.5	27.5
Endcap spacer contact area	[mm ²]	490	410
Endcap spacer mean radius	[mm]	13.5	12.5
Endcap spacer axial height	[mm]	1.5	1.5
Cone spring			
F _{ax} max tolerance	[N]	577.3	565.0
F _{ax} min tolerance	[N]	440.6	482.0
Minimum internal diameter	[mm]	16.2	18.2
Maximum external diameter	[mm]	30.0	27.1
Main spring			
Safety factor	[-]	1.5	1.5
σ_a max	[MPa]	1181	1199
σ_{amin}	[MPa]	1079	1050
σ_{inst}	[MPa]	1448	1590
Material	[-]	VDSiCr	VDSiCr
Working condition	[-]	Winding	Winding
Wire section type	[-]	Flat wire	Flat wire
Wire section sizes	[mm x mm]	2.3 x 2.3	2.3 x 2.3
n _a (free state)	[-]	4.09	5.05
mbd	[mm]	41	36.8
h _{spring}	[mm]	14.8	14.9

$\vartheta_{\text{free state}}$	[deg]	328.3	342
ϑ_{nom}	[deg]	206.7	223.2
Bolt			
T_{bolt}	[Nm]	19.64	20.00
$F_{\text{ax bolt}}$	[N]	14254	N/A
σ_{bolt}	[MPa]	442.74	N/A
τ_{bolt}	[MPa]	239.94	N/A
$\sigma_{\text{eqv bolt}}$	[MPa]	607.23	N/A
$\sigma_{\text{under bolt head}}$	[MPa]	203.37	N/A
σ_{thread}	[MPa]	289.08	N/A
Bolt format	[-]	M8 x 1.25	M8 x 1.25
Bolt material class	[-]	8.8	8.8
Tilting - Sliding verification			
Pivot base contact surface	[mm ²]	359.06	361.52
Avg contact surface pressure	[MPa]	45.27	47.12
Tilting safety factor	[-]	2.56	2.62
Sliding safety factor	[-]	2.50	2.54

Table 10. 1st case study simulation output summary

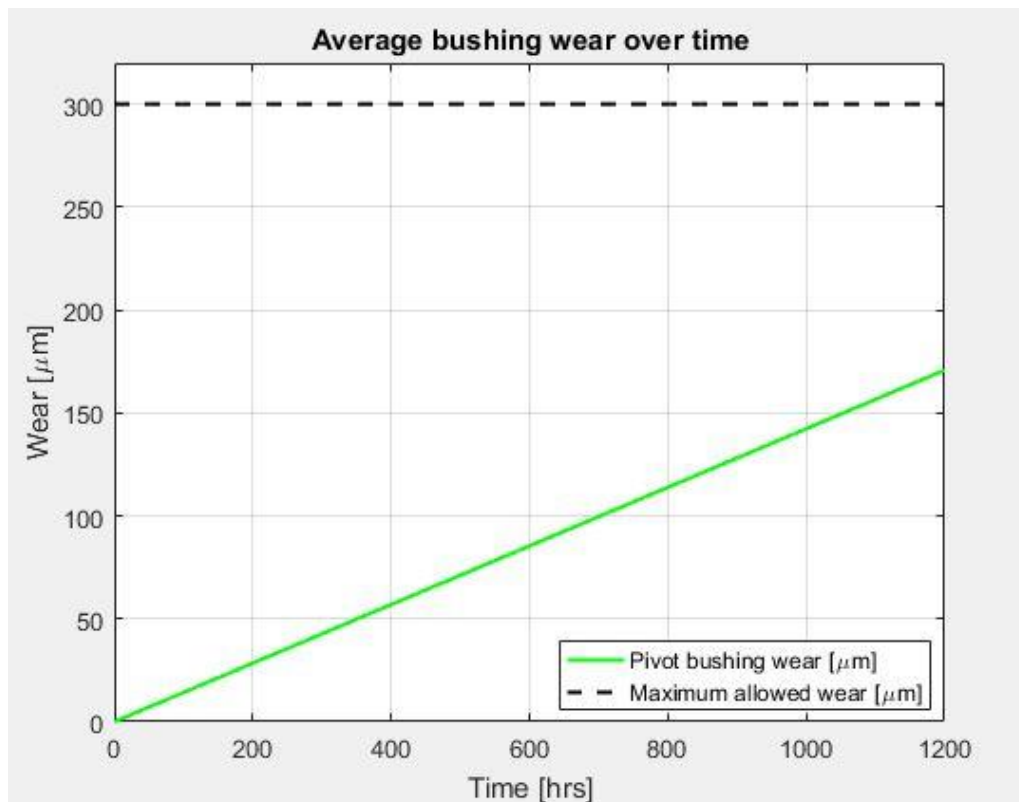


Figure 79. 1st case study bushing wear vs. time

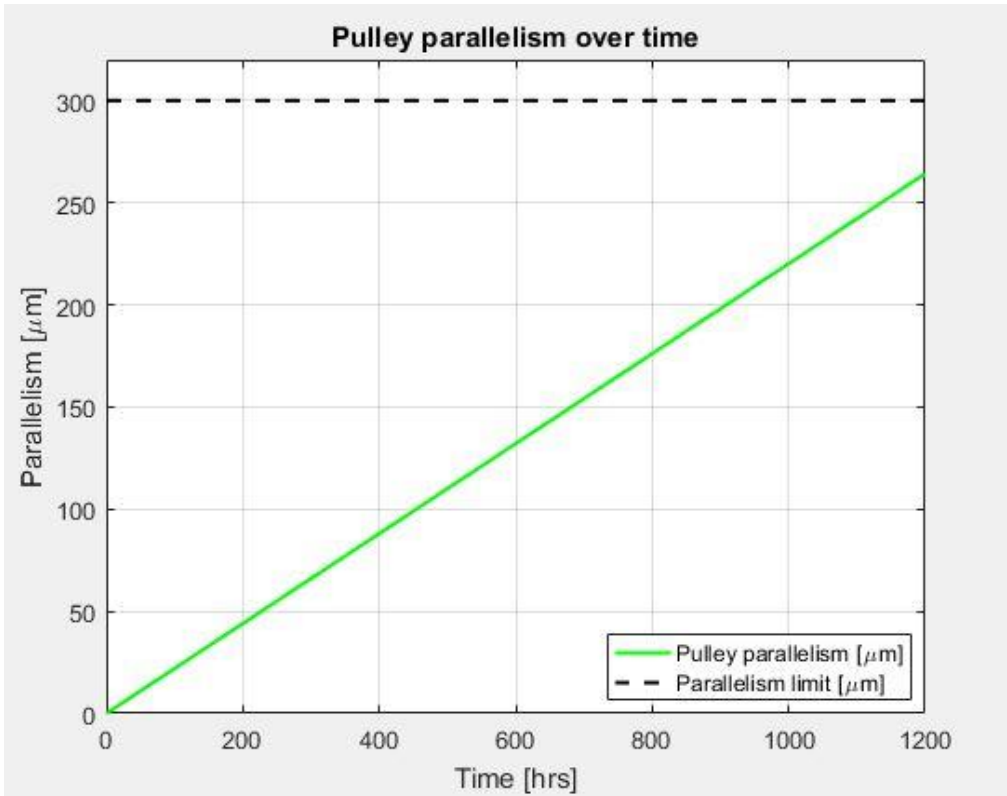


Figure 80. 1st case study pulley parallelism vs. time

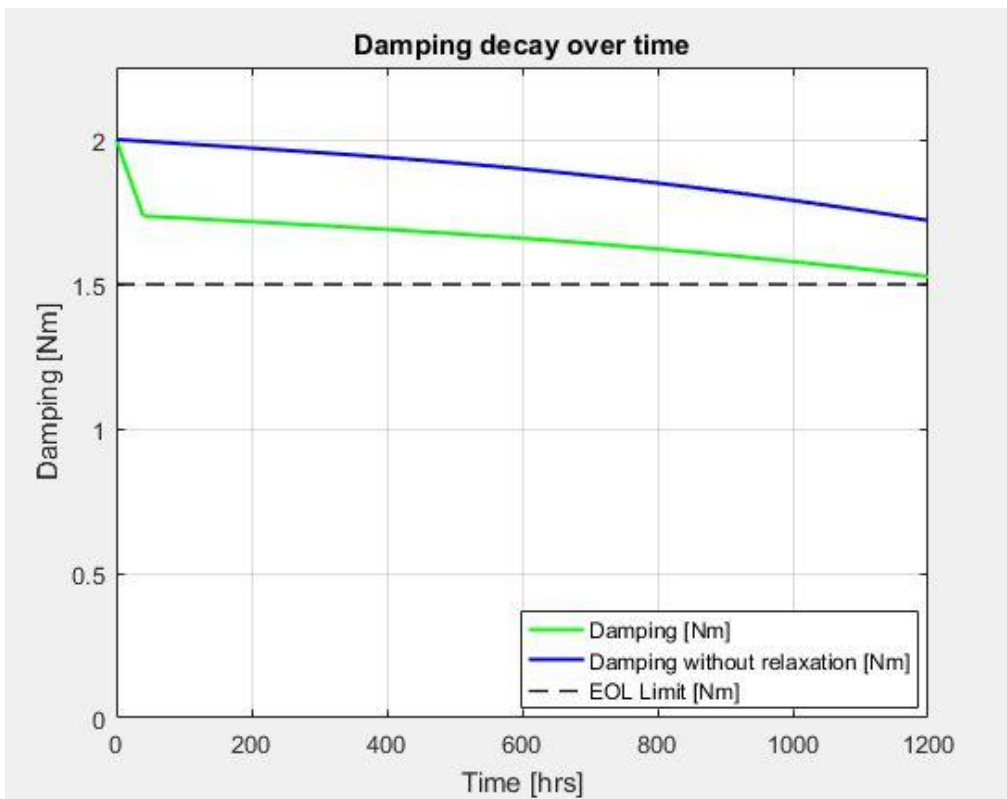


Figure 81. 1st case study damping decay vs. time

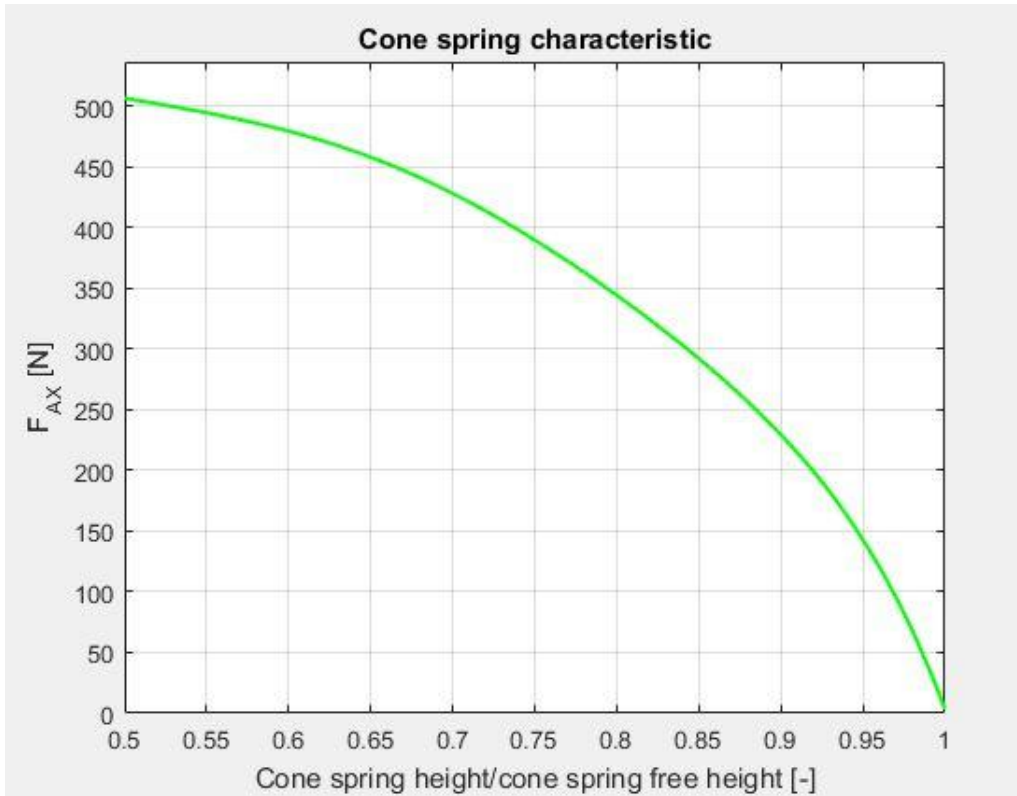


Figure 82. 1st case study cone spring characteristic

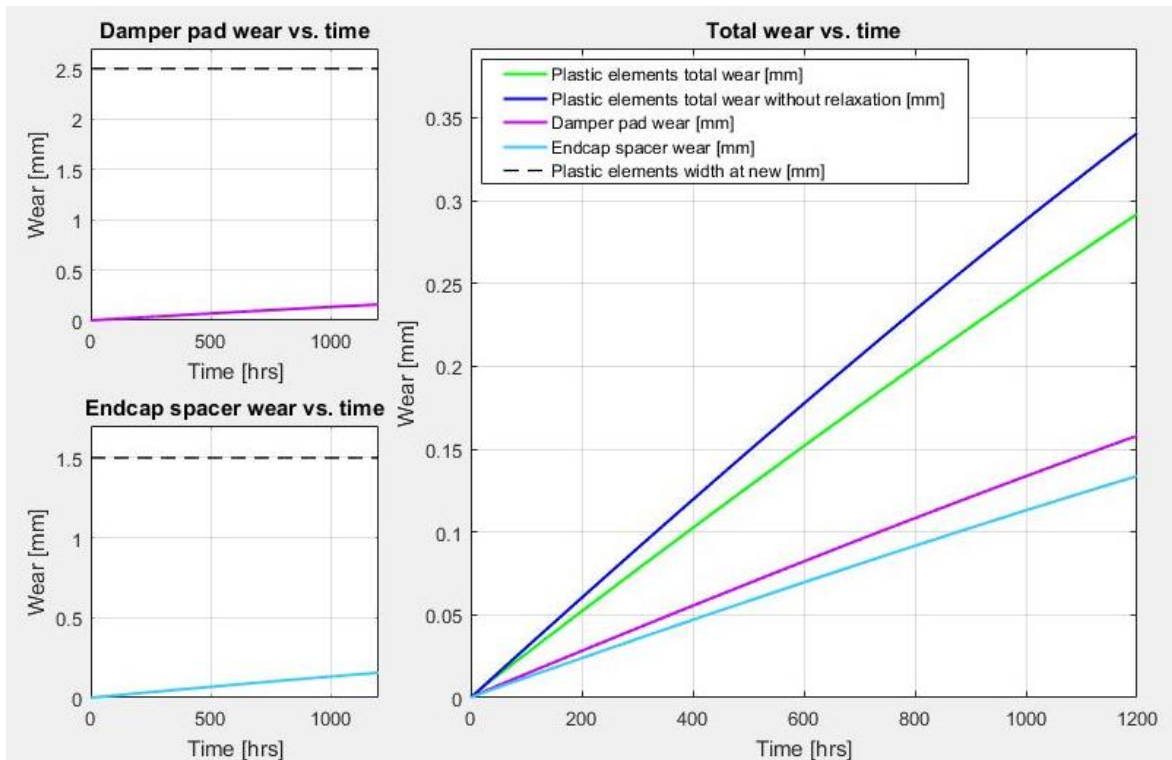


Figure 83. 1st case study plastic friction elements wear vs. time

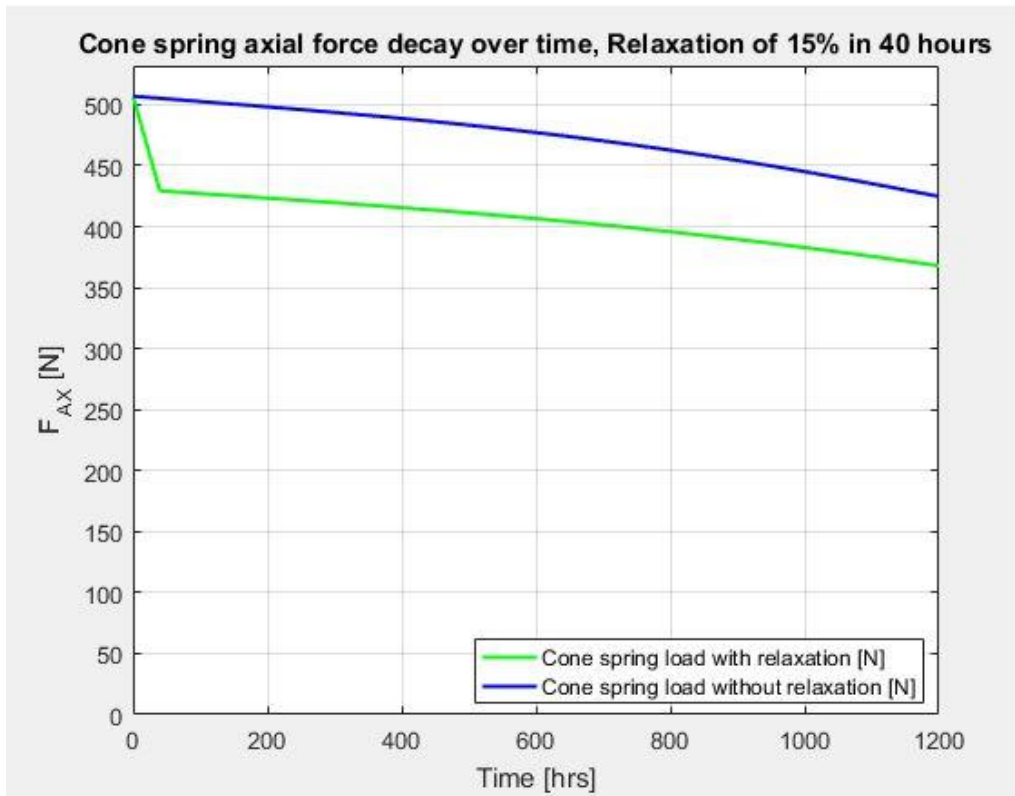


Figure 84. 1st case study cone spring axial force vs. time

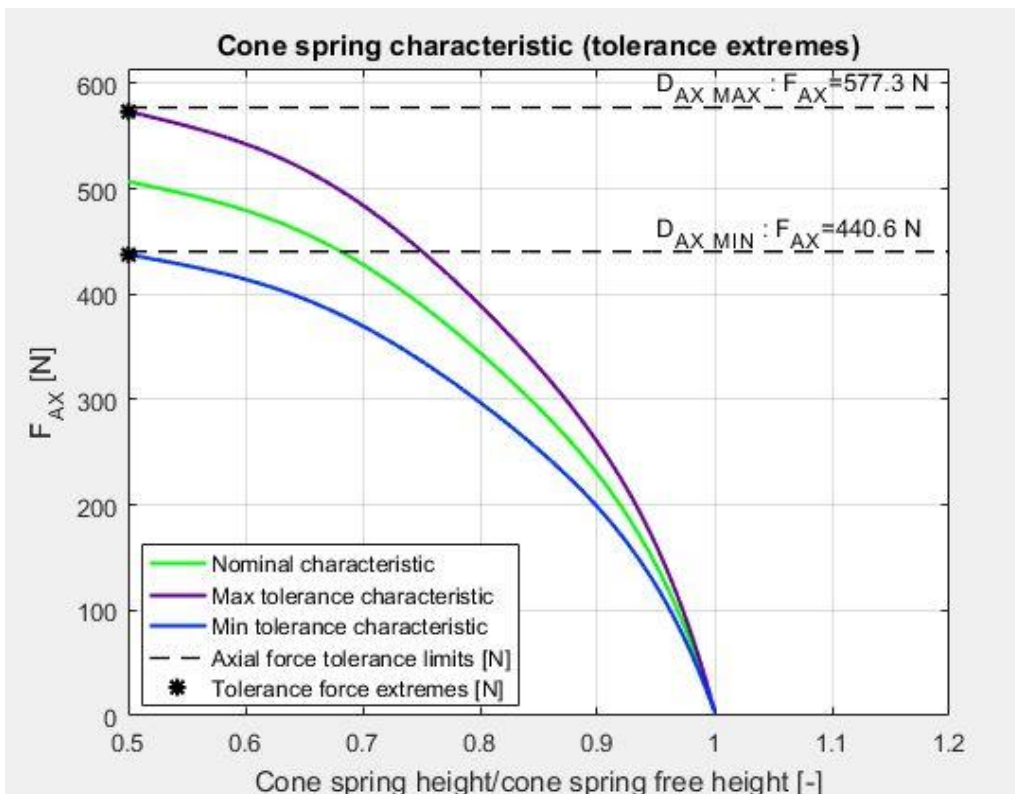


Figure 85. 1st case study cone spring force tolerance

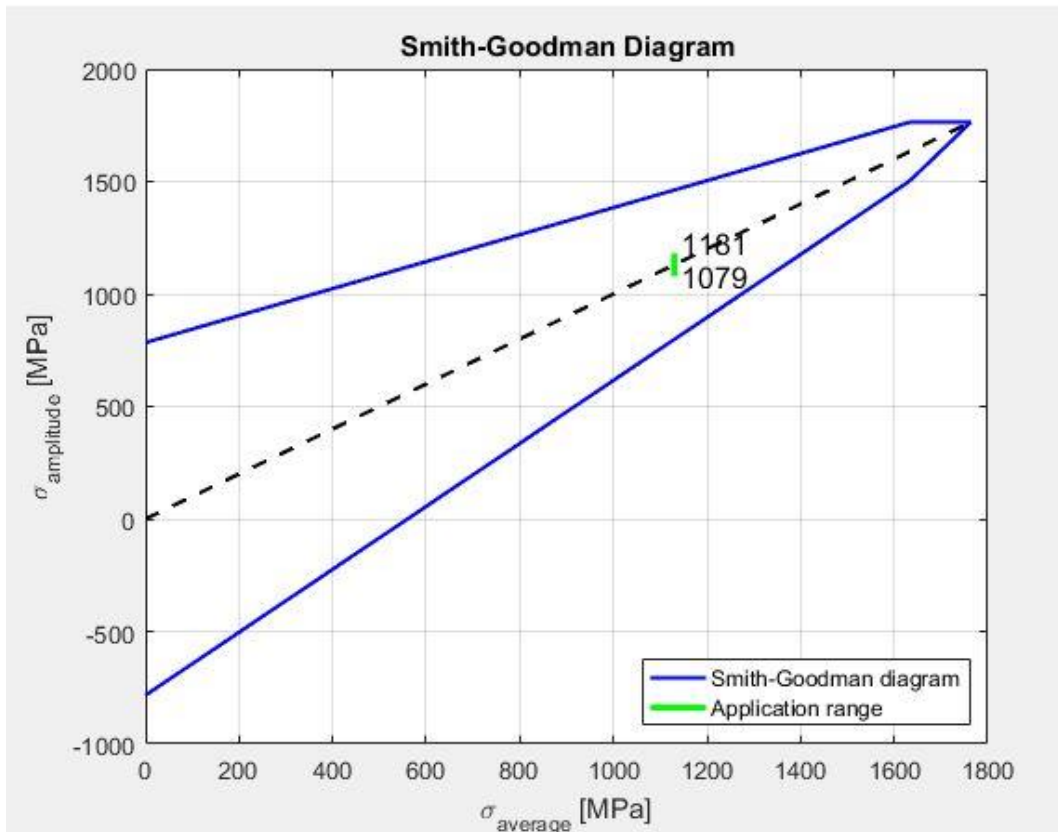


Figure 86. 1st case study Smith-Goodman diagram

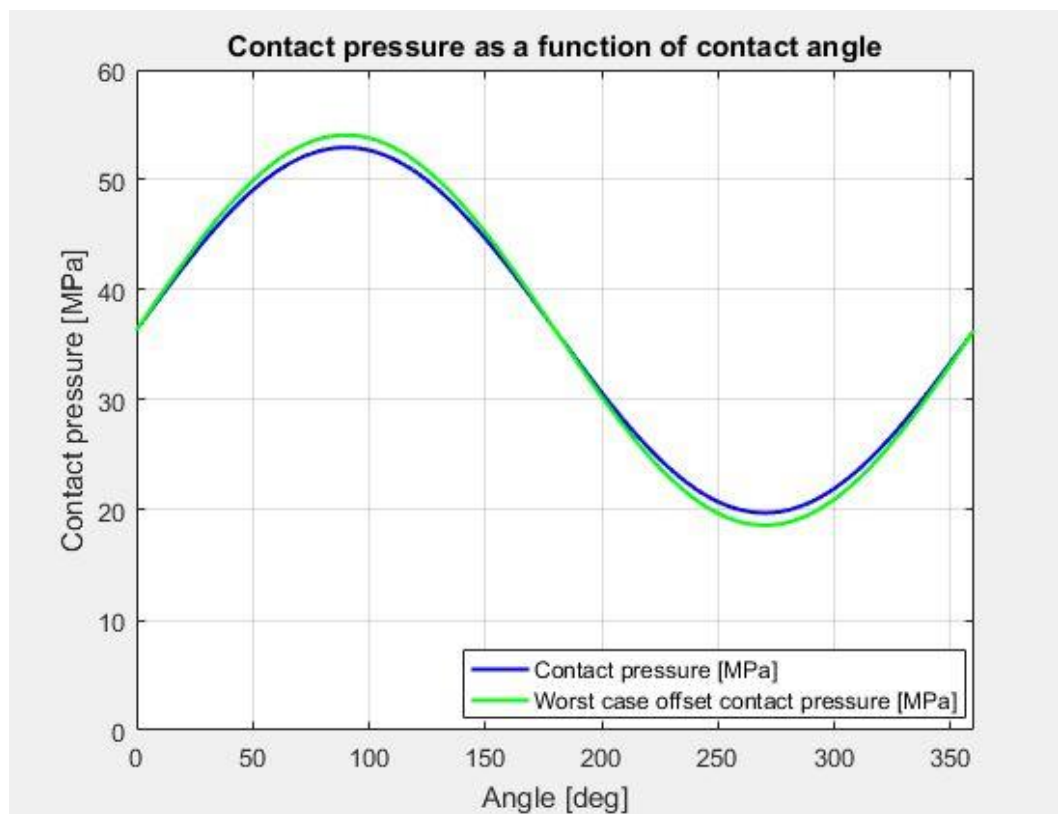


Figure 87. 1st case study pivot base contact pressure vs. contact angle

In table 10, the outputs deriving from the automatic design tool and the real ones regarding the 1st case study are compared:

- Tensioner architecture:
It is a function of the middle plane belt height and brings in both cases to a standard layout.
- Pulley:
As a function of the belt width, the pulley width is selected. The suggested value coincides with the real one.
- Ball bearing:
There is a complete alignment between simulation and real product.
- Pivot:
Pivot diameter is selected as an input. It is then checked to avoid critical issue. If the real value is inserted, the verification is achieved. A difference can be detected for the pivot bushing length. For what concerns the computed value, the verification is achieved at the first re-iteration, so the pivot bushing length coincides with its diameter. The real pivot bushing is longer, since it is not available in such a format.
- Tensioner characterization:
By evaluating the tensioner mathematical model, the axial damping system is assumed to be needed in order to fulfil the tensioner specifications, reaching in this way an alignment with the real condition. Axial and radial damping contributions disjunction is needed only from a mathematical point of view, so it is not specified in the tensioner drawings. A mathematical model output comparable with the components specifications is, instead, the spring torque at nominal position. In this case a discrepancy of about 5% can be detected.
- Plastic friction elements:
As it can be seen from picture 81, tensioner is verified at the first re-iteration, without the need for increasing the plastic friction elements dimensions. It is worth to notice that the margin is quite narrow, whose main reason is the enhanced cone spring relaxation. This aspect is heavily influencing the tensioner damping trend, since, in this configuration, the axial damping is almost the 80% of the total one.
In this section a weak alignment between the automatic design tool and the real tensioner arises. This difference is to be ascribed to the out-of-standard plastic friction elements dimensions of the real tensioner. So, this aspect has not to be seen as an error, because the aim of the automatic design tool is not only to fasten the design procedure. In fact, besides this, it is aimed to boost the components standardization too.
- Cone spring:
The automatic design tool shows as output maximum and minimum tolerance values for the cone spring axial force. These threshold values are evaluated considering the cone spring gap height tolerance, together with the tensioner damping tolerance. The upper limit computed by the automatic design tool is comparable with the actual

one. A different situation is found in the lower limit. In fact, the actual limit is considerably higher than the computed one. This difference is brought by the asymmetric tolerance with respect to the cone spring nominal force applied by the supplier. Moving the attention to the cone spring packaging constraints, a general misalignment can be noticed. The internal diameter difference is to be ascribed to the fact that the cone spring-pivot coupling is an out-of-standard. The external diameter difference, instead, is due to the different damper pad dimensions.

➤ Main spring:

As discussed above, a spring nominal torque shift has been experienced. Since the safety factor and the spring stresses in the considered conditions are depending on the spring torque at nominal position, a shift in these values can be experienced as well (again about 5%). This difference does not influence the spring typology and its working conditions. Moving the attention to the mean body diameter, a strong difference can be detected (more than 10%). This is due to the different plastic friction elements dimensions. In fact, if even the smallest standard format would be implemented, the spring of the real tensioner, during its winding, would lock onto the spring bushing, bringing to a non-linear behaviour. This misalignment influences the number of active coils at free state. In fact, in the real tensioner a higher number of active coils can be noticed. This difference permits to obtain the same value of torsional stiffness.

➤ Bolt & Tilting-Sliding Verification

Minimum tilting safety factor and sliding safety factor are imposed as inputs. As a result, a very similar torque with respect to the real one has been obtained. This brings to the same bolt choice and bolt material class. As it can be observed, the computed contact surface pressure is very similar to the real one. Finally, the actual safety factors can be analysed: the computed sliding safety factor is equal to the target one. The tightening torque that permits to reach this result is fulfilling the tilting safety factor as well, with a small margin.

Case study nr.2

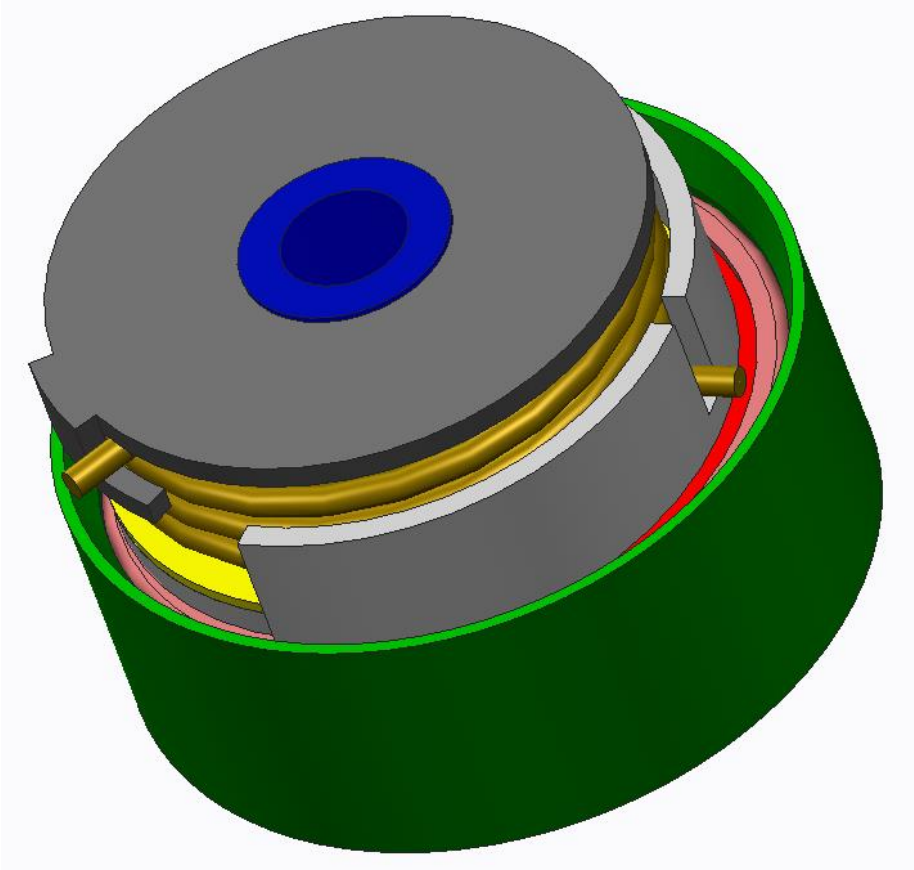


Figure 88. 2nd case study 3D model

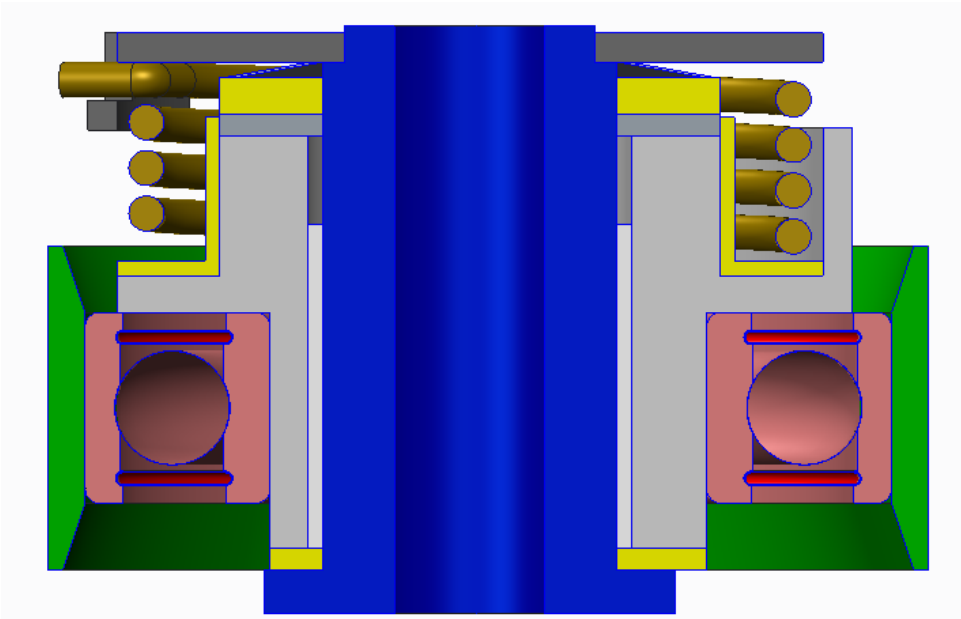


Figure 89. 2nd case study 3D model (section view)

Input list

Engine application		
Application type	[-]	Belt In Oil
Engine fuel	[-]	Diesel
Pulley		
Pulley shell type	[-]	Flat
Pulley diameter	[mm]	60.0
Pulley max parallelism EOL	[mm]	0.3
Tensioner geometrical data		
Belt loading type	[-]	Autosetting
Working arm length	[mm]	2.5
Loading arm length	[mm]	-
Differential angle	[deg]	79
Wrap angle	[deg]	N/A
Nom arm angle with respect to H.E.R.	[deg]	83
Belt		
Belt width	[mm]	18.0
Middle plane belt height	[mm]	14.0
Middle plane belt height increment (worst case)	[mm]	2.0
Lock-up pin		
Lock-up pin position radius	[mm]	N/A
Lock-up pin angular position	[deg]	N/A
Lock-up pin diameter	[mm]	N/A
Space constraints		
Max pivot height	[mm]	40.0
Min belt-crankcase clearance	[mm]	2.0
Pivot		
Pivot class diameter	[mm]	20
Pivot bushing radial thickness	[mm]	1
Durability test		
Theta peak-to-peak	[deg]	16
Frequency	[Hz]	50
Duration	[hrs]	1200
Tensioner specifications		
Calculated torque target	[Nm]	1.75
Damping target	[Nm]	1.10
Damping tolerance	[Nm]	0.25
Damping EOLife limit	[Nm]	0.70
Main spring		
Spring stiffness	[Nm/deg]	0.0131
Spring torque tolerance	[%]	8%
Bolt		
Tilting safety factor	[-]	4.50
Sliding safety factor	[-]	4.50
Fixation dimensional features		
Engine support internal diameter	[mm]	10.2
Engine support external diameter	[mm]	28.0
Contact angle	[deg]	360
Bolt head contact external diameter	[mm]	0.0156

Number of active threads	[-]	3
σ_{YS} support (compression)	[MPa]	400
σ_{YS} support (traction)	[MPa]	400

Table 11. 2nd case design input

Output list			
		Automatic design tool	Real tensioner
Tensioner architecture			
Tensioner architecture typology	[-]	Rotary, Reverse	Rotary, Reverse
Pulley			
Pulley width	[mm]	22	21.3
Ball bearing			
Ball bearing typology	[-]	6006	6006
Pivot			
Pivot diameter	[mm]	20	20
Pivot bushing length	[mm]	22	22
Tensioner characterization			
Axial damping	[Y/N]	Yes	Yes
Axial damping	[Nm]	0.71	N/A
Radial damping	[Nm]	0.39	N/A
Spring torque @ nominal position	[Nm]	1.50	1.47
Plastic friction elements			
Damper pad contact area	[mm ²]	490	490
Damper pad mean radius	[mm]	13.5	13.5
Damper pad axial height	[mm]	2.5	2.5
Damper pad outer diameter	[mm]	34.5	34.5
Endcap spacer contact area	[mm ²]	670	670
Endcap spacer mean radius	[mm]	14.5	14.5
Endcap spacer axial height	[mm]	1.5	1.5
Cone spring			
F _{ax} max tolerance	[N]	267.4	260
F _{ax} min tolerance	[N]	150.4	160
Minimum internal diameter	[mm]	20.2	20.2
Maximum external diameter	[mm]	33.0	32.5
Main spring			
Safety factor	[-]	1.3	1.3
σ_a max	[MPa]	1331	1303
σ_{amin}	[MPa]	1170	1148
σ_{inst}	[MPa]	1650	1610
Material	[-]	VDSiCr	VDSiCr
Working condition	[-]	Winding	Winding
Wire section type	[-]	Round wire	Round wire
Wire section sizes	[mm]	2.4	2.4
n _a (free state)	[-]	3.234	3.517
mbd	[mm]	44	43.9
h _{spring}	[mm]	13.5	15.5

$\vartheta_{\text{free state}}$	[deg]	275.9	184
ϑ_{nom}	[deg]	151.96	56
Bolt			
T_{bolt}	[Nm]	48.86	50.00
$F_{\text{ax bolt}}$	[N]	32090	N/A
σ_{bolt}	[MPa]	511.96	N/A
τ_{bolt}	[MPa]	220.01	N/A
$\sigma_{\text{eqv bolt}}$	[MPa]	637.37	N/A
$\sigma_{\text{under bolt head}}$	[MPa]	293.27	N/A
σ_{thread}	[MPa]	290.40	N/A
Bolt format	[-]	M10 x 1,50	M10 x 1,50
Bolt material class	[-]	8.8	9.8
Tilting - Sliding verification			
Pivot base contact surface	[mm ²]	534.04	534.04
Avg contact surface pressure	[MPa]	58.82	60.09
Tilting safety factor	[-]	11.02	11.15
Sliding safety factor	[-]	4.50	4.58

Table 12. 2nd case study simulation output summary

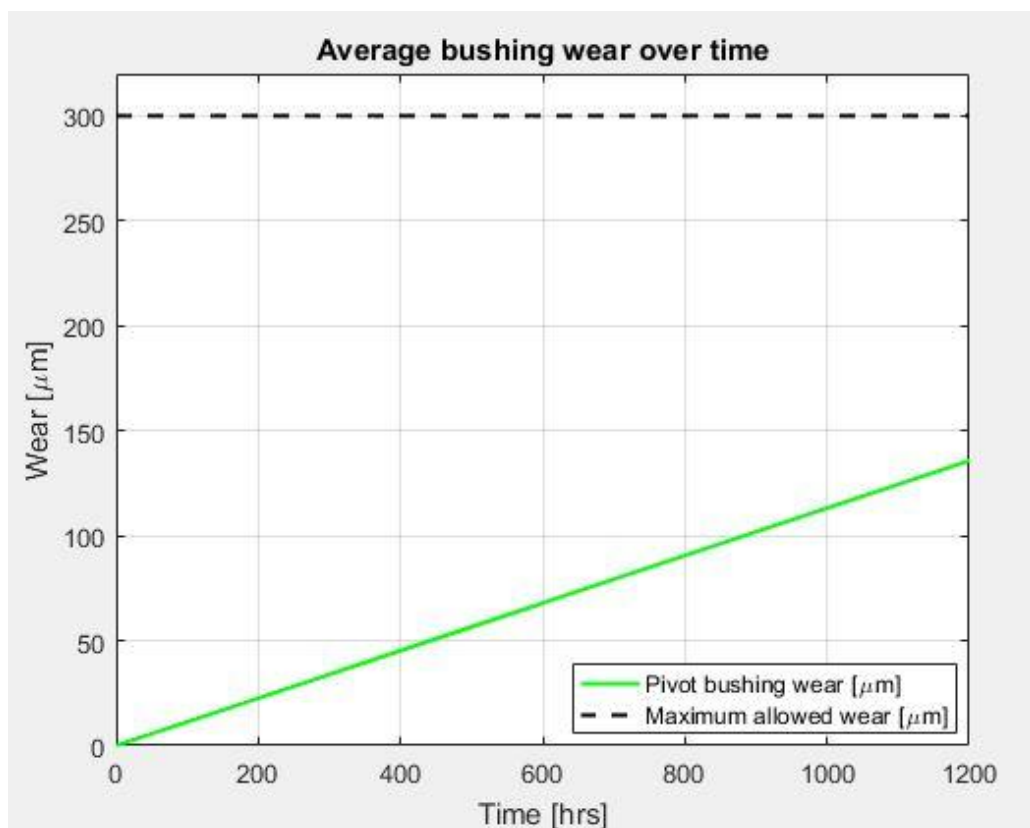


Figure 90. 2nd case study bushing wear vs. time

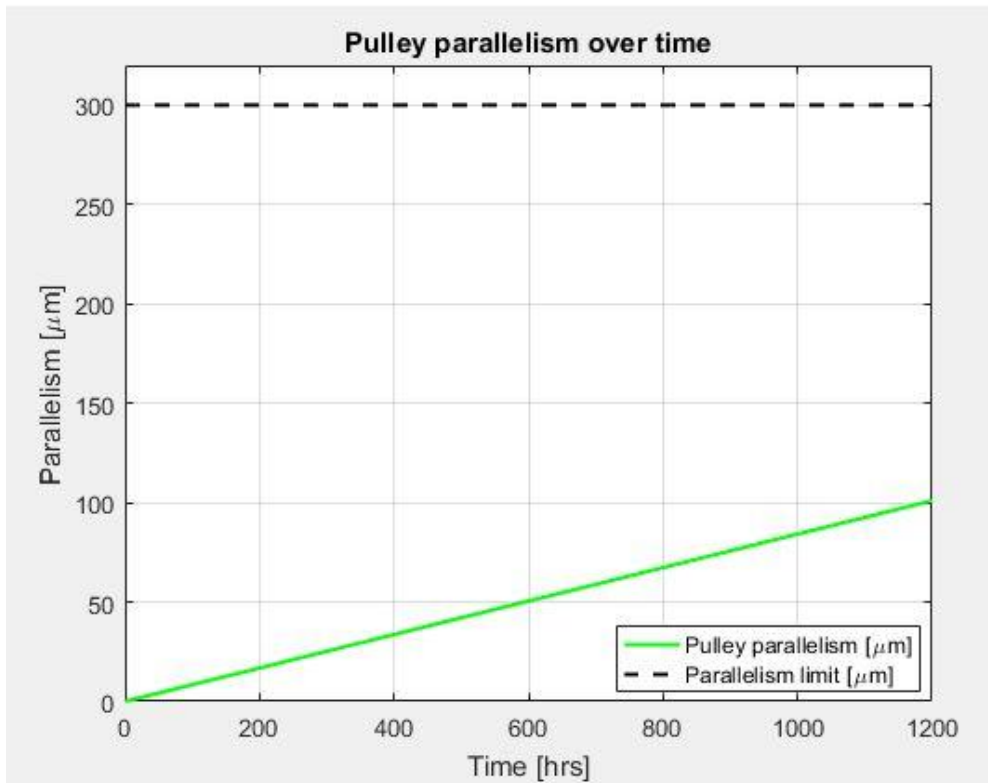


Figure 91. 2nd case study pulley parallelism vs. time

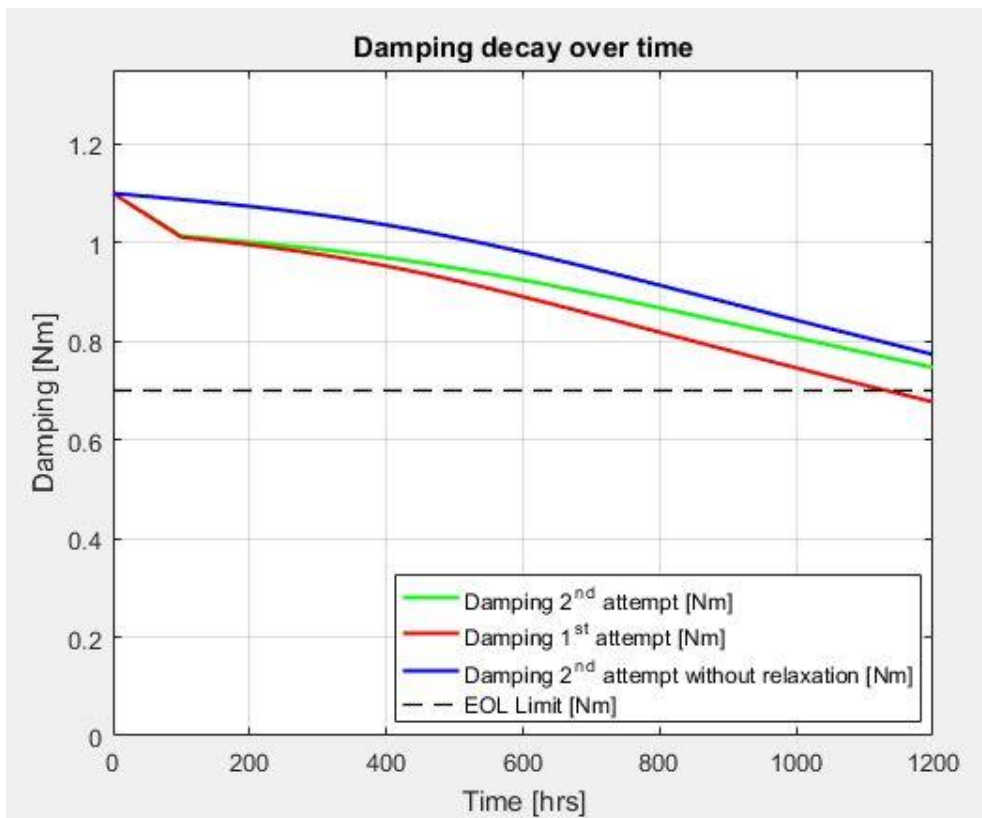


Figure 92. 2nd case study damping decay vs. time

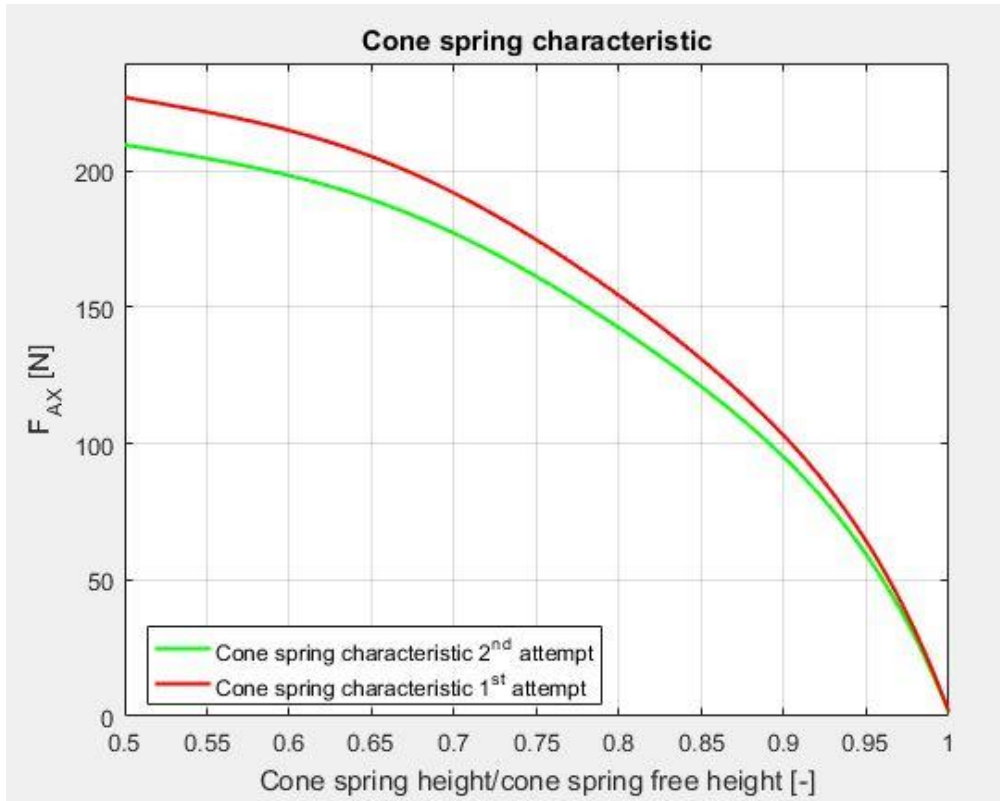


Figure 93. 2nd case study cone spring characteristic

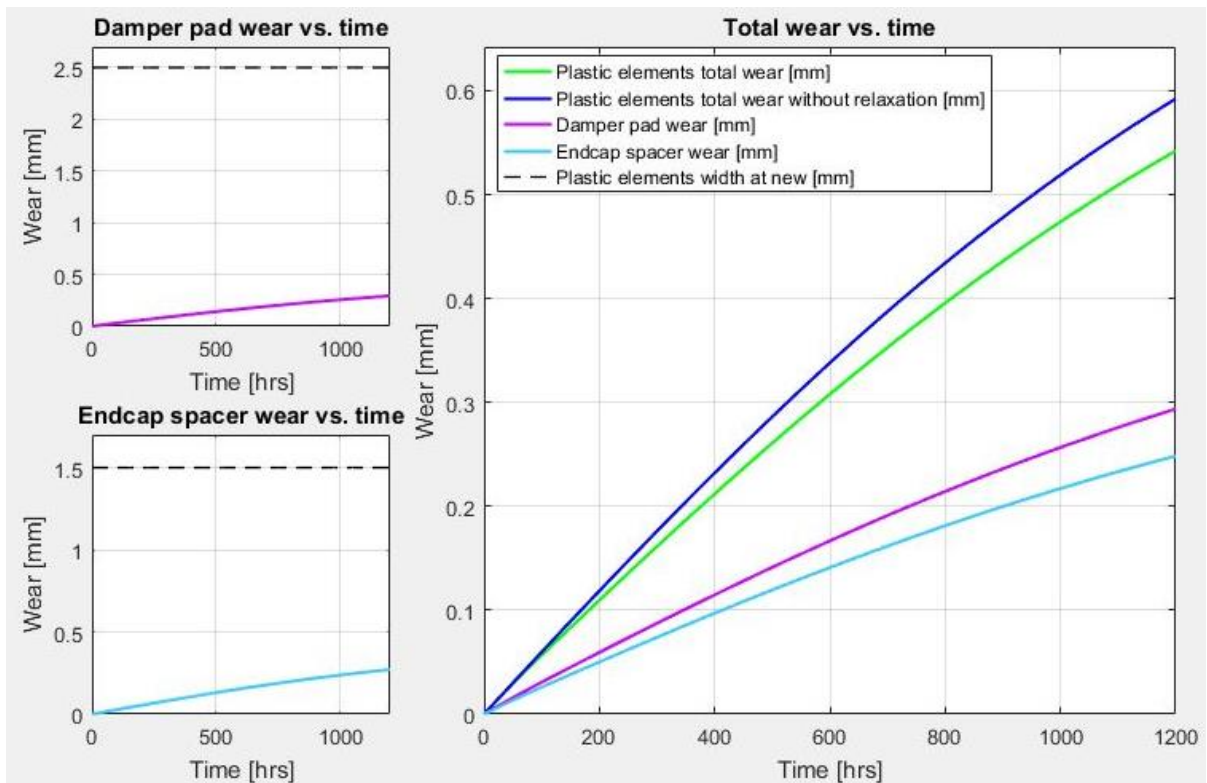


Figure 94. 2nd case study plastic friction elements wear vs. time

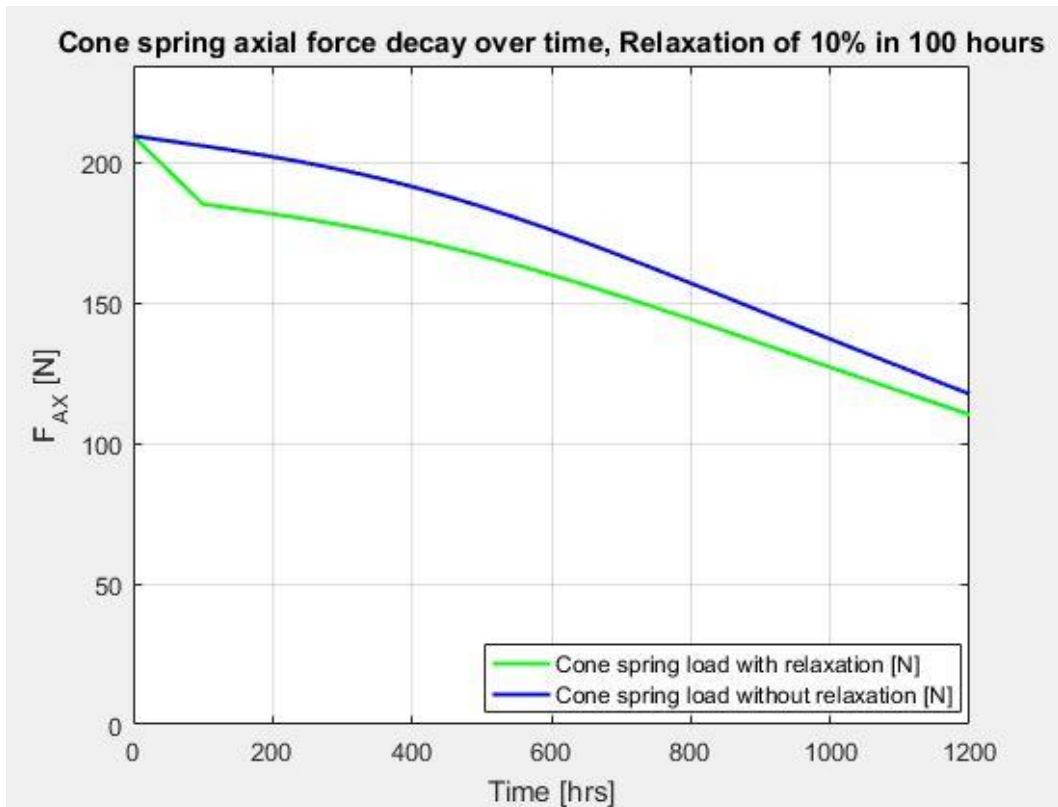


Figure 95. 2nd case study cone spring axial force vs. time

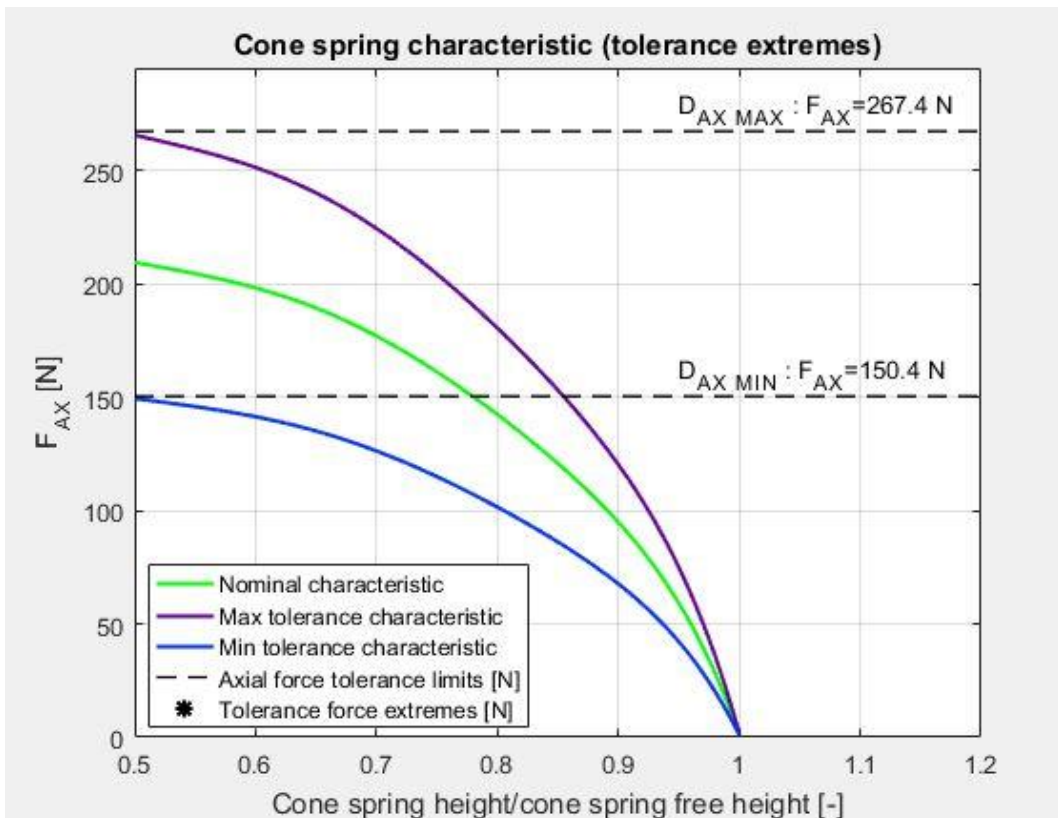


Figure 96. 2nd case study cone spring tolerance

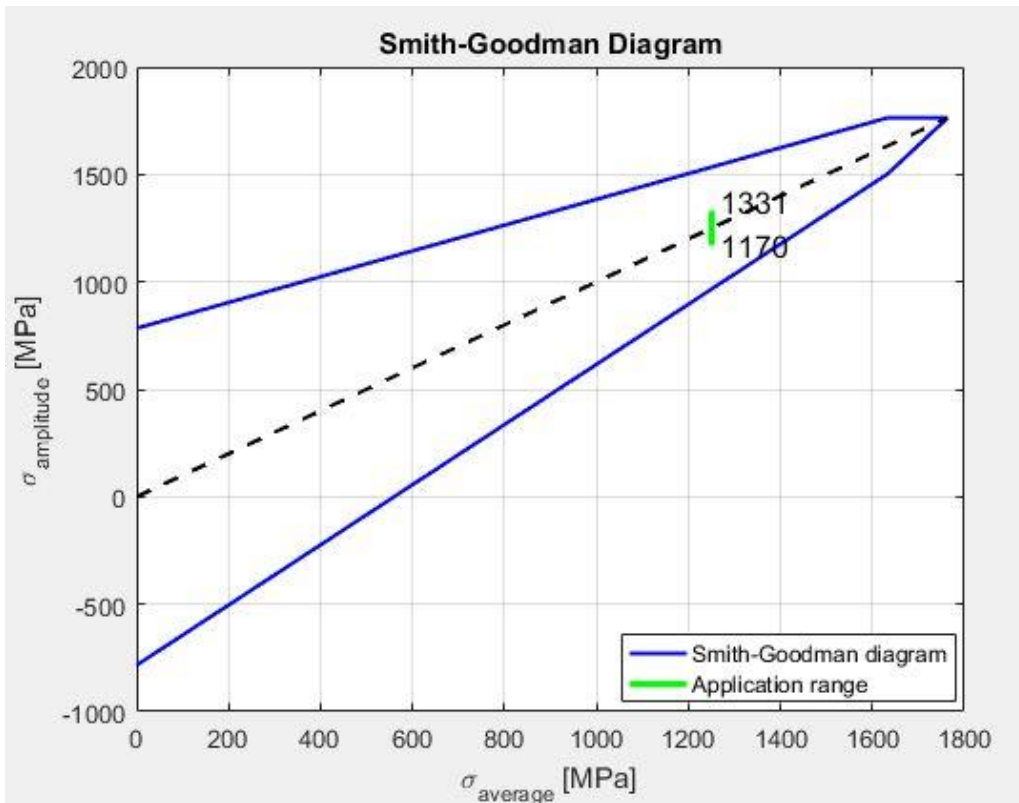


Figure 97. 2nd case study Smith-Goodman diagram

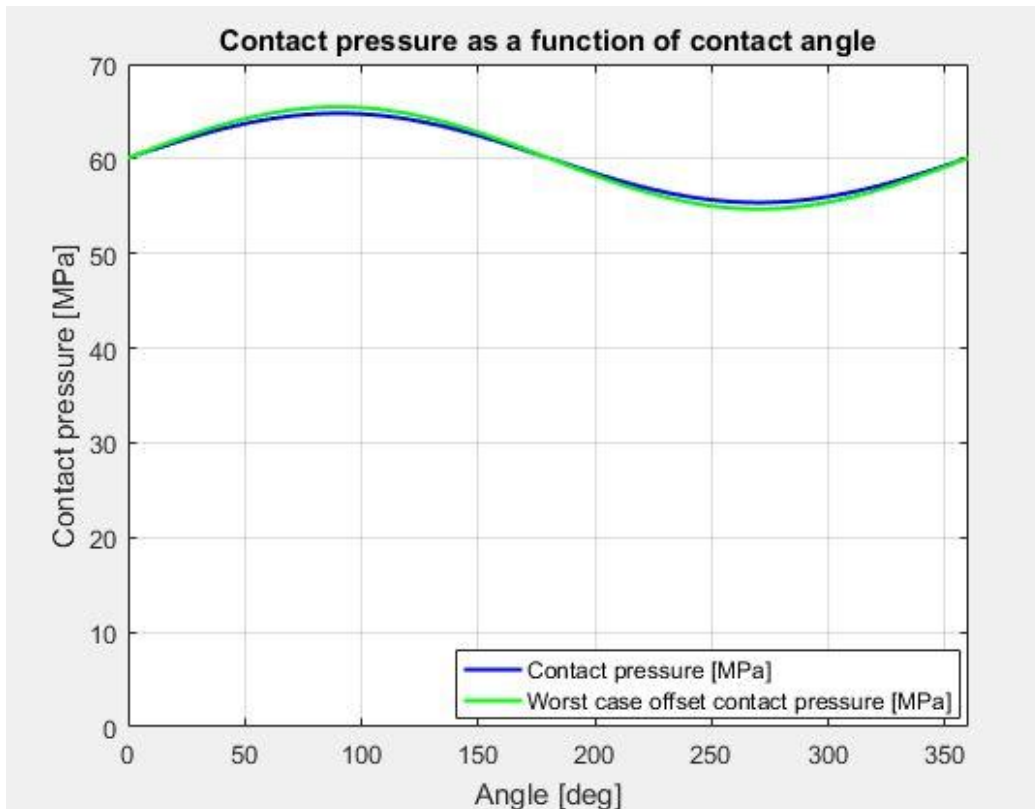


Figure 98. 2nd case study pivot base contact pressure vs. contact angle

In table 12, the outputs deriving from the automatic design tool and the real ones regarding the 2nd case study are compared:

- Tensioner architecture:
It is a function of the middle plane belt height and brings in both cases to a reverse layout.
- Pulley:
By selecting the actual belt width, a pulley width value different from the real one is suggested. However, the user can decide to change the suggested value to cope with already existing production codes (this choice has been done for the real tensioner). By selecting the real pulley width, the tensioner is verified as well.
- Ball bearing:
There is a complete alignment between simulation and real product.
- Pivot:
Pivot diameter is selected as an input. It is then checked to avoid critical issue. If the real value is inserted, the verification is achieved. Pivot bushing length suggested by the automatic procedure is the same implemented in the real component. The automatic design tool achieves the pivot bushing length verification at the second re-iteration.
- Tensioner characterization:
By evaluating the tensioner mathematical model, the axial damping system is assumed to be needed in order to fulfil the tensioner specifications, reaching in this way an alignment with the real condition. Axial and radial damping contributions disjunction is needed only from a mathematical point of view, so it is not specified in the tensioner drawings. A mathematical model output comparable with the components specifications is, instead, the spring torque at nominal position. In this case a discrepancy of about 2% can be detected.
- Plastic friction elements:
As it can be seen from picture 92, tensioner plastic friction elements verification is achieved at the second re-iteration. Initially they were set according to the axial damping interval, but the resulting EOLife damping value was below the threshold (red line). As a consequence, contact surfaces have been increased and simulation run again. The resulting damping trend over time is represented by the green line. The green colour highlights the positive outcome, in fact the EOLife damping value of the second simulation results to be higher than the minimum threshold. These final plastic friction elements dimensions correspond to the real tensioner ones.
- Cone spring:
The automatic design tool shows as output maximum and minimum tolerance values for the cone spring axial force. These threshold values are evaluated considering the cone spring gap height tolerance, together with the tensioner damping tolerance. The limits computed by the automatic design tool are comparable with the actual ones. Moving the attention to the cone spring packaging constraints, a general

alignment between computed and real dimensions can be noticed. This is achieved due to the standard pivot-cone spring coupling (for what concerns the inner diameter) and due to the same damper pad dimensions (for what concerns the outer diameter).

➤ Main spring:

As discussed above, a spring nominal torque shift can be noticed. Since the safety factor and the spring stresses in the considered conditions are depending on the spring torque at nominal position, a shift in these values can be experienced as well (again about 2%). This difference does not influence the spring typology and working conditions. Number of active coils at free state is deviating from the automatic tool output to the real tensioner since, in this last situation, the theoretical value is increased of 0.25. This is due to the spring stress distribution which is resulting when it is installed in the tensioner. In fact, within 90 degrees from the spring hooks, the stress shows a triangular distribution. For this reason, since each application requires two hooks, there are two 90 degrees wide areas that present this behaviour, so they have to be accounted as two 45 degrees wide areas. This difference can be found also in the angle between hooks in free state and in nominal condition.

Moving the attention to the mean body diameter, an almost complete alignment between the automatic design tool and the real tensioner can be noticed.

Different considerations have to be adduced for what concerns the spring cavity height. There is, in fact, a remarkable difference between the computed value and the real one. This is a critical dimension, since particular care must be payed to avoid spring coils contact. The difference is due to two components lower axial thickness with respect to standard: the arm and the spring bushing. This has been performed in order to gain some additional space, since, at early design stages, the tensioner spring stiffness was lower (a higher number of active coils was needed).

➤ Bolt & Tilting-Sliding Verification

Minimum tilting safety factor and sliding safety factor are imposed as inputs. As a result, a very similar torque with respect to the real one has been obtained. This brings to the same bolt choice, but this is not true for the bolt material class. In fact, the automatic design tool suggests a lower class with respect to the real one. This is due to the slightly lower tightening torque, bringing to an equivalent stress in the bolt very near to the limit between a material class and the following one (computed equivalent stress equal to 637.37, where the limit is 640.00). As it can be observed, the computed contact surface pressure is very similar to the real one. Finally, the actual safety factors can be analysed: the sliding safety factor is equal to the target one, while the tensioner is verified against tilting with a significant margin in comparison with the imposed target (they could also be different between each other). This aspect has to be ascribed to the tensioner architecture typology: a reverse tensioner is characterized by a contained belt offset, which brings to a low tilting moment.

Case study nr. 3

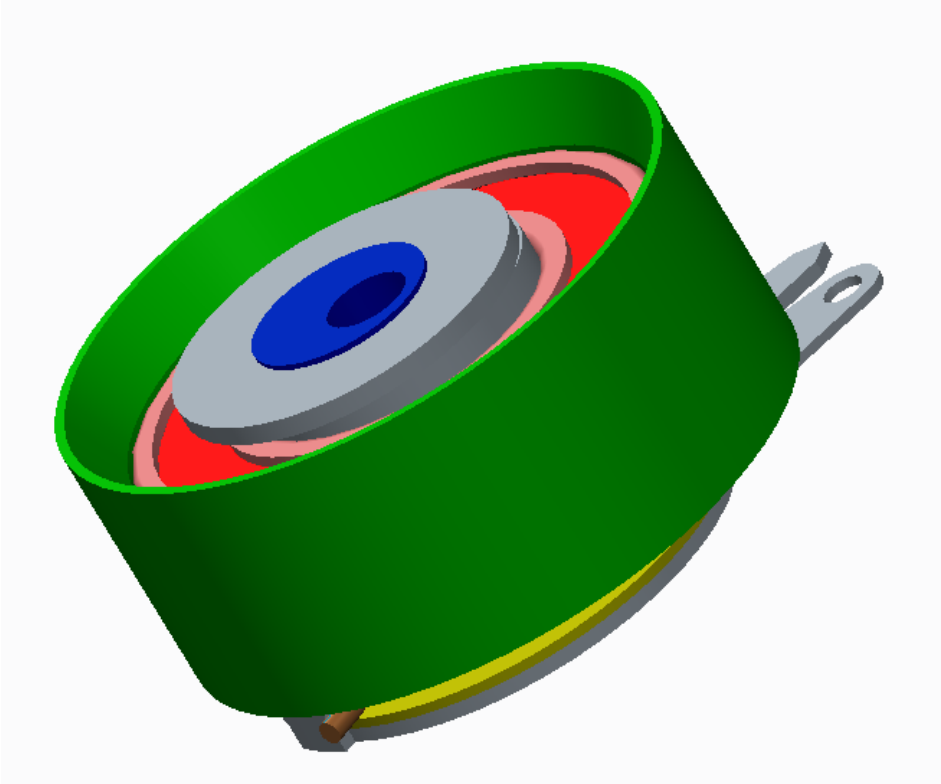


Figure 99. 3rd case study 3D model

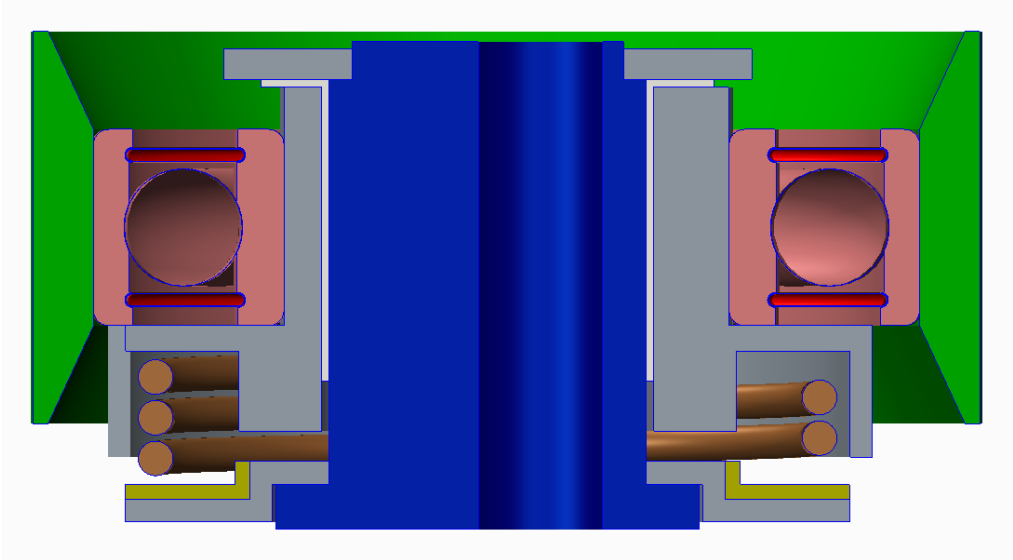


Figure 100. 3rd case study 3D model (section view)

Input list

Engine application		
Application type	[-]	Dry
Engine fuel	[-]	Diesel
Pulley		
Pulley shell type	[-]	Flat
Pulley diameter	[mm]	65.5
Pulley max parallelism EOL	[mm]	0.5
Tensioner geometrical data		
Belt loading type	[-]	Double eccentric
Working arm length	[mm]	4.0
Loading arm length	[mm]	3.0
Differential angle	[deg]	90
Wrap angle	[deg]	N/A
Nom arm angle with respect to H.E.R.	[deg]	290
Belt		
Belt width	[mm]	26.0
Middle plane belt height	[mm]	20.0
Middle plane belt height increment (worst case)	[mm]	2.0
Lock-up pin		
Lock-up pin position radius	[mm]	N/A
Lock-up pin angular position	[deg]	N/A
Lock-up pin diameter	[mm]	N/A
Space constraints		
Max pivot height	[mm]	34.0
Max axial displacement	[mm]	36.3
Pivot		
Pivot class diameter	[mm]	20
Pivot bushing radial thickness	[mm]	0.5
Durability test		
Theta peak-to-peak	[deg]	16
Frequency	[Hz]	50
Duration	[hrs]	1200
Tensioner specifications		
Calculated torque target	[Nm]	1.85
Damping target	[Nm]	0.45
Damping tolerance	[Nm]	0.20
Damping EOLife limit	[Nm]	0.30
Main spring		
Spring stiffness	[Nm/deg]	0.0164
Spring torque tolerance	[%]	8%
Bolt		
Tilting safety factor	[-]	3.00
Sliding safety factor	[-]	3.00
Fixation dimensional features		
Engine support internal diameter	[mm]	8.2
Engine support external diameter	[mm]	28.0
Contact angle	[deg]	360
Bolt head contact external diameter	[mm]	0.011

Number of active threads	[-]	2.6
σ_{YS} support (compression)	[MPa]	400
σ_{YS} support (traction)	[MPa]	400

Table 13. 3rd case study design input

Output list			
		Automatic design tool	Real tensioner
Tensioner architecture			
Tensioner architecture typology	[-]	Rotary, Standard	Rotary, Standard
Pulley			
Pulley width	[mm]	30.0	30.0
Ball bearing			
Ball bearing typology	[-]	6006	6006
Pivot			
Pivot diameter	[mm]	21.0	21.0
Pivot bushing length	[mm]	21.0	22.0
Tensioner characterization			
Axial damping	[Y/N]	No	No
Axial damping	[Nm]	-	N/A
Radial damping	[Nm]	0.45	N/A
Spring torque @ nominal position	[Nm]	1.56	1.60
Plastic friction elements			
Damper pad contact area	[mm ²]	-	-
Damper pad mean radius	[mm]	-	-
Damper pad axial height	[mm]	-	-
Damper pad outer diameter	[mm]	-	-
Endcap spacer contact area	[mm ²]	-	-
Endcap spacer mean radius	[mm]	-	-
Endcap spacer axial height	[mm]	-	-
Cone spring			
F _{ax} max tolerance	[N]	-	-
F _{ax} min tolerance	[N]	-	-
Minimum internal diameter	[mm]	-	-
Maximum external diameter	[mm]	-	-
Main spring			
Safety factor	[-]	1.3	1.3
σ_a max	[MPa]	1338	1303
σ_{amin}	[MPa]	1114	1096
σ_{inst}	[MPa]	1626	1610
Material	[-]	VDSiCr	VDSiCr
Working condition	[-]	Winding	Winding
Wire section type	[-]	Round wire	Round wire
Wire section sizes	[mm]	3.0	3.0
n _a (free state)	[-]	2.18	2.52
mbd	[mm]	44.0	39.1
h _{spring}	[mm]	8.8	9.0
$\vartheta_{free\ state}$	[deg]	295.56	197

ϑ_{nom}	[deg]	211.86	117.7
Bolt			
T_{bolt}	[Nm]	22.60	25
$F_{ax\ bolt}$	[N]	14500	N/A
σ_{bolt}	[MPa]	394.67	N/A
τ_{bolt}	[MPa]	214.05	N/A
$\sigma_{eqv\ bolt}$	[MPa]	541.72	N/A
$\sigma_{under\ bolt\ head}$	[MPa]	343.41	N/A
σ_{thread}	[MPa]	228.14	N/A
Bolt format	[-]	M8 x 1,25	M8 x 1,25
Bolt material class	[-]	8.8	8.8
Tilting - Sliding verification			
Pivot base contact surface	[mm ²]	562.94	562.94
Avg contact surface pressure	[MPa]	25.76	28.34
Tilting safety factor	[-]	5.18	5.25
Sliding safety factor	[-]	3.00	3.12

Table 14. 3rd case study simulation output summary

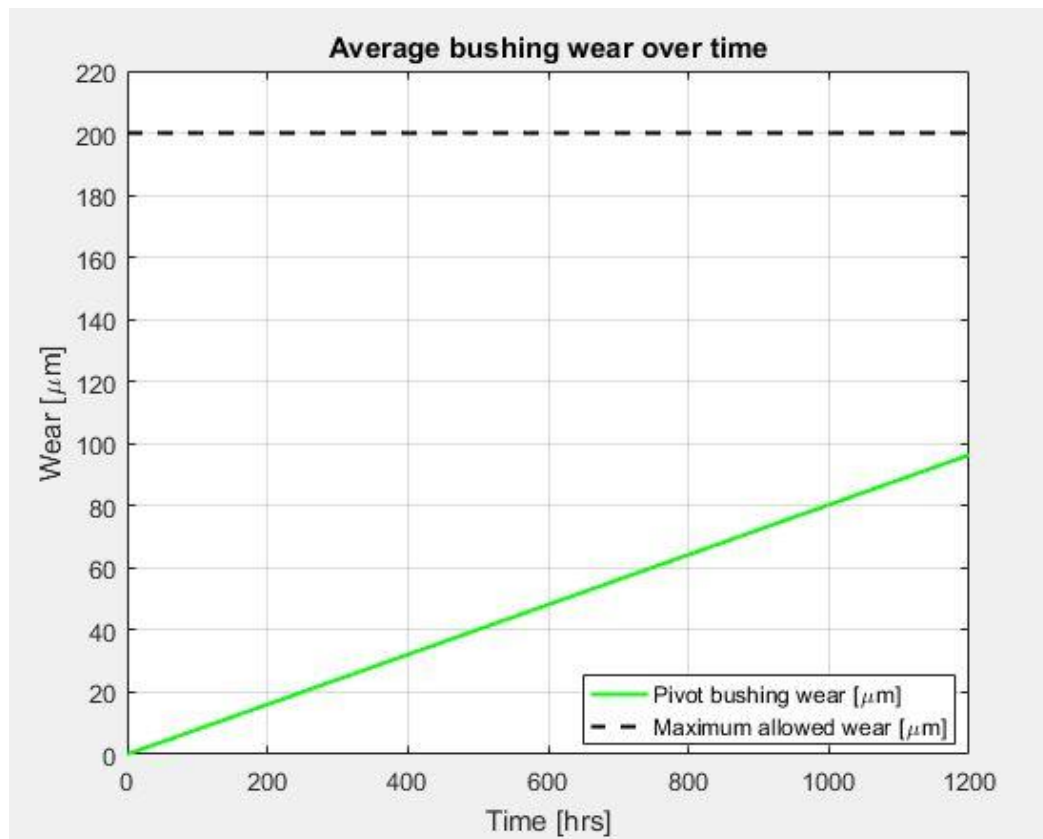


Figure 101. 3rd case study bushing wear vs. time

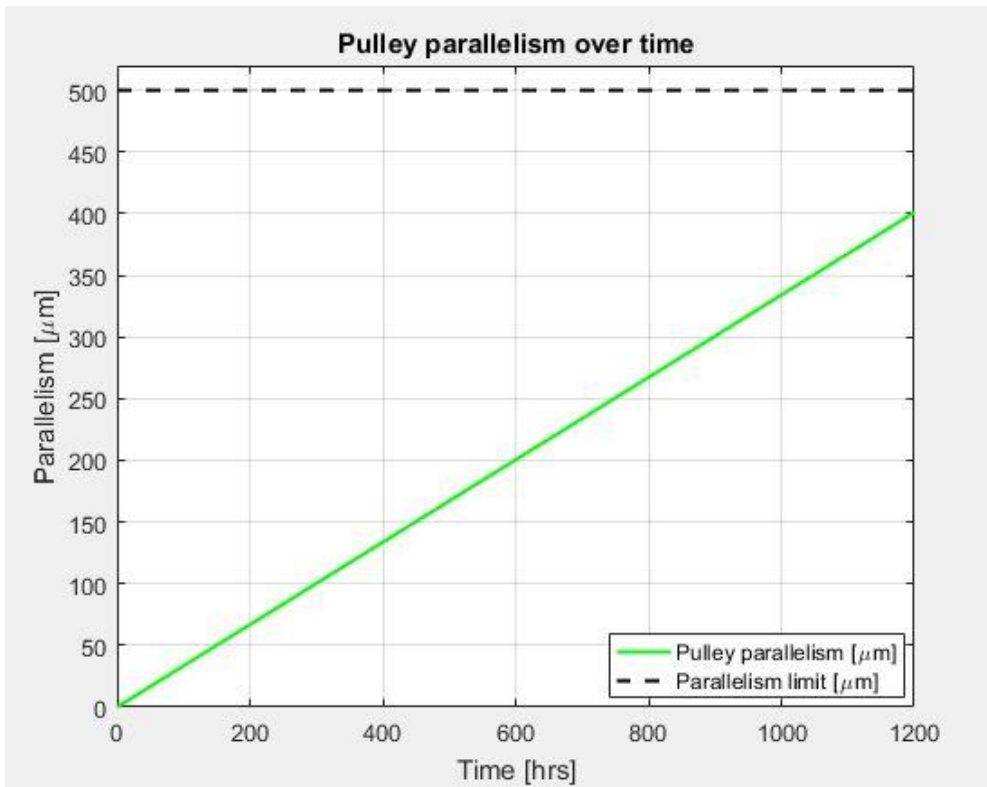


Figure 102. 3rd case study pulley parallelism

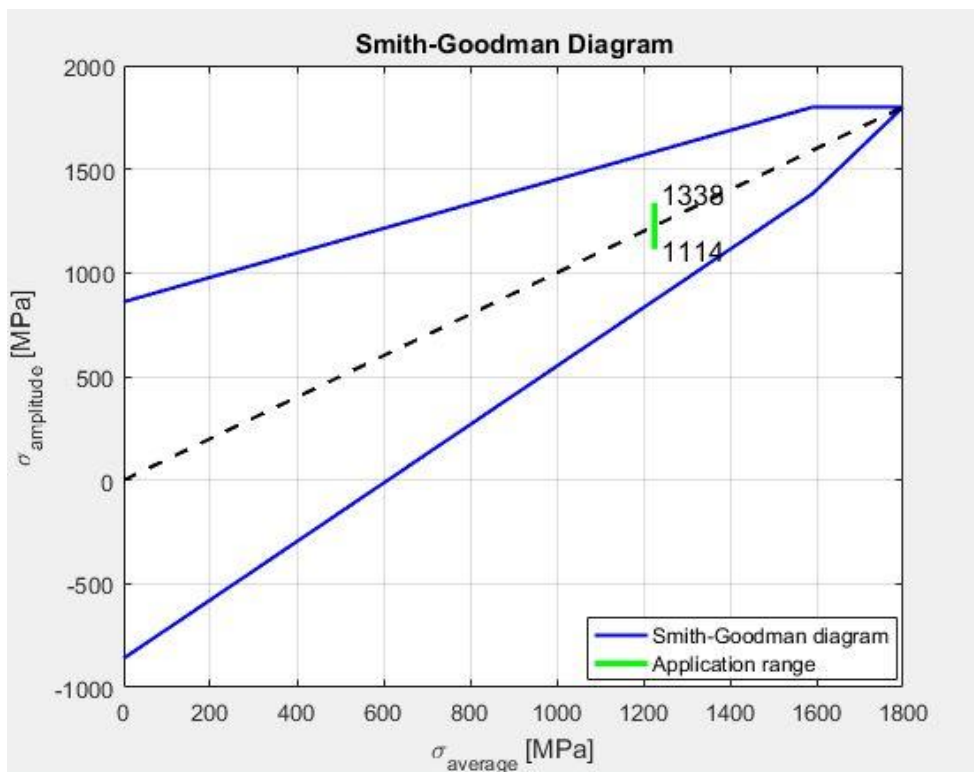


Figure 103. 3rd case study Smith-Goodman diagram

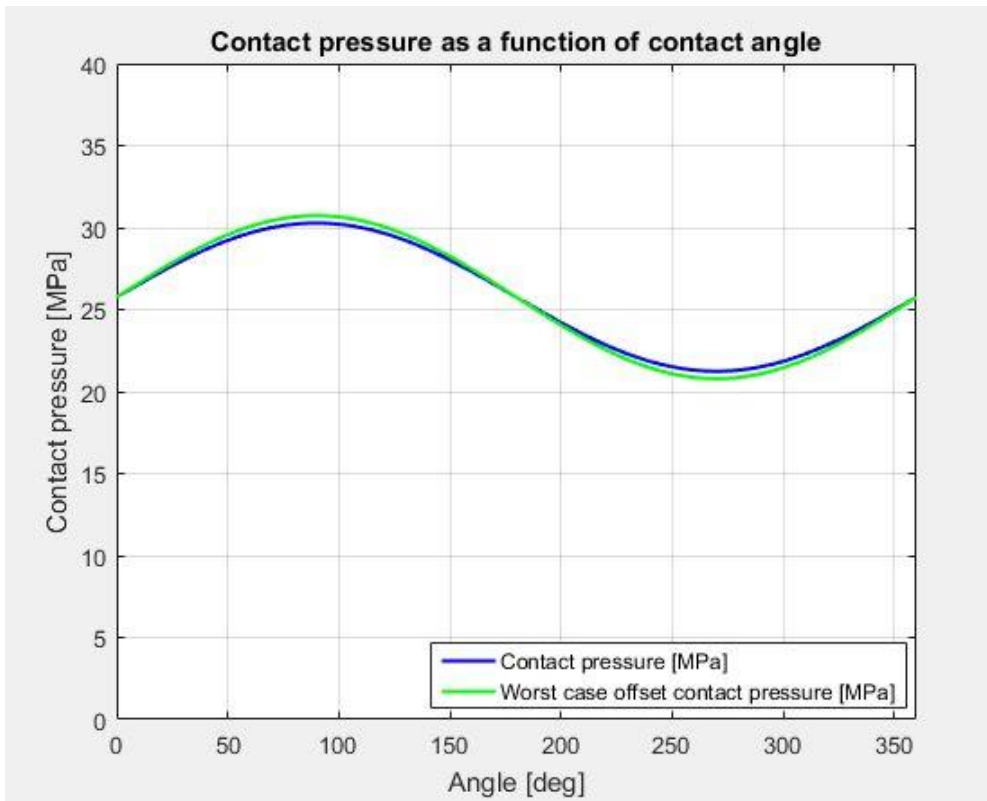


Figure 104. 3rd case study pivot base contact surface vs. contact angle

In table 14, the outputs deriving from the automatic design tool and the real ones regarding the 3rd case study are compared:

- Tensioner architecture:
It is a function of the middle plane belt height and brings in both cases to a standard layout.
- Pulley:
By selecting the actual belt width, the correct pulley width is suggested by the automatic design tool.
- Ball bearing:
There is a complete alignment between simulation and real product.
- Pivot:
Pivot diameter is selected as an input. It is then checked to avoid critical issue. If the real value is inserted, the verification is achieved. For what concerns the pivot bushing length, instead, a misalignment between computed value and real one can be detected. In fact, a pivot bushing 21mm long would be sufficient for the application, but it is not available in such a format, so in the real tensioner a 1mm longer pivot bushing can be found.
- Tensioner characterization:
By evaluating the tensioner mathematical model, the axial damping system is assumed to not be needed in order to fulfil the tensioner specifications, reaching in this way an alignment with the real condition, so only radial damping is present. A mathematical model output comparable with the components specifications is the spring torque at nominal position. In this case a discrepancy slightly above 2% can be detected.
- Plastic friction elements:
for this application the axial damping is not needed, so plastic friction elements have not to be implemented.
- Cone spring:
for this application the axial damping is not needed, so cone spring has not to be implemented.
- Main spring:
As discussed above, a spring nominal torque shift has been experienced. Since the safety factor and the spring stresses in the considered conditions are depending on the spring torque at nominal position, a shift in these values can be experienced as well (again about 2%). This difference does not influence the spring typology and working conditions. Number of active coils at free state computed by the automatic design tool has to be incremented of 0.25. This is due to the spring stress distribution which is resulting when it is installed in the tensioner. In fact, within 90 degrees from the spring hooks, the stress shows a triangular distribution. For this reason, since each application requires two hooks, there are two 90 degrees wide areas that present this behaviour, so they have to be accounted as two 45 degrees wide areas.

However, this is not sufficient to justify the difference between the real value and the computed one. In fact, it is influenced also by the mean body diameter, which shows a not negligible difference between the real value and the computed one.

This difference is then reflected in the angle between hooks in free state condition, which in turn influences the same angle at nominal.

Moving the attention to the spring cavity height, an almost complete alignment between the automatic design tool and the real tensioner can be noticed.

➤ Bolt & Tilting-Sliding Verification

Minimum tilting safety factor and sliding safety factor are imposed as inputs. As a result, a comparable torque with respect to the real one has been obtained. This brings to the same bolt choice, as well as the bolt material class. As it can be observed, the computed contact surface pressure is very similar to the real one. Finally, the actual safety factors can be analysed: the sliding safety factor is equal to the target one, while the tensioner is verified against tilting with a significant margin in comparison with the imposed target (they could also be different between each other). This aspect has to be ascribed to the tensioner architecture typology: despite the standard layout, the belt offset is very low, so tilting moment is quite small.

Conclusions

The aim of this work is to permit to shorten the time needed for a timing belt tensioner development. This is done through a dimensioning flowchart, a consequential process that, given the required design input, generates as a result a raw but verified 3D model. The final outcome cannot be a ready-to-produce model, since each application needs for some adaptation, which are different from one to another. For this reason, this automatic design tool has to be thought as a help for the designer, who will maintain a key role in the design process.

The organized structure of the dimensioning flowchart permits to avoid time-wasting trial and error procedures. This is not the only benefit with respect to the traditional procedure. The standardization is, in fact, promoted as well. This is a fundamental aspect, since it permits an easier management of different projects and improves the weight of the company know-how in similar applications. Then, the economical aspect must not be neglected: an higher standardization permits to lower both purchasing and production costs. Lower costs are achieved also thanks to design verification at early stage. From this point of view the most important part of this work is the tensioner damping variation over time simulation due to plastic friction elements wear. This is a critical aspect since a not optimized initial dimensioning of these elements would bring to a difficult adaptation of the surrounding components. In addition, the wear simulation, if properly tuned on the basis of similar in-production items, permits to avoid, or at least reduce, prototypes building and testing. Tensioner required specifications are becoming always more and more stringent, bringing to always more and more demanding tests. For this reason, they require quite a long time to be run. So, design verification at early stage means also a faster time-to-market, a relevant aspect in a global competitors-crowding environment.

An important source of improvement of this work could be the implementation of a look-up-table for the friction coefficients involved in the tensioner characterization as a function of temperature and wear. The running-in is, in fact, a relevant aspect to be accounted for. Some layout result to be more stable from this point of view, while others are more affected by this phenomenon. In this last case the need for differentiate the product specifications at new and after running-in can arise. Once the mathematical model considering this aspect is built, several simulations could be performed in order to choose all the components in such a way to obtain the desired behaviour. As an example, in products with both axial and radial damping, once the pivot bushing coefficient trend over time is known, the cone spring can be selected in such a way to compensate it, ideally obtaining a completely stable tensioner. Besides this, this work could be refined by linking the dimensioning flowchart with the components costs. A proper algorithm should consider the cost per unit of each element as a function of the actual volumes and how much it would decrease considering the growing volumes due to the new application implementation. In this way standardization would be further increased helping at the same time several divisions:

- research and development team: they would have to deal with a lower number of codes, easing the drawings management, together with the worldwide drawing alignment (in case of an international company).
- testing team: they could reduce the number of tests, reducing the number of new components. Resources could then be invested on the most used items, permitting to go in more detail.
- purchasing team: due to the lower number of suppliers deriving from this situation, purchasing team would have to deal with bigger orders. This would enable them to exert more power on suppliers, achieving lower costs and, in case of emergency, a higher timeliness.
- logistics team: material flow to the line would be easier, having a lower differentiation of codes. Besides this, stocks in the warehouse would be easier to be managed.
- production team: same components implementation means also same assembling procedure. This would bring to a shorter learning curve, with a more efficient production. Another aspect that is worth to notice is that this would permit a higher flexibility in the human capital management.

References

- G. Genta, L. Morello, The Automotive Chassis, Vol. 1 : Components Design, Springer, 2009
- G. Genta, L. Morello, The Automotive Chassis, Vol. 2 : System Design, Springer, 2009
- L. Morello, L. Rosti Rossini, G. Pia, A. Tonoli, The Automotive Body, Vol. 1 : Components Design, Springer, 2011
- L. Morello, L. Rosti Rossini, G. Pia, A. Tonoli, The Automotive Body, Vol. 2 : System Design, Springer, 2011
- R. C. Juvinall, K. M. Marshek, Fundamentals Of Machine Component Design, John Wiley & Sons, Inc., 2011
- www.schnoor.com
- www.scherdel.com